Journal of the National Academy of Forensic Engineers®

http://www.nafe.org

ISSN: 2379-3252

DOI: 10.51501/jotnafe.v39i1

Vol. 39 No. 1 June 2022

National Academy of Forensic Engineers®

Journal Staff

Technical Review Process

The Technical Review Committee Chair chooses the reviewers for each Journal manuscript from amongst the members and affiliates of the NAFE according to their competence and the subject of the paper, and then arbitrates (as necessary) during the review process. External reviewers may also be utilized when necessary. This confidential process concludes with the acceptance of the finished paper for publication or its rejection/withdrawal. The name(s) of authors are included with their published works. However, unpublished drafts together with the names and comments of reviewers are entirely confidential during the review process and are excised upon publication of the finished paper.

National Academy of Forensic Engineers®

Board of Directors

President
Samuel Sudler, PE, DFE
Senior Member

President-Elect
Joseph Leane, PE, DFE
Fellow

Senior Vice President
Steven Pietropaolo, PE, DFE
Senior Member

Vice President
Michael Aitken, PE, DFE
Senior Member

Treasurer
Bruce Wiers, PE, DFE
Senior Member

Secretary
Richard Rice, PE, DFE
Fellow

Past Presidents
Liberty Janson, PE, DFE
Senior Member

James Petersen, PE, DFE
Fellow

John Certuse, PE, DFE
Fellow

Directors at Large
Daniel Couture, PEng, DFE
Member

Robert Peruzzi, PhD, PE, DFE
Member

Executive Director
Rebecca Bowman, PE, Esq.

Journal of the National Academy of Forensic Engineers®

Editorial Board

Submitting Proposed Papers to NAFE for Consideration

Please visit the Journal's author page at
http://journal.nafe.org/ojs/index.php/nafe/information/authors for submission details.

We are looking for NAFE members who are interested in giving presentations on technical topics that will further the advancement and understanding of forensic engineering at one of the academy's biannual meetings and then developing those presentations into written manuscripts/papers, which will go through a single-blind peer review process before publication. Only papers presented at a NAFE regular technical seminar and have received oral critique at the seminar will be accepted for review and publication. We recommend that you review the About the Journal page for the journal's section policies as well as the Author Guidelines listed on the Submissions page. Authors need to register with the journal prior to submitting, or (if already registered) they can simply log in and begin the process. The first step is for potential authors to submit a 150-word maximum abstract for consideration at an upcoming conference into the online journal management system.

Copies of the Journal

The Journal of the National Academy of Forensic Engineers® contains papers that have been accepted by NAFE. Members and Affiliates receive a PDF download of the Journal as part of their annual dues. All Journal papers may be individually downloaded from the NAFE website. There is no charge to NAFE Members & Affiliates. A limited supply of Volume 33 and earlier hardcopy Journals (black & white) are available. The costs are as follows: $15.00 for NAFE Members and Affiliates; $30.00 for members of the NSPE not included in NAFE membership; $45.00 for all others. Requests should be sent to Mary Ann Cannon, NAFE, 1420 King St., Alexandria, VA 22314-2794.

Comments by Readers

Comments by readers are invited, and, if deemed appropriate, will be published. Send to: Ellen Parson, Journal Managing Editor, 3780 SW Boulder Dr, Lee's Summit, MO 64082. Comments can also be sent via email to journal@nafe.org.

Material published in this Journal, including all interpretations and conclusions contained in papers, articles, and presentations, are those of the specific author or authors and do not necessarily represent the view of the National Academy of Forensic Engineers® (NAFE) or its members.

 ISSN: 2379-3252

Table of Contents

+ Paper presented at the NAFE seminar held in January 2019 in Orlando.

§ Paper presented at the NAFE seminar held in January 2020 in San Diego.

‡ Paper presented at the NAFE seminar held in July 2021 in Providence.

Paper presented at the NAFE seminar held virtually in January 2021.

FE Analysis and Visual Presentation Methodology of Mechanical Systems

By David A. Danaher, PE, DFE (NAFE 703F) and Sean M. McDonough, PE (NAFE 1146M)

Abstract

The operation of a large industrial or other complex mechanical system incorporates a variety of mechanical and electrical subsystems to perform a given task, some of which require interaction by an operator or worker to oversee and control the process. As with anything mechanical, the system also requires periodic maintenance and replacement of worn parts. During the operation of industrial systems, problems can occur and result in catastrophic failures and/or injury. When applying forensic analysis to such failures, a methodical approach is necessary to allow for a deeper understanding of the overall operation of the system. However, once the forensic analysis has been performed, conveying the findings of such a complex system can be challenging. To assist in describing the system and failure, the use of visualization is a powerful tool to clearly convey the findings as well as normal operation. The following paper outlines the process of building a methodology to investigate and lay the proper foundation for visually presenting the findings. To demonstrate the methodology outlined in this paper, a case study involving a boiler system will be used.

Keywords

Mechanical, visualization, failure, operator, maintenance, animation, graphics, boiler, design, pressure vessel, forensic engineering

Introduction

Before any detailed graphics or animation can be produced, a forensic analysis must be performed of the mechanical system. For the purposes of this paper, an outline will be discussed to assist with the steps needed to produce a compelling visualization.

There are three main areas of focus: operation of the system during normal operation (including the interaction of the operators and maintenance performed); operation of the system at the time of the failure (including the actions of operators and any work or maintenance performed leading up to the failure); and analysis of the failure (including specific components, processes, maintenance, or operator error).

Analysis of mechanical systems failures requires an engineer to first understand the processes, components, and materials that comprise the system — and what functions they perform during normal operation. While there are endless types and variations of mechanical systems, a basic understanding of the parts and steps performed can be developed through reviewing available resources and creating a simple model of the order of operations. When a mechanical systems analysis is required, a failure in the system and/or an injury to an operator or bystander has occurred. Therefore, it is beneficial to start with identifying the likely locations or components in the system that were involved in the failure or injury. Focusing the analysis on specific components or subsystems can simplify the analysis process of a larger system.

Normal Operation

The first step in performing a forensic analysis is to determine the operation of the system under normal circumstances. Forensic engineering investigations include varying levels of documentation, such as photographs or drawings of the system. It is common to encounter systems that are commercially available, in which case research into the product or system can provide significant information on the operation and components. However, some failure analyses will be performed on proprietary systems or something adapted without formal documentation during operation to improve function of the system. In these cases, reviewing operator and witness statements, formal and informal notes, technical drawings, and/or any available photographs or video is the best resource for developing an understanding of the system operation.

David A. Danaher, PE, 6070 Greenwood Plaza Blvd., Suite 200, Greenwood Village, CO 80111; 303-733-1902; ddanaher@kineticorp.com

Identifying Failure

Identifying the point of failure or injury during operation of a mechanical system begins with reviewing six possible sources of mechanical failure: system design, construction/installation, maintenance, operator actions, modifications, and passive safety (such as safety guards, warnings, and labels).

System Design: The original design of a system can be analyzed through review of provided technical drawings, proposals, or requests for bids for construction and statements or testimony from the manufacturer, architects, or engineers involved with the design of the mechanical system. There are times when the design has not been fully vetted prior to the introduction into the public, and a failure due to design can occur. However, most designs are thoroughly reviewed and tested prior to distribution with factors of safety incorporated into the system for their intended use. Therefore, it is important to review the original design intents of the system or its components, as this can aid the engineer in determining possible failure modes in the system.

Construction/Installation: Mechanical system construction or installation is a potential source of failure and/or injury. Improper installation or construction can introduce unintended failure points that were not part of the initial design or intent. Review of "as-built" drawings, if available, and comparison with photographs of the system at the time of failure can provide insight as to whether the installation or construction meets the requirements of the system manufacturer — or if there are any deviations from original design that may introduce issues in the system that result in failure or injury.

Maintenance: System maintenance should be considered and reviewed for its adherence to manufacturers' specifications or service intervals, along with the actual maintenance performed. Determine if maintenance was conducted properly with the correct components or with the appropriate repairs. Deferred or incorrectly performed maintenance is an obvious point at which problems can begin for a complicated mechanical system, such as ignoring a low oil pressure warning light on a vehicle's dashboard until the engine seizes due to lack of lubrication.

Operator Actions: Most mechanical systems require human interaction at some point in the processes for proper function, or, at a minimum, require oversight and analysis of system conditions during operation. Identifying the locations and functions of each operator associated with the system is important to defining the normal operation of the system, since the points at which operators or monitors are present can often be keys to determining where the process began to go wrong during a failure or injury incident. Much like the pilot of a plane, at times, the most vital cog in a mechanical process is the person interacting with the system.

Modifications: There are times when the design and construction or installation was done properly but was modified at some point during operation. Sometimes, the operator may bypass a safety feature for convenience, the parts for replacement were not available, and the system was changed to accommodate continued operation. The demands of the system or equipment may change from the original intent, resulting in overexerting the design and failure. Modifications can be determined by understanding the original intended operation or design and comparing it to the operation or design at the time of the failure.

Passive Safety: The design or operation of a mechanical system, at times, may pose certain hazards to operators or the public due to the utility of the system. Controlling operator exposures to hazards can be achieved using a safety hierarchy. The safety hierarchy has been expressed in several ways by various authors and governing bodies; however, the main ideal is the same: design, guard, and warn. One example of this principle is from the National Institute for Occupational Safety and Health (NIOSH).

NIOSH focuses on controlling the exposure to occupational hazards to implement feasible and effective control solutions. NIOSH outlines a hierarchy of controls that rates the most effective solution to the least effective[1]. The following outlines the NIOSH Hierarchy of Controls:

1. Elimination — Physically remove the hazard.
2. Substitution — Replace the hazard.
3. Engineering Controls — Isolate people from the hazard.
4. Administrative Controls — Change the way people work.
5. PPE — Protect the worker with personal protective equipment.

In *Safety and Health for Engineers*, Brauer lists a set of priorities that is helpful in selecting controls for hazards

that some call the "Design Order of Precedence" as[2]:

1. Eliminate the hazard.
2. Reduce the hazard level.
3. Provide safety devices.
4. Provide warnings.
5. Provide safety procedures (and protective equipment).

Manuele, in *On the Practice of Safety,* cites the hierarchy of controls from ANSI/ASSE Z590.3, the Prevention through Design standard[3]. The standard outlines the following as:

1. Eliminate hazards and risks through system design and redesign.
2. Reduce risks by substituting less hazardous methods or materials.
3. Incorporate safety devices (fix guards, interlocks).
4. Provide warning systems.
5. Apply administrative controls (work methods, training, etc.).
6. Provide personal protective equipment.

The above provides a general outline to the safety hierarchy; however, there are more specific standards for differing types of equipment, such as ANSI B11.19 (Performance Criteria for Safeguarding), ANSI B11.0 (Safety of Machinery-General Requirements and Risk Assessment), ANSI Z244.1 (Control of Hazardous Energy: Lockout), and ANSI Z10 (Occupational Health & Safety Management Systems) to list a few.

During the design process, any potential hazards should be eliminated through design revisions. However, there are times when the hazard cannot be removed without taking away the utility of the machine/process or introducing unintended consequences. When the potential hazard cannot be eliminated, the manufacturer should guard against it with physical devices and/or electric switches. Many exposed hazards, such as rotating machinery or pinch points, can be physically guarded to prevent inadvertent interaction from an operator. If access is needed into the guarded area, a movable guard equipped with electrical interlocks can be installed to assure that the guard is in place before the machine is operated. As a next layer of protection from a hazard, warnings, labels, training, and procedures should be used to inform the operator of the potential for injury and the steps to prevent hazards from occurring.

While analyzing the failure, review the potential hazards, warnings, and procedures to determine relevance to the incident and adherence by the operator. At times, the guards designed by the manufacturer are circumvented by the operator or owner of the machine, or the warnings are ignored. The owner of the machine is typically responsible for the equipment maintenance and complying with the manufacturer's recommendations on the proper use and operation of the machine. At other times, the guards and warnings are not present, and the user unknowingly places him or herself in harm's way.

Operation at the Time of the Failure

After a failure has occurred, there can be catastrophic damage system-wide that complicates finding the source of the failure. Therefore, the first step in the analysis is to focus on what took place right before the failure occurred to assist in narrowing down the root cause. Compare the conditions of the system and the personnel leading up to the failure. There are three main areas to focus on: recent maintenance, operation parameters, and operators/personnel.

Recent Maintenance or Repairs: Starting from the time of the failure, review any recent maintenance that was performed or any changes in process that may have occurred just prior to the failure. Work backward in time by reviewing the history of the maintenance or repairs, and determine if there is a pattern or reoccurring issue that caused or contributed to the ultimate failure. If there is a reoccurring issue presented in the maintenance records, the cause could be due to the parts installed, the original construction/installation, or the repairs performed. It may be found that the maintenance or repair was proper; however, the application of that part or system was undersized or under-designed to accommodate the requirements of the system.

Operation Parameters: This leads to the next phase of evaluating the failure — the controls and operating conditions of the system at the time of the failure. Review any reports, statements, recorded data, and/or video that may show what the operating conditions of the system were at

the time of the incident. Compare the operating temperatures, pressures, speeds, and sequences to that of normal operation. If any of the parameters differ from that of normal operation, determine if they contributed to or caused the ultimate failure.

Operators and Personnel: The operators may have also contributed to the incident. A procedure or step in the process may have been omitted for the sake of time, apathy, or miscommunication. The operator may be required to perform a safety check that was skipped or did not notice warnings presented. Additionally, an inexperienced or inadequately trained operator may not understand the proper and safe operation of the machine. Review of the operator's training records may be helpful in determining whether the operator had proper training prior to the incident.

Sometimes, the cause of the incident or failure can be a combination of the above that occurred in the right sequence to lead to an unstable condition. For example, the replaced part was in the process of failing; however, the monitoring systems showed a drop in pressure or reduction in speed that was missed, ignored, or misinterpreted. The problem persists and is allowed to continue until the ultimate failure occurs.

Case Study

To help illustrate the analysis procedure, the following case study outlines a failure of a boiler system. It does not incorporate every aspect of potential failure sources in a mechanical system, but it does encompass many of the areas associated with a catastrophic failure. It discusses the events leading up to the failure, but, more importantly, the time line and analysis are explained with the use of graphics. Unfortunately, dynamic animations of the operation of the system cannot be included due to the limitations of a static paper.

The incident, which occurred in April 2017, involved a storage tank that stored steam condensate, which was used in a commercial manufacturing process. The tank measured 30 inches in diameter and 17.5 feet tall and weighed approximately 2,000 pounds. At the time of the incident, the tank contained approximately 510 gallons of condensed steam at a temperature of 330°F and pressure of 100 psig[1]. The tank, which is referred to as a "semi-closed receiver" or SCR, received surplus steam from the plant, and allowed additional hot water makeup from an external reservoir with a vent to the environment. **Figure 1** shows an exemplar tank highlighted with a yellow circle.

Figure 1
Exemplar SCR highlighted by the yellow circle (photograph taken by Kineticorp).

At the time of the incident, the bottom cap of the tank failed, allowing the pressurized water in it to flash instantly into steam. The volume of steam produced was approximately 75 times that of the water volume of the tank[4]. The amount of energy instantaneously released was equivalent to 350 pounds of TNT, which was mainly directed in rocketing the tank through the roof of the building and propelling it 425 feet into the air. The tank traveled in a parabolic trajectory for more than 10 seconds and landed 520 feet laterally away from its original location at a speed of approximately 120 mph at impact[4]. The tank crashed through the roof of a neighboring commercial building and fatally injured three individuals. **Figure 2** shows the final resting location of the SCR tank in the commercial building.

System Design: The system is semi-closed, which means that some of the steam (energy) is lost due to use by the machines in the plant and environment. The steam

Figure 2
Resting location of the SCR tank through the roof of the commercial building[4].

is produced by heating water in a steam generator, which is powered by natural gas, and then fed into a separator. The steam to the plant operates at 175 psi and 375°F. The separator splits the steam into dry steam, which feeds the machines in the plant, and wet condensate, which is fed back into the top of the SCR tank. In order to recoup energy in the system, the SCR tank also receives excess steam from the plant, which is fed into the top of the SCR. The SCR tank stores the condensed steam at 100 psi and 330°F, and feeds the steam generator during operation, creating a loop.

Due to various inefficiencies (such as venting when the pressure is too high or leaks present in the system), the process loses steam. When a sufficient loss of water occurs — and the level in the SCR tank drops below a specified limit — an atmospheric temperature-controlled makeup tank (labeled a Hotwell) feeds heated water into the top of the SCR. The makeup water supplied to the SCR tank is filtered and treated to reduce impurities and maintain a proper pH balance. **Figure 3** shows a diagram of the steam generating process with annotations by the author showing the flow direction of the steam. This sketch was created as an early step of system understanding and documentation.

SCR Tank Design: The entirety of the SCR tank was constructed of SA-516-70 carbon steel and designed to meet ASME Section VIII Div. 1 recommendations of Construction of Pressure Vessels[5]. The SCR was inspected and registered with the National Board of Boiler and Pressure Vessel Inspectors (NBBI) in February of 1997[4].

The SCR tank is vertically mounted and capped at both ends with an ellipsoidal steel dome. The bottom of the tank is fitted with a steel skirt that allows the tank to rest level on the ground and room for a drain at the bottom of the tank. According to provided plant operations procedures, the tank was drained weekly to remove any sediment or contaminants that accumulated during use.

At the upper portion of the tank are two spargers that receive condensed steam from the boiler and recovered steam from the plant. The bottom portion of the tank has an outlet to the boiler and a drain mounted to the very bottom of the ellipsoidal dome. **Figure 4** shows the SCR labeled with the respective components and a shadow outline of an average male adult for scale.

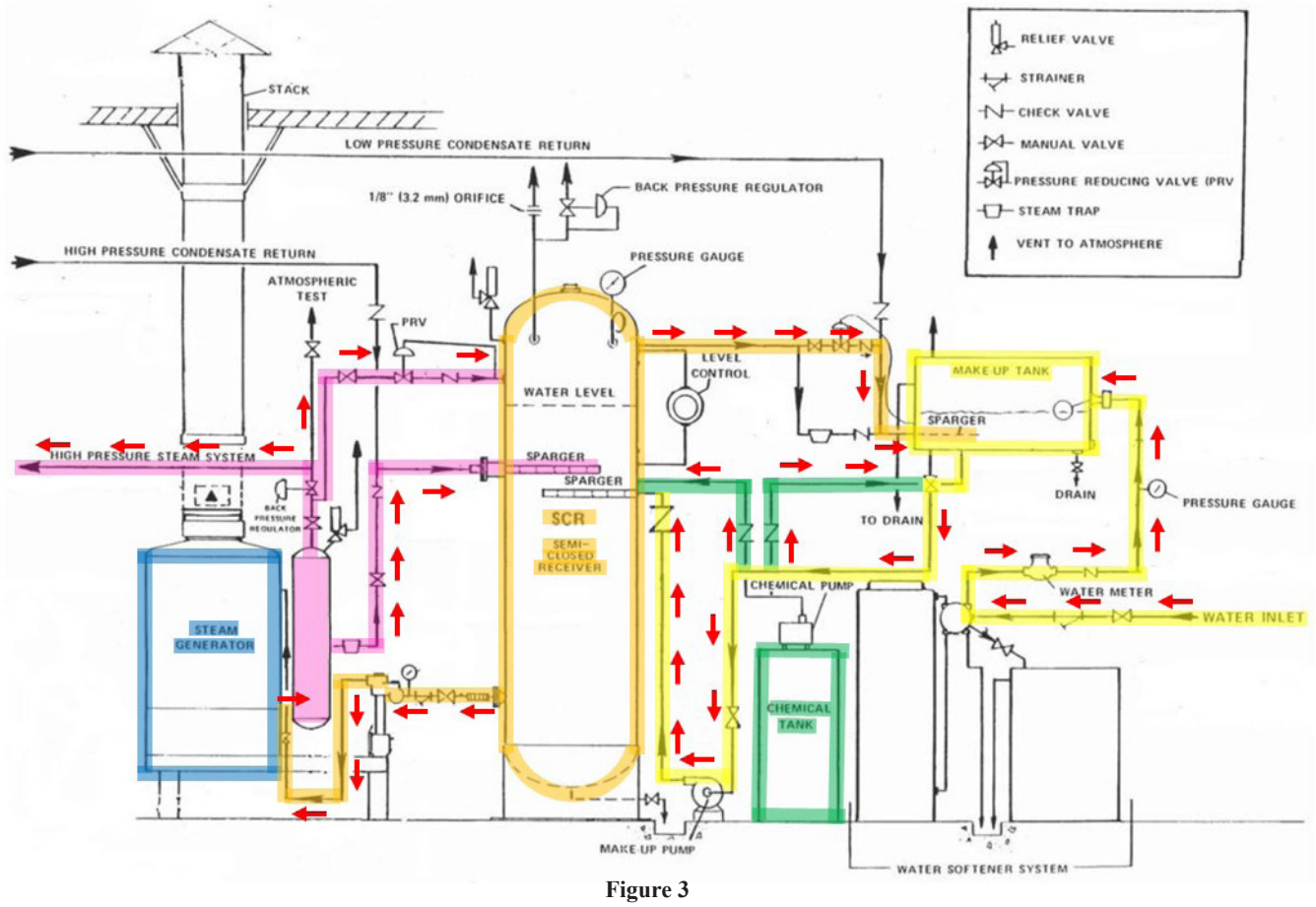

Figure 3
Schematic of the steam generation process, showing direction of flow highlighted by the author.

Repair and Maintenance: In 2012, plant maintenance engineers noticed a leak originating from under the skirt of the SCR tank. They preliminarily inspected the source of the leak by cutting a small access hole in the side of the skirt and determined that the source of the leak was originating from the bottom of the tank. The engineers then contacted an independent engineering company to perform the repairs in the SCR tank.

Inspection of the inside of the tank showed that the lower ellipsoidal dome became pitted and had the appearance similar to the "surface of the moon"[4]. It was decided that the bottom of the head should be sectioned off and repaired. The location of the cut was made at the welded union between the skirt and the side of the tank for ease of repair. The lower section of the skirt (as well as the bottom) were removed. See **Figure 5** for location of the cut on the skirt and the bottom cap.

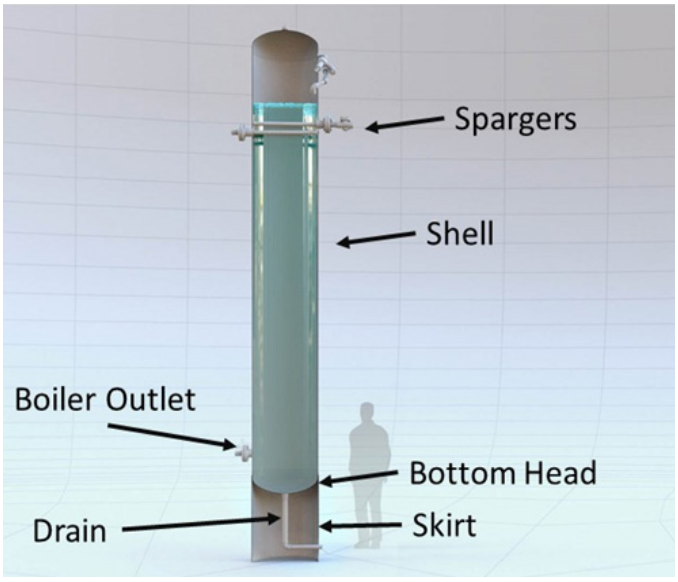

Figure 4
SCR with labeled components with a shaded outline of an average adult male (image produced by Kineticorp).

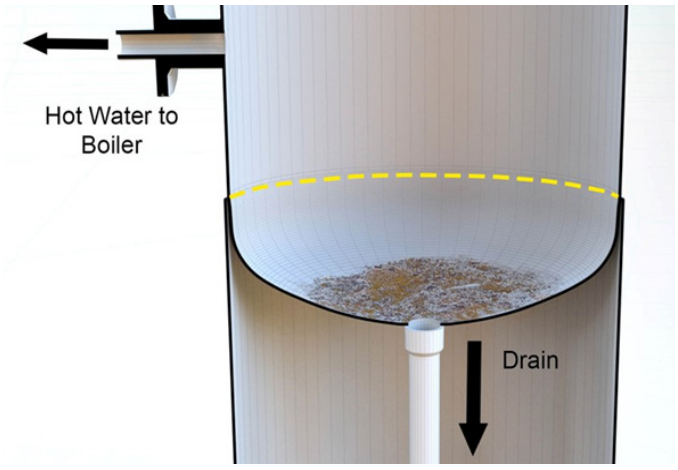

Figure 5
The yellow line shows where the skirt was cut to access the bottom cap (image produced by Kineticorp).

After removing the skirt, a 24-inch-diameter circular section was cut and removed from the center of the bottom cap and replaced with a new steel piece to act as a patch. After the removal of the 24-inch diameter section, 6 inches remained of the original bottom cap. **Figure 6** shows the 24-inch-diameter section removed with 6 inches of the original bottom cap remaining.

The new patch was then welded to the remaining 6-inch ring from the original ellipsoidal cap, and a hole was cut in the patch where the drain was then welded in place. The repaired bottom cap and the skirt were then reattached to the tank of the SCR using a 1-inch-wide and 0.25-inch-thick backing ring behind the weld. **Figure 7** shows the backing ring, 6-inch ring, and patch after the repair.

The repair company followed up 25 days later with a proposal to fabricate and replace the entire lower 4 feet of the tank, including the bottom cap with a new 2:1 elliptical design. The material used would also be 50 percent thicker to allow for corrosion. The 4-foot tank bottom replacement never occurred[4].

Failure: Four and half years after the repair was performed, the plant engineer again noticed a leak originating from the bottom of SCR tank on March 31, 2017. Using the access hole cut in the skirt in 2012, the plant engineer took a picture of the bottom cap of the SCR tank to

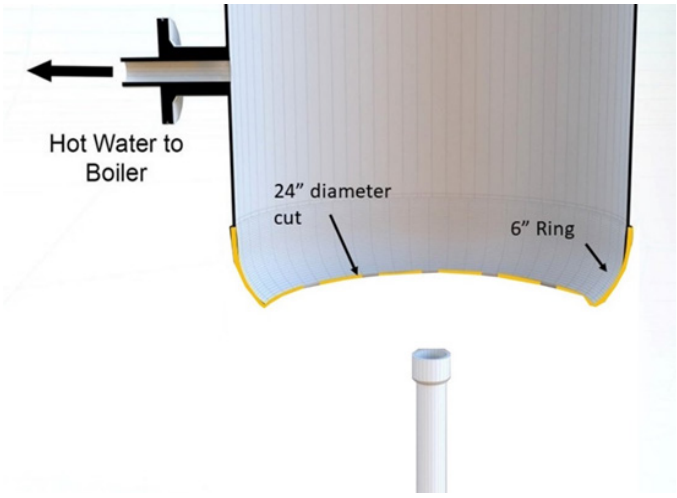

Figure 6
24-inch diameter section removed from bottom cap with the original 6-inch ring of cap remaining (image produced by Kineticorp).

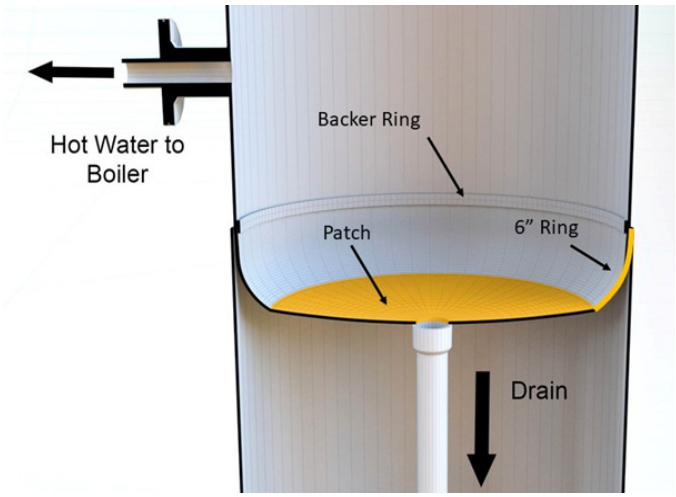

Figure 7
Backer ring, 6-inch ring and repair patch (image produced by Kineticorp).

document the leak. **Figure 8** is the photo taken by the plant engineer showing the leak. In the photograph, the seam can be seen where the 24-inch-diameter patch was welded to the original 6-inch bottom cap. The image shows two locations where the wet and rusted paths originated from the seam where the patch was welded to the bottom cap.

The system was shut down, and the repair company was contacted to come out and perform repairs the following afternoon on April 3. That morning, the steam generation system was started up, and the catastrophic failure occurred at the end of the startup process — three days after the initial leak was first found.

Analysis of the Failure: The cause of the mechanical failure can be attributed to several issues present in the tank. The Chemical Safety Board (CSB) investigated the incident and found that "the vessel failed due to corrosion of the 6-inch ring of the original bottom head, resulting in the circumferential split of the ring and subsequent separation of the entire tank circle from the SCR."[4] The CSB found the original 6-inch ring that was left in place during the repair was heavily corroded, and the reduced thickness of the material provided an inherent circumferential weakness that allowed the patch to separate from the tank.

Figure 8
Picture taken by the plant engineer showing the leak from the bottom cap of the SCR.

Inspection of the bottom cap shows that the separation occurred above the weld and originated on the 6-inch ring. **Figure 9** shows the repaired bottom cap with the 24-inch patch after the failure with labels showing the patch, weld, and original 6-inch ring. An image from the CSB report, **Figure 10** shows the steel shell (patch), which was clean, and the original 6-inch ring, which was heavily corroded.

The thickness of the 6-inch ring at the time the SCR

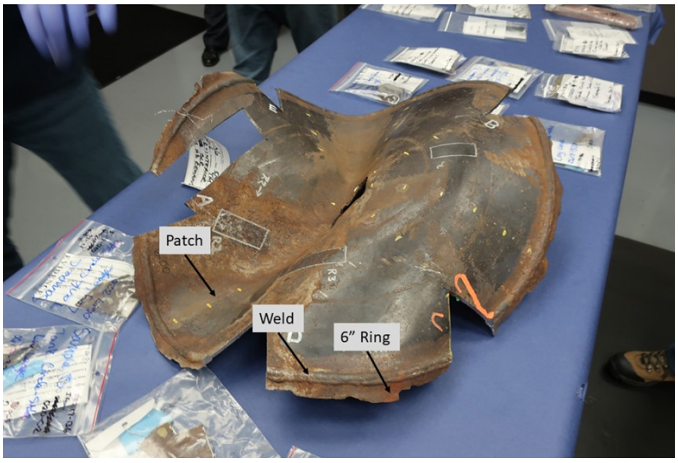

Figure 9
Repaired bottom cap with the 24-inch patch after the failure (photograph taken by Kineticorp).

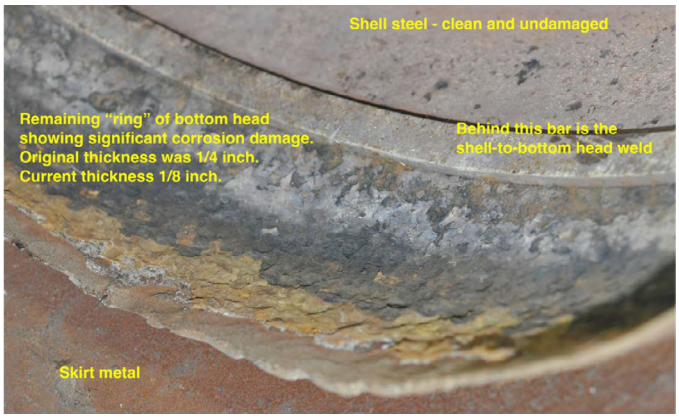

Figure 10
An image from the CSB report showing the corrosion of the 6-inch ring.

tank was manufactured was ¼ inch. After the failure, the thickness of the 6-inch ring was measured at $^1/_8$ inch, a reduction in material of $^1/_8$ inch. To better visualize the reduction of thickness, **Figure 11** shows a cross-section of the skirt, the original 6-inch bottom cap, and the backing plate.

Although the reduction in the thickness due to corrosion of the original 6-inch bottom cap was the ultimate cause of the failure, the shape and design of the 24-inch patch also played a role. When the patch was installed, the size was sufficient to cover the removed bottom section; however, the shape did not match the original ellipsoidal profile. **Figure 12** shows the shape of the bottom cap with the repaired patch piece compared to the original bottom cap. As can be seen in **Figure 13**, the patch piece is much flatter compared to the original ellipsoidal-shaped bottom cap with the maximum deviation of 2.4 inches measured at the apex.

The ellipsoidal bottom cap is also called a 2:1 ellipsoidal head due to the relationship of the height of the head relative to the diameter (D), where the distance to the top of the head is a quarter of the diameter (d = 0.25D). The standards and codes related to pressure vessels are prescribed by the American Society of Mechanical Engineers (ASME). The design of the ellipsoidal head is outlined by ASME in paragraph UG-32 Code Section VIII, Division 1[5]. The height to the center of the cap in the original bottom cap measured approximately 6.8 inches while the new patch height measured 4.4 inches. The difference in height changes the distribution of the forces along the surface of the bottom cap, which, in turn, increases the stress. The combination of the reduced wall thickness and the increased stress results in an accelerated failure.

The repair to the head of the pressure vessel changed the shape. The original certified shape was a 2:1 ellipsoidal. After the repair, the shape of the head became torispherical. A torispherical surface is obtained from the intersection of a spherical cap with a torus tangent. The radius of the sphere is called the crown radius, and the radius of the torus is called the knuckle radius. The torispherical shape of the head of the pressure vessel increased the stress and reduced the safe operating pressure. **Equation 1** below is the calculation for the max allowable internal pressure of a 2:1 ellipsoidal head[6], and **Equation 2** is the calculation for the max allowable internal pressure in a torispherical head[6].

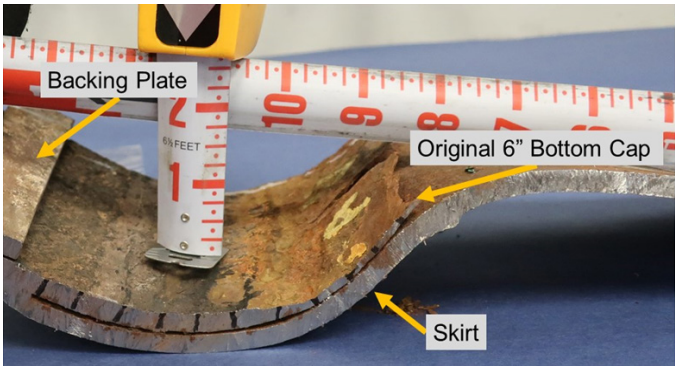

Figure 11
Cross-section of the skirt, the original 6-inch bottom cap, and the backing plate (image taken by Kineticorp).

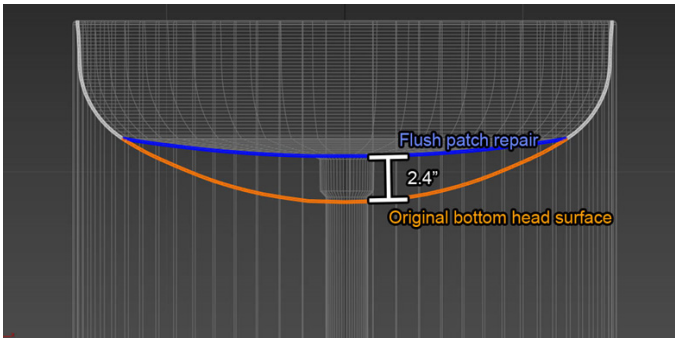

Figure 12
Comparison of the flat patch piece to the original ellipsoidal bottom cap (image produced by Kineticorp).

$$p = \frac{2SEt}{KD_0 - 2t(K-0.1)} \quad \text{Equation 1}$$

Where: p = pressure in psi
S = allowed stress in psi
E = efficiency
t = wall thickness in inches
K = factor (K=1 for 2:1 ellipsoidal heads)
D_0 = outside diameter in inches

$$p = \frac{2SEt}{ML - t(M-0.2)} \quad \text{Equation 2}$$

Where: p = pressure in psi
S = allowed stress in psi
E = efficiency
t = wall thickness in inches
M = factor, $M = \frac{1}{4}\left(3 + \sqrt{\frac{L}{r_k}}\right)$
L = crown radius in inches
r_k = knuckle radius in inches

When comparing the maximum pressure allowed with the two formulas in **Equation 1** and **Equation 2**, the maximum pressure is reduced 78% from changing the head from an ellipsoidal to a torispherical shape. The change in the geometry of the head at the time of the repair was a contributing factor in the cause of the failure.

The failure of not replacing the temporary bottom cap with the properly designed ellipsoidal cap was a significant factor in the ultimate cause of the failure. Additionally, the procedural failure of not initiating a lockout/tagout of the system — and allowing the boiler to be restarted after the additional leak was identified — also contributed to the failure.

Case Summary: The above case study was one example of a mechanical failure that led to a catastrophic failure. The full details of the events leading up to the incident, the research performed to determine the normal operation of the boiler system, and the events leading to the failure (as well as the analysis performed) are too great for the scope of this paper. The point of the case study was to show all the various entities and parties involved that led to the ultimate failure.

What the case study shows is that although the ultimate failure was sudden and spectacular, the events leading up to the event took place over a long period of time. A problem with the tank was recognized early on, and the repair to the bottom cap was insufficient. However, when a proper repair proposal was submitted to the plant, it was ignored. Even with the insufficient repair, the SCR tank stayed in operation for another 4.5 years before another problem occurred. When the final leak was found, the system was shut down, and a request was made for repairs. However, the boiler was started back up in the morning before the repair could be made. There were multiple signs of problems along the road to the ultimate failure — had any of them been properly addressed, the sudden rupture of the tank may not have occurred.

Presentation

Once an understanding of the system operation has been developed, articulating its basic design and function to others is the next challenge. Presentation of mechanical systems analysis to the layperson is a complicated undertaking, as the system is often technical and involves physics, thermodynamics, or statics to perform a function or output a final product.

Boiling down the system operations and components into a basic flow chart is the first step toward producing a system diagram that outlines the main components, functions, and operators (if required) for normal operation of the mechanical system. Utilizing simplified models of the components of a system in visual form helps relate the models to their real-life counterparts seen in photographs or video of the system. Simple 3D models of components in the system can be placed into an environment where the flow chart of system functionality can be presented from various angles or perspectives, allowing the presenter to show different segments of the system dynamically. **Figure 13** shows the boiler system from the above case study, along with the simplified 3D model of the system.

As shown in **Figure 13**, the steam generator, semi-closed receiver, makeup tank, and associated piping are all present in the 3D model with similar sizes and shapes as the actual components. However, the wire frame model is easier to digest for viewers (with color coding of components and labels for clarity and identification).

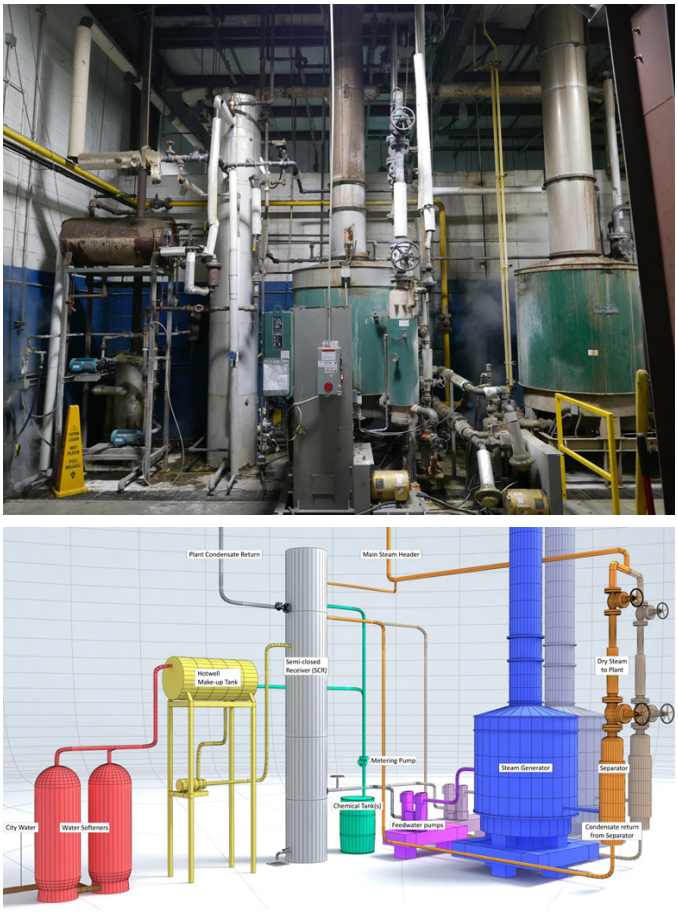

Figure 13
3D model flow (image produced by Kineticorp)
with comparison photograph (taken by Kineticorp).

The 3D model animation style has additional benefits, such as being able to isolate sections of the system for further detailed visualization. In the case of the example, the semi-closed receiver is of particular interest. In the 3D model, the section of the system encompassing the semi-closed receiver and its associated components in the system processing sequence can be isolated and shown with additional information, as shown in **Figure 14**.

In addition to isolating sections of the system, alternate camera perspectives can be applied to the same 3D models to illustrate other functional components or features — in this case, the blow-down process for the semi-closed receiver. As shown in **Figure 15**, the initial camera position showing the entire 3D model of the system can rotate and focus in on the bottom of the SCR tank to show the drain out the bottom of the tank and through the tank skirt, along with the blow-down valve for draining the tank.

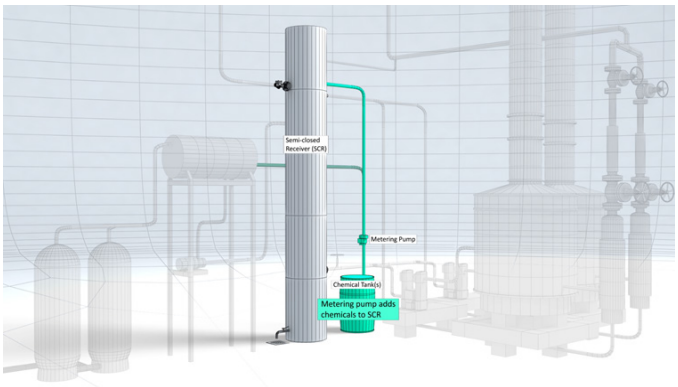

Figure 14
3D model isolating SCR and chemical tanks
(image produced by Kineticorp).

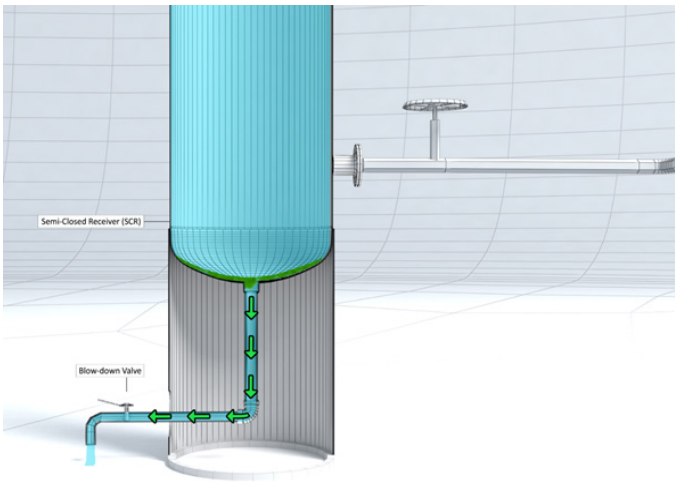

Figure 15
Secondary camera perspective of 3D model
(image produced by Kineticorp).

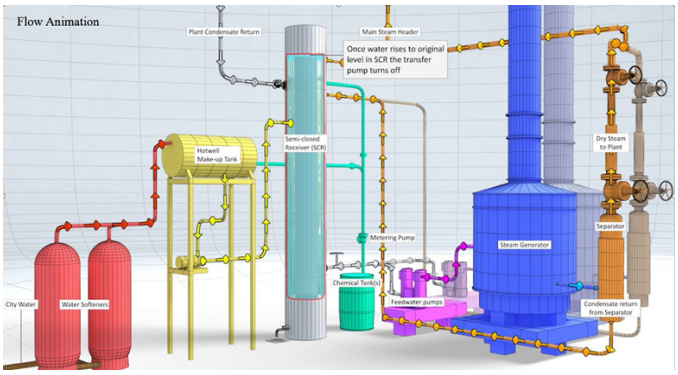

Figure 16
Graphic showing the direction of flow with
equipment labeled (image produced by Kineticorp).

In the animation that the image is taken from, the arrows move to show fluid flow in the drain piping, and the water level and sediment (green) inside the SCR tank flow out through the drain valve as the animation progresses. The ability to articulate flow visually with animations offers a more easily understood explanation of system functionality to the end viewer than just still images or diagrams. **Figure 16** shows the system in operation with arrows, depicting the direction of flow and labels for the corresponding equipment.

Conclusion

The takeaway of this paper is that when you are first presented with a mechanical failure, there is a process to follow to determine the cause of the incident. The first step is to understand how the system or design was intended to operate and then determine the cause of the failure by looking at the six possible sources of failure: system design, construction/installation, maintenance, operator actions, modifications, and safety guards, warnings, and labels.

Once an understanding of how the system operates and the cause of the failure are determined, the next step is conveying that understanding to others. This last step cannot be overlooked: Conveying your understanding of the system to others is really the main purpose of the investigation. It does not matter how much you understand; it matters what your audience understands. Presenting your findings clearly with graphics and animations is an essential part of showing your knowledge of the system and ultimate failure to others who have little concept of what any of these mechanical systems do. Ultimately, these large mechanical system failures reduce to a few core issues that can be explained and shown simply in visual form.

References

1. NIOSH, website: https://www.cdc.gov/niosh/topics/hierarchy/default.html, Centers for Disease Control and Prevention, CDC, Washington DC, 2021.

2. R. Brauer, Ph.D., P.E., *Safety and Health for Engineers*, Second Edition, Hoboken, New Jersey: John Wiley & Sons, Inc., 2006.

3. F. Manuele, *On the Practice of Safety*, Fourth Edition, Hoboken, New Jersey: John Wiley & Sons, Inc., 2013.

4. Chemical Safety and Hazard Investigation Board, "Factual Investigation Update, Catastrophic Pressure Vessel Failure,": Washington DC, CSB Chemical Safety and Hazard Investigation Board, 2018.

5. American Society of Mechanical Engineers, Boiler and Pressure Vessel Committee, VIII Rules for Construction of Pressure Vessels, Division 1, New York: American Society of Mechanical Engineers, 2017.

6. P. Michael R. Lindeburg, *Mechanical Engineering Reference Manual for the PE Exam,* 13th Edition, Belmont: Professional Publications Inc, 2013.

Forensic Engineering Research and Testing of Building Copper Tube Water Piping System Freeze Failures

By Joseph G. Leane, PE, DFE (NAFE 524F)

Abstract

Forensic engineers investigating water loss incidents, caused by water leaking from damaged copper tube piping systems inside buildings, are tasked with determining if that damage is from the piping being exposed to subfreezing temperatures or some other cause. This paper provides guidance for such investigations and factual basis for such opinions, including presenting the results of experimental testing of water-filled copper tube piping systems exposed to subfreezing conditions. It also discusses piping standards and building codes. When ice forms a solid plug inside a pipe, the portion of the piping downstream of that plug becomes isolated. As the ice plug grows, the pressure in the isolated portion of the piping system increases dramatically from hydraulic pressure until the strength of the "weak link" is exceeded, which causes a rupture that relieves the pressure. Oftentimes, no significant water flows through the rupture at that time because the ice plug prevents water flow through the pipe. However, significant water flow occurs once the plug melts. This paper demonstrates why it is critically important for forensic engineers to understand this sequence of events.

Keywords

Water, freeze, ice, copper tube, pressure, rupture, damage, forensic engineering, testing, freeze failure, piping, plumbing

Introduction and Background

For forensic engineers to be permitted to testify in federal court on their opinions in a particular matter, their work is required to comply with Federal Rules of Evidence, Rule 702[1]. That rule requires that an expert witness' "testimony is based on sufficient facts or data." This paper provides facts and data for an expert to rely on when investigating a water damage incident involving copper tube plumbing systems.

The cost of frozen pipe water damage incidents is significant. In fact, approximately 250,000 buildings are damaged by frozen pipes every year. Other estimates indicate the average cost per incident is $15,000[2]. This data suggests the annual cost is on the order of $3.75 billion. The following hypothetical case study illustrates the various issues a forensic engineer may encounter when investigating a potential pipe freeze incident.

Case Study

A forensic engineer, retained to investigate a water damage incident to a single-family home, inspected the building and discovered a rupture in a length of copper tube water line. The water line extended from the basement upward through an exterior wall and horizontally through a second-floor joist space to a second-floor bathroom. The rupture was located in the horizontal tube 10 feet from the exterior wall. The engineer documented the outdoor temperature was well below freezing for days immediately before the date the water damage incident was discovered, and rose above freezing on the day of the incident. The engineer also documented the heating system inside the house was set low (but above freezing) during that time. The engineer concluded the temperature inside the house dropped below freezing, and the copper tube water line froze and burst, permitting a large volume of water to flow through the rupture and cause extensive water damage inside the house.

The forensic engineer was subsequently asked two questions by an attorney representing an adverse party during a deposition: 1) If the tube burst from freezing,

Joseph G. Leane, PE, 1144 Ensell Road, Lake Zurich, IL 60047, leane@hkleng.com

why didn't the burst occur inside the exterior wall where it would have been first exposed to subfreezing temperatures and froze? 2) What caused the tube to burst 10 feet inboard of the exterior wall where it was surrounded by the warmer temperatures? This paper provides experimental test data that answers those questions.

Codes and Standards

A brief discussion of some codes and standards forensic engineers should be aware of when conducting this type of water damage incident follows. Building codes contain requirements for water service and distribution systems. For example, the International Residential Code (IRC) states the maximum allowable pressure for residential water piping systems is 80 p.s.i., and pressure-reducing valves are required when the pressure exceeds that number[3]. Thermal expansion control and water hammer arrestors may also be required. The IRC also specifies the allowable types of copper tube for water distribution systems are types K, L, and M[4]. The International Property Maintenance Code (IPMC) requires hot water to be supplied at a minimum temperature of 110ºF[5].

Requirements for components of copper tube water systems are contained in the following standards. These requirements include dimensions and tolerances, temperature and pressure ratings, and testing requirements.

- ASME B16.18 Cast Copper Alloy Solder Joint Pressure Fittings[6]
- ASME B16.22 Wrought Copper and Copper Alloy Solder-Joint Pressure Fittings[7]
- ASTM B32 Standard Specification for Solder Metal[8]
- ASTM B88 Standard Specification for Seamless Copper Tube[9]

Copper Tube Specifications

A popular choice for building domestic water and hydronic heating systems, copper tubing was introduced around 1927, and its use grew to include about 90 percent of indoor water piping. Currently, more than 5.7 million miles of copper tubing has been installed in homes and commercial buildings in the United States[10]. Piping systems of other materials include galvanized pipe and plastic pipe (PVC, CPVC, and PEX) to name a few. However, this paper focuses on copper.

A well-known excellent conductor of electricity and heat energy, copper has low thermal resistance (inverse of thermal conductivity) when compared to other piping materials. For comparison purposes, the thermal conductivity of copper is about 10 times the value for steel and more than 2,000 times the value for PVC[11,12,13]. Consequently, water inside copper tube will cool and freeze quickly. Ice plugs will form earlier in a freezing event when compared to other piping materials.

The wall thickness of the allowable types of copper tube for water distribution systems varies by type (for ½ in. tube): Type K = 0.049 in.; Type L = 0.040 in.; and Type M = 0.028 in., which correlates with their rated pressures. **Figure 1** provides basic copper tube specifications, including rated and burst pressures[14]. The rated and burst pressures decrease with increased pipe size. Information printed on the tube is color coded to the Type. Copper tube is available in annealed and drawn products. Since the allowable maximum pressure for residential and light commercial building water supply is 80 p.s.i., the lowest rated pressure for drawn tube is at least 10 times the expected water pressure in a piping system, and the burst pressure is at least 75 times. Straight lengths of pre-cut individual tube are typically drawn but may be annealed. Coiled tube is annealed only. Drawn tube is stiffer and has a greater rated pressure, while annealed tube is more ductile. The use of solder having a lead content greater than 0.2 percent has been banned for potable water systems since 1986.

Pipe Freeze Failure Mechanism

When a water-filled piping system is subjected to subfreezing conditions, portions of the system may freeze when one or more ice plugs form and expand in the piping. Water expands as it freezes to ice, which causes the water pressure in "closed" portions of the system to increase dramatically. If the piping or components have insufficient strength to withstand the pressures they encounter, they will fail at the weakest points and relieve the pressure.

If the pressure can be relieved, then a pipe rupture may be avoided. Accordingly, the practice of opening a faucet to maintain minimal water flow during cold spells permits the pressure in the piping system to dissipate without reaching damaging levels.

Air chambers or air pockets in the piping system may protect the system from freeze failures. The water being displaced by the growing ice plug can partially fill the air space, thereby limiting the pressure rise. However, piping ruptures can occur when the water occupies enough

Type	Color Code	Nominal Size/Dia. (in.)	O.D. (in.)	Wall Thickness (in.)	Rated Pressure (P.S.I.)		Burst Pressure (P.S.I.) @ Room Temperature	
					Annealed	Drawn	Annealed	Drawn
K	Green	½	.625	.049	891 @ 100F 446 @ 400F	1534 @ 100F 1400 @ 400F	4535	9840
		¾	.875	.065	852 @ 100F 426 @ 400F	1466 @ 100F 1338 @ 400F	4200	9300
		1	1.125	.065	655 @ 100F 327 @ 400F	1126 @ 100F 1028 @ 400F	3415	7200
L	Blue	½	.625	.040	722 @ 100F 361 @ 400F	1242 @ 100F 1133 @ 400F	3885	7765
		¾	.875	.045	582 @ 100F 291 @ 400F	1002 @ 100F 914 @ 400F	2935	5900
		1	1.125	.050	494 @ 100F 247 @ 400F	850 @ 100F 776 @ 400F	2650	5115
M	Red	½	.625	.028	494 @ 100F 247 @ 400F	850 @ 100F 776 @ 400F	n/a	6135
		¾	.875	.032	407 @ 100F 204 @ 400F	701 @ 100F 639 @ 400F	n/a	4715
		1	1.125	.035	337 @ 100F 169 @ 400F	701 @ 100F 639 @ 400F	n/a	3865
Source: Copper Tubing Handbook								

Figure 1
Table of copper tube specifications.

volume of the original air space to compress the air to the piping burst pressure.

When a water-filled piping system is exposed to subfreezing conditions, heat energy transfers from the water through the piping wall to the environment, cooling the water to 32°F (0°C). The water in the piping freezes at one or more locations, with an ice plug forming inside the pipe at each location. Copper tube has low thermal resistance when compared to other piping options, so it provides minimal insulating value to resist the heat loss of the water inside the tube.

Ice plugs may form at different locations where the piping system is exposed to subfreezing temperatures in the building, such as in an inadequately insulated exterior wall, floor/crawl space, ceiling/attic, or near an area with air infiltration (e.g., door, window, crack in a wall, or other opening). Portions of the system downstream of the ice plugs become isolated and closed. Increased pressure in the portion of the system upstream of the plug may dissipate backward toward the water source. Ice plugs inside the tube expand longitudinally within the pipe as more water freezes. A 9 percent volumetric expansion of the ice in a closed portion of the piping system causes the water pressure in that section to increase dramatically, creating very high hydraulic pressures.

The pressures increase until the burst pressures of the weakest points in the closed sections are exceeded, causing piping component failures. Ruptures are typically not due to direct contact with ice plugs[15]. There may not be any significant water leakage at the time of rupture because the ice plugs prevent water flow through the pipes. When the piping containing the ice plugs warms above freezing, the ice plugs melt, and water flows through the ruptures, causing water damage.

As the pipe is cooled, the water temperature decreases by several degrees below 32°F, supercooling the water. Supercooling is based on a concept that the ice nucleation temperature is different than the phase change equilibrium temperature[16]. Supercooling may last for an extended period of time, and has been documented in testing to last up to 80 consecutive hours[12]. The metastable (marginally stable) water initiates ice nucleation, and ice crystals begin to form

on the inner surface of the tube wall, growing in the dendritic form[12,13]. Ice nucleation is the point where the phase change begins when water freezes to ice. When ice begins to form, the temperature abruptly increases to the phase change equilibrium temperature and remains there during the freeze process. The noted abrupt increase in temperature is caused by the initiation of the phase transition from water to ice. This process releases energy (latent heat of fusion), which increases the temperature. The latent heat of fusion is the heat energy needed to change the state of a substance from a solid to a liquid. The abrupt temperature increase indicates the point of dendritic ice formation, resembling the branches of a tree (**Figure 2**). Once the water has fully phase changed from water to ice, the temperature then progressively decreases as the ice gets colder.

As water undergoes the phase transition to ice during a freezing process, the density decreases and the volume increases, which is why ice cubes float in a glass of water. When water freezes to ice at 0°C, the densities are 0.9998 g/cm^3 for water and 0.9167 g/cm^3 for ice, revealing the change in volume is 1.091. Likewise, at -10°C, those values are 0.9993 and 0.9196, for a change in volume of 1.087[17]. Accordingly, there is a 9 percent increase in volume when water freezes to ice. **Figure 3** presents this information in tabular form.

An ice structure then grows from the tube wall inward at the phase change temperature until it has formed a plug when all the water in the area has frozen solid. However, the tube typically does not fail at the plug. This condition is the basis of pipe freeze kits used to intentionally freeze sections of pipes (forming ice plugs) to isolate and drain downstream portions of the piping and perform maintenance work[18].

Flash freezing of water (where water instantly freezes to ice) at the pipe rupture location has been documented. This condition is caused by the high system pressure depressing the phase change temperature. Then, when the rupture occurs, the pressure suddenly drops to atmospheric, causing a flash freeze of the water discharging from the opening in the pipe. This phenomenon is explained by the phase diagram for water (**Figure 4**)[19]. The negative slope of the boundary line between the solid and liquid phases is significant because it indicates the freeze temperature decreases as the pressure increases, and vice versa. For example, the phase change temperatures at 14.7 p.s.i. (1 atmosphere) and 14,504 p.s.i. are 32.0°F and 15.8°F, respectively[17].

Figure 2
Photo of dendritic ice formation on needles on a tree.

Temperature	Water Density	Ice Density	ΔV
0°C	0.9998 g/cm^3	0.9167 g/cm^3	0.09
-10°C	0.9993	0.9196	0.09

Figure 3
Table of water and ice densities.

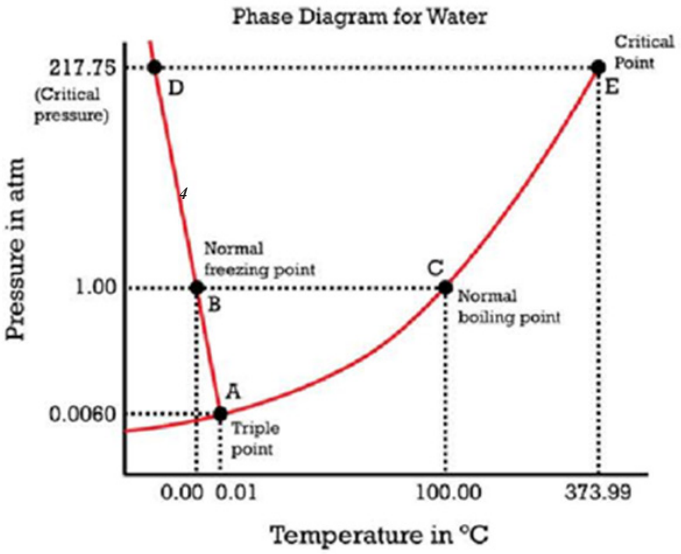

Figure 4
Phase diagram for water.

The pressure that is developed is dependent on the size of the ice plug and the volume of the closed portion of the piping system downstream of that plug. Since water is essentially incompressible, the volume of the water displaced by the ice toward the closed end of the system causes the pressure increase. The increased pressure causes the piping to expand both radially and longitudinally. This increased volume of the piping compensates for some of the ice expansion. However, the piping ruptures when the stress exceeds the ultimate strength of the material.

The length of closed portion of the piping system, downstream of the ice plug, is a key factor in whether a rupture will occur. If the volume of the closed portion of the piping is sufficiently large relative to the size of the ice plug, the burst pressure will not be reached, and the piping will not rupture. A rupture occurs when the change in volume of the fluid exceeds the allowable change in volume of the piping. The critical length of the piping to cause a rupture can be calculated as follows[15].

The change in volume of the fluid is:

$$\Delta V_f = I L_f \frac{d^2 \pi}{4}$$

Where: ΔV_f = the change in fluid volume

I = volume increase from water freezing to ice (9 percent)

L_f = the length of pipe frozen beyond the initial freeze

d = the inside diameter of the pipe

The change in volume of the pipe to cause a rupture is:

$$\Delta V_p = l d^2 \frac{\pi}{4} \left[(1+\sigma_{hoop}/E)^2 (1 + \sigma_{axial}/E) - 1\right]$$

Where: ΔV_p = change in pipe volume

l = length of pipe not frozen beyond the initial freeze plug

σ_{hoop} = hoop stress corresponding to the critical "burst" pressure of the piping

σ_{axial} = axial stress corresponding to the critical "burst" pressure of the piping

E = modulus of elasticity

The critical length is found by solving for L_f when ΔV_p equals ΔV_f at the critical pressure:

$$L_f = \frac{l}{I} \left[(1+\sigma_{hoop}/E)^2 (1+\sigma_{axial}/E) - 1\right]$$

Experiments

Physical experiments were performed in a laboratory on ½-inch nominal diameter copper tube assemblies exposed to subfreezing conditions to:

1. Evaluate downstream pressures generated from ice plugs forming and growing inside a piping system, including the pressures necessary to fail copper tube, copper fittings (elbows and caps), solder joints, push-connect components, and compression components.

2. Determine whether the failures occur at the point of the ice formation (ice plug) where the tube was in direct contact with the ice or in liquid filled closed portions of the system due to increased water pressure from ice plug growth inside the piping.

3. Investigate the process of ice plug formation inside copper tube.

Three experiments were conducted. The first utilized copper tube assemblies connected to a refrigerated galvanized pipe test apparatus where temperatures and water pressures were recorded. The second utilized "U"-shaped copper tube assemblies open at both ends (filled with water and frozen inside the freezer). Only temperatures were recorded. The first and second test apparatuses were generally consistent with test apparatuses utilized in similar water pipe freeze testing[13,15]. The third test utilized a straight section of copper tube extending through a cold chamber. Windows were present on the ends of the tube, and the tube was filled with water. The formation of ice inside the tube was documented, and temperatures were recorded. Distilled water was used during the testing to control variations in the freeze temperature from minerals and impurities in the water. The initial pressure in all tests was atmospheric.

Ice Plug Expansion Pressure Experiment

Tests were performed on a closed piping system of galvanized pipe and copper tube (**Figures 5** and **6**). The test apparatus was in the shape of an inverted "L" of ¾-inch galvanized pipe. Galvanized pipe was used because it had a significantly higher burst pressure than

copper tube to assure any failures occurred within the copper tube system. The piping was carefully filled completely with water to eliminate any air entrapment. A new and calibrated 10,000 p.s.i. pressure transducer (error +/- 0.05 FS) and data logger was located in the branch port of a tee fitting of the galvanized pipe. A ½-inch reducer bushing was threaded into the end of the short leg, and the ½-inch copper tube test assemblies were screwed into the test apparatus there. The vertical leg was insulated with a progressively thicker layer starting with no insulation on the lowermost 6 inches and stepped up thicker layers every 6 inches, progressing toward the top.

The vertical leg was placed inside an electric freezer and projected out the top of the freezer (**Figure 7**). The copper tube assembly was positioned horizontally above the freezer in the room environment, and remained well above freezing during the testing.

This configuration assured an ice plug formed near the bottom of the vertical leg and grew upward, progressively increasing the water pressure above the ice. The pressure within the liquid portion of the system was recorded along with various temperatures. New K-type thermocouples (accuracy +/-2°F) were installed on the lower portion of the galvanized pipe vertical leg where no insulation was present (T1), on the copper tube piping assembly (T2), inside the freezer measuring the air temperature (T3), and

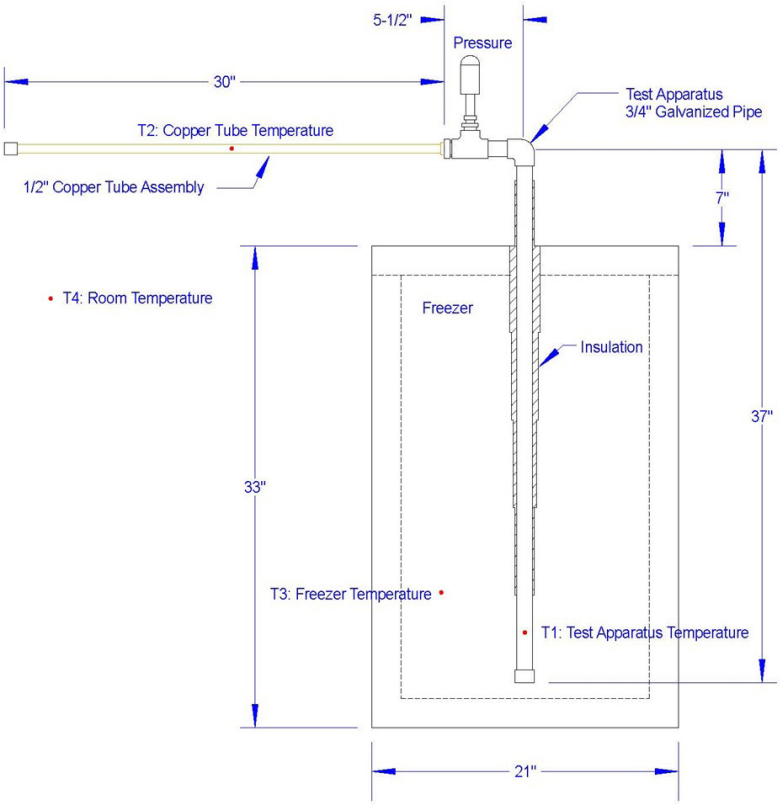

Figure 5
Diagram of ice plug expansion test apparatus.

Figure 6
Photo of the galvanized pipe test apparatus, showing pressure transducer and copper tube test assembly attached. Different configurations of copper tube assemblies were tested. Accordingly, this copper tube assembly is different than the one illustrated in **Figure 5**.

Figure 7
Photo of the test setup, showing test apparatus installed in freezer.

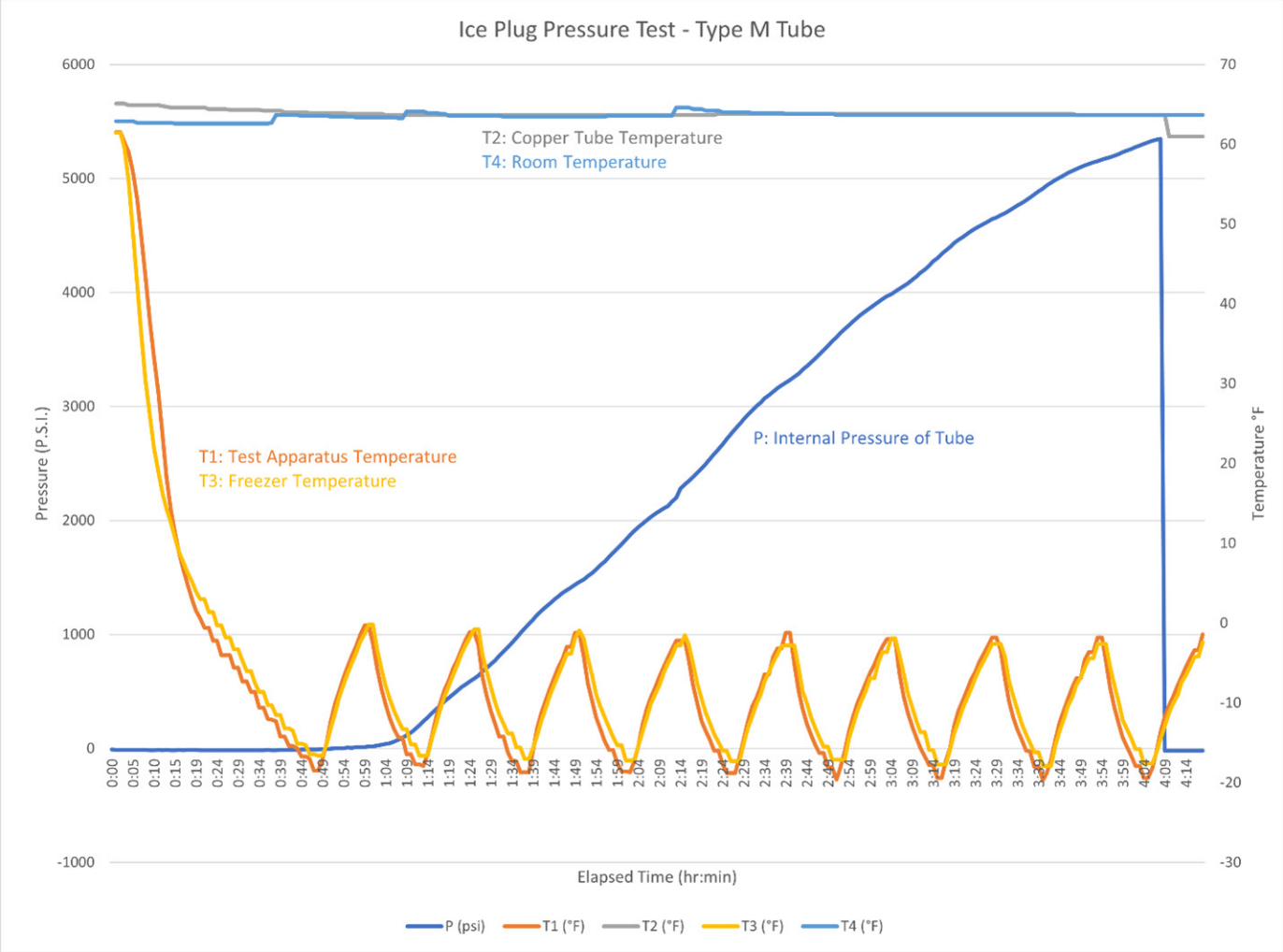

Figure 8
Graph of pressure and temperature data from Type M copper tube test.

measuring the room temperature (T4). The pressure transducer measured the water pressure in the upper portion of the test apparatus, which remained water filled. **Figure 8** illustrates the pressure and temperature data for a test run.

The test apparatus temperature (T1) closely followed the freezer temperature (T3). Likewise, the copper tube temperature (T2) closely followed the room temperature (T4). The pressure began to increase approximately 1 hour into the test and then increased fairly consistently for about 3 hours where it then dropped suddenly back to atmospheric pressure when the tube ruptured. The maximum pressure attained was approximately 5,300 p.s.i.

Group 1 tests: Caps and threaded male adapters were soldered onto straight sections of Type M copper tube. Lead-free silver bearing solid wire solder (complying with ASTM B32) was utilized in all tests. The tube was attached to the test apparatus and carefully filled with distilled water to prevent air pockets. The freezer was then turned on, and the temperatures/pressures were recorded every minute. The copper caps ruptured in "fish-mouth"-type failures at an average pressure of 5,048 p.s.i. (**Figure 9**). Burst pressure readings from different trial runs were within 3 percent of each other. The burst

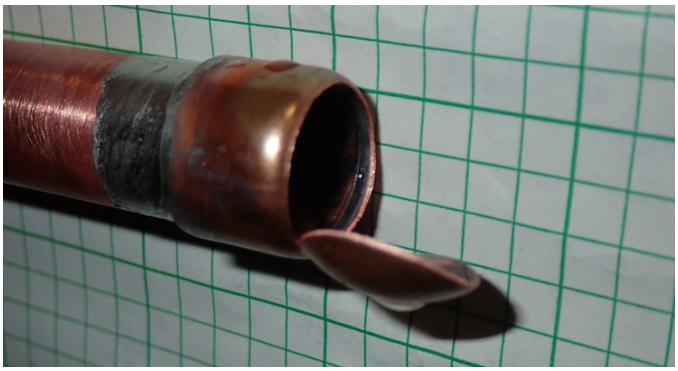

Figure 9
Photo of a "fish-mouth" rupture of copper cap.

pressures may have been lowered when the annealed strength of the material was reduced from the heat of the torch during the soldering process, where the rupture locations were within the heat-affected zones of the fittings.

Group 2 tests: The cap was replaced with a second male adapter and a galvanized cap, permitting higher pressures to be developed inside the tube. The tube was again attached to the test apparatus, filled with water, and the freezer was turned on. The Type M copper tube split longitudinally at an average pressure of 5,373 p.s.i. (**Figure 10**). Burst pressure readings from different trial runs were within 2 percent of each other. The splits generally occurred in the middle of the tube well away from any potentially heat-affected areas at the ends where the adapters had been soldered to the tube.

Group 3 tests: The copper tube configuration was the same as the Group 2 tests except the Type M copper tube was replaced with Type L (greater wall thickness). No failures occurred, and the maximum pressure attained was 7,133 p.s.i. Note: At those high pressures, small, slow drip-type leaks developed in threaded joints in the galvanized pipe assembly, which permitted enough water loss to limit any further pressure increases.

Group 4 tests: "L"-shaped copper tube assemblies with a copper 90° elbow fitting and a capped threaded adapter on the end were attached to the test apparatus. All ruptures occurred at the elbow fittings in longitudinal-type failures at an average pressure of 4,682 p.s.i. (**Figure 11**). Burst pressure readings from different trial runs were within 5 percent of each other.

Group 5 tests: Push-to-connect caps were fully pressed onto the ends of copper tube so there was full engagement. The caps began to drip water at an average pressure of 1,029 p.s.i. (**Figure 12**). Failure pressure readings from different trial runs were within 30 percent of each other. Some movement of the caps on the tube was observed. In later tests, the caps were installed on copper tube and frozen solid (**Figure 13**). During those tests, the metal outer caps were pushed off the tube by the expanding ice. However, the inner plastic components remained on the tube.

Group 6 tests: Compression stop valves were installed onto the ends of the copper tubes, so there was full engagement with the tube. Brass ferrule rings were used in the compression joints. The stop valves were in the closed position during the tests, and the outlet ports of the valves were capped. Drips developed at the valve outlet port caps.

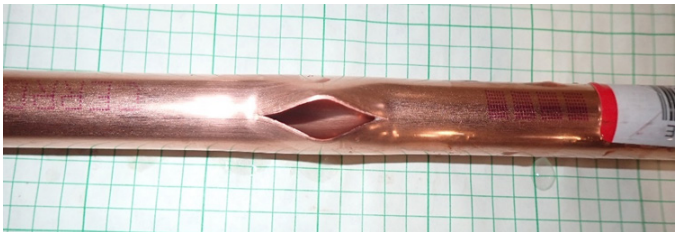

Figure 10
Photo of a longitudinal rupture in Type M copper tube.

Figure 11
Photo of a longitudinal rupture in copper elbow fitting.

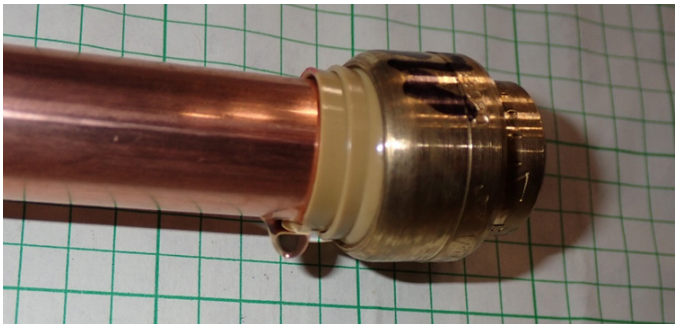

Figure 12
Photo of a push-to-connect cap dislocated on copper tube.

Figure 13
Photo of a push-to-connect cap separated from frozen solid copper tube.

The maximum pressure obtained averaged 1,365 p.s.i. (**Figure 14**). Failure pressure readings from different trial runs were within 26 percent of each other. An audible pop was observed immediately prior to the dripping, suggesting the internal valve mechanisms may have failed. There was no visible movement of the valve on the tube. The stop valve may have been pushed along the tube, including being pushed off by expansion of the ice if all the water in the tube froze.

Figure 15 summarizes the test results in tabular form. At no time did any of the solder joints fail, including exposure to internal pressures exceeding 7,000 p.s.i. Each test was repeated at least once, and the results were compared to evaluate repeatability.

Tube Rupture in Water or Ice Section Experiment

Tests were performed to observe whether the ruptures occurred in areas that were frozen solid at ice plugs or in areas of liquid water trapped in closed sections isolated by the ice plugs. A "U"-shaped copper tube assembly was comprised of three straight tube sections and two elbows (**Figures 16** and **17**). The vertical legs were 14 inches long, and the horizontal leg was 13 inches long. The top ends of the two vertical legs were open, and the middle horizontal leg of the tube was insulated. A thermocouple was installed at the middle of each straight section (T1, T2, and T3), and the freezer air temperature was measured (T4).

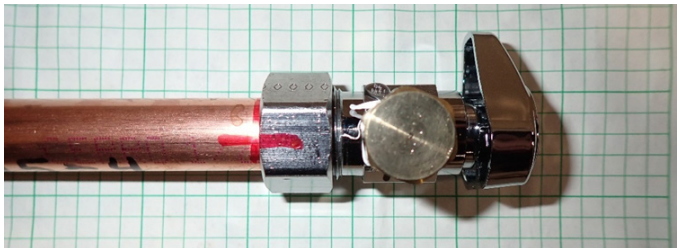

Figure 14
Photo of a compression stop valve installed on copper tube.

The tube was filled with water and placed upright inside the freezer (**Figure 18**). The insulation was utilized to cause the two vertical legs to freeze first, thereby creating a closed section between the two ice plugs. **Figure 19** illustrates the data from a U-shaped tube freeze test.

The temperatures of the three legs of the test U-tube

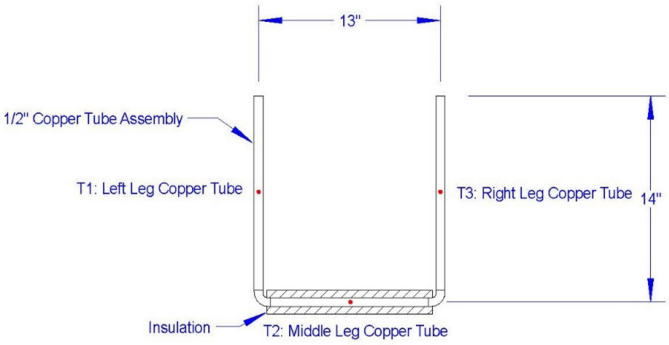

Figure 16
Diagram of U-shaped copper tube rupture location test apparatus.

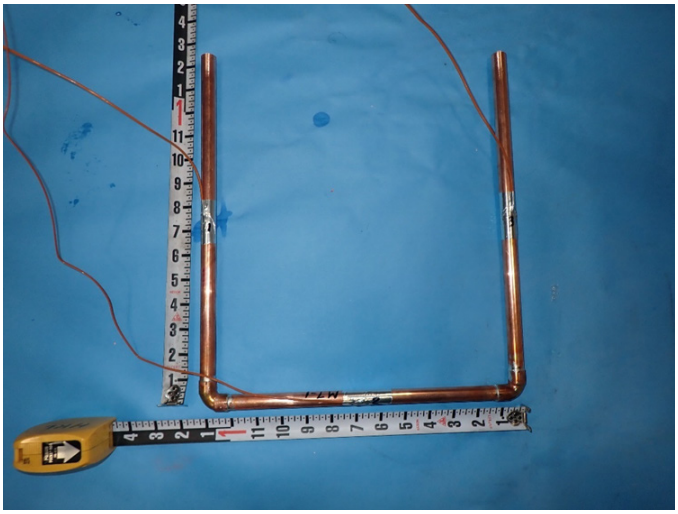

Figure 17
Photograph of the U-shaped copper tube test apparatus, without insulation, showing thermocouple locations.

Failed Component	Failure Pressure (p.s.i.)	Failure Mode
Copper cap fitting	5048 +/- 3%	Fish-mouth rupture
Type M copper tubing	5373 +/- 2%	Longitudinal rupture
Tyle L copper tubing	7133 max	No failure
Copper 90° elbow fitting	4682 +/- 5%	Longitudinal rupture
Push-to-connect cap	1029 +/- 30%	Water drip, no visible failure
Compression stop valve	1365 +/- 26%	Water drip at valve outlet, no visible failure

Figure 15
Table summarizing test results from ice plug pressure tests.

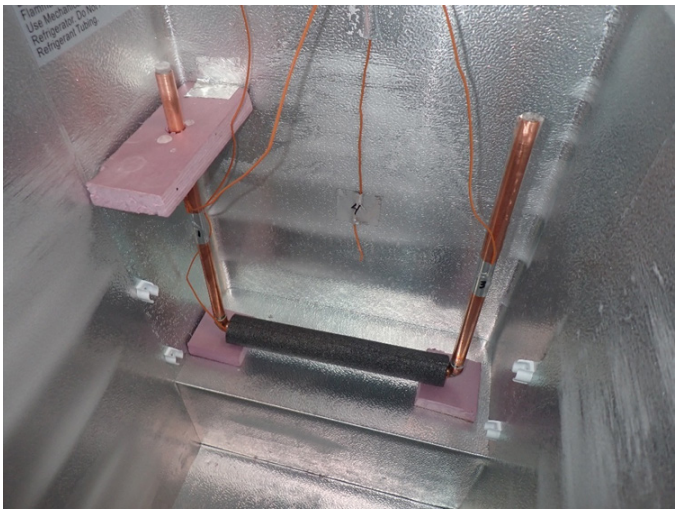

Figure 18
Photo of U-shaped copper tube test apparatus installed in freezer.

(T1, T2, and T3) all decreased gradually until the water in became supercooled. The middle leg (T2) decreased less due to the insulation. Freezing started when dendritic ice began to form, and the temperature of all three legs abruptly increased to 32°F. The temperature then remained roughly constant as the water froze. The two vertical legs (T1 and T3) froze solid first, trapping liquid water in the horizontal leg. As the ice plugs grew, the water pressure in the horizontal leg increased until the tube ruptured.

The tube burst was documented by a sudden increase in temperature. The equilibrium freeze temperature was reduced with increased pressure. For example, at 2,000 p.s.i., the temperature is reduced about 1.8°F (1.0°C). Likewise, at 4,600 p.s.i., the temperature is reduced about 4.3°F (2.4°C)[12]. When a burst occurs, the pressure in the area of the rupture instantly drops to atmospheric, causing the freeze temperature to suddenly jump to 32°F (0°C). The cause of this effect is apparent in the negative slope of the boundary line between the solid and liquid area of the phase diagram.

During trial runs, the horizontal legs ruptured generally near the middle in longitudinal hoop stress type

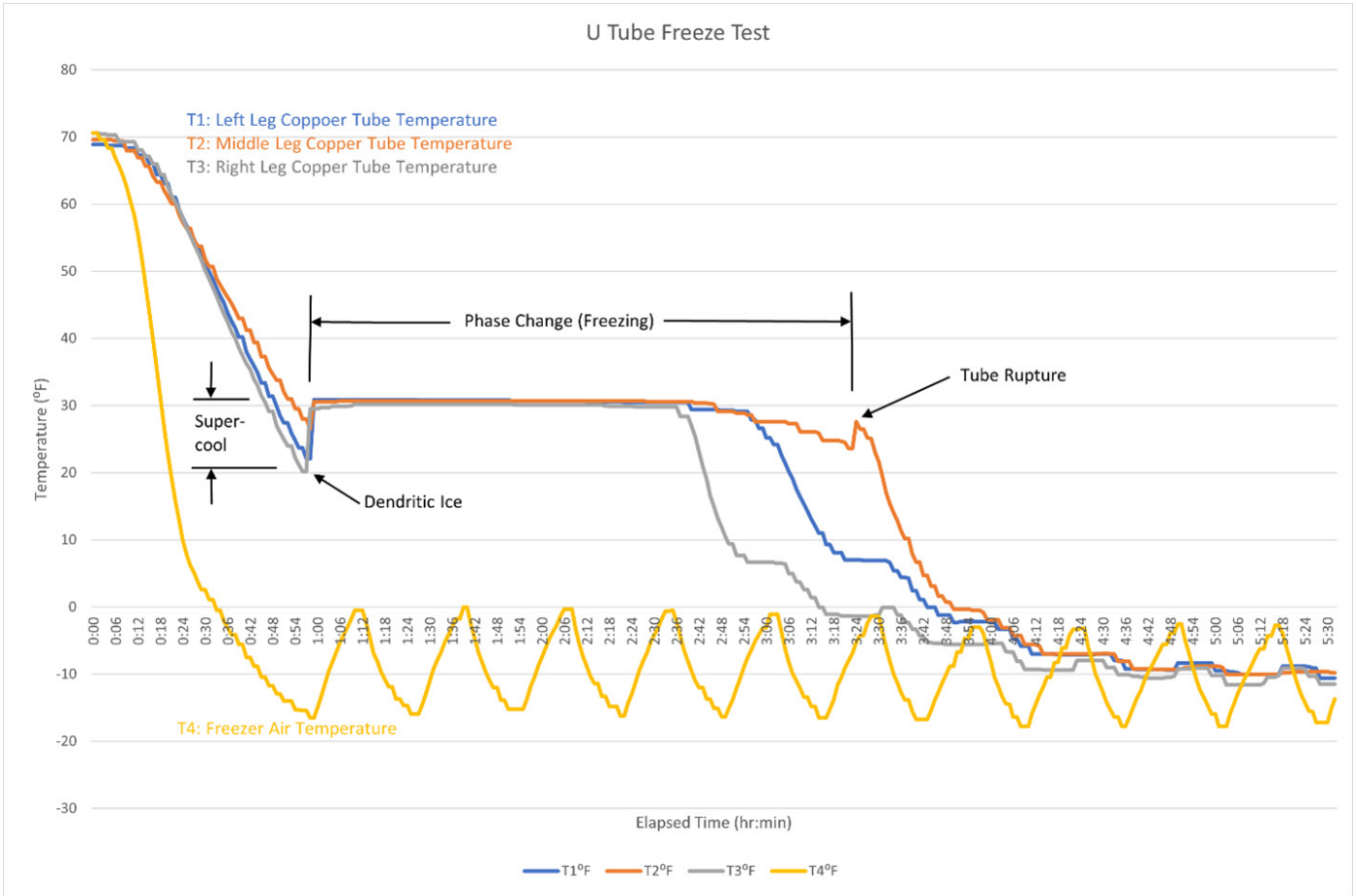

Figure 19
Graph of U-shaped tube freeze test data.

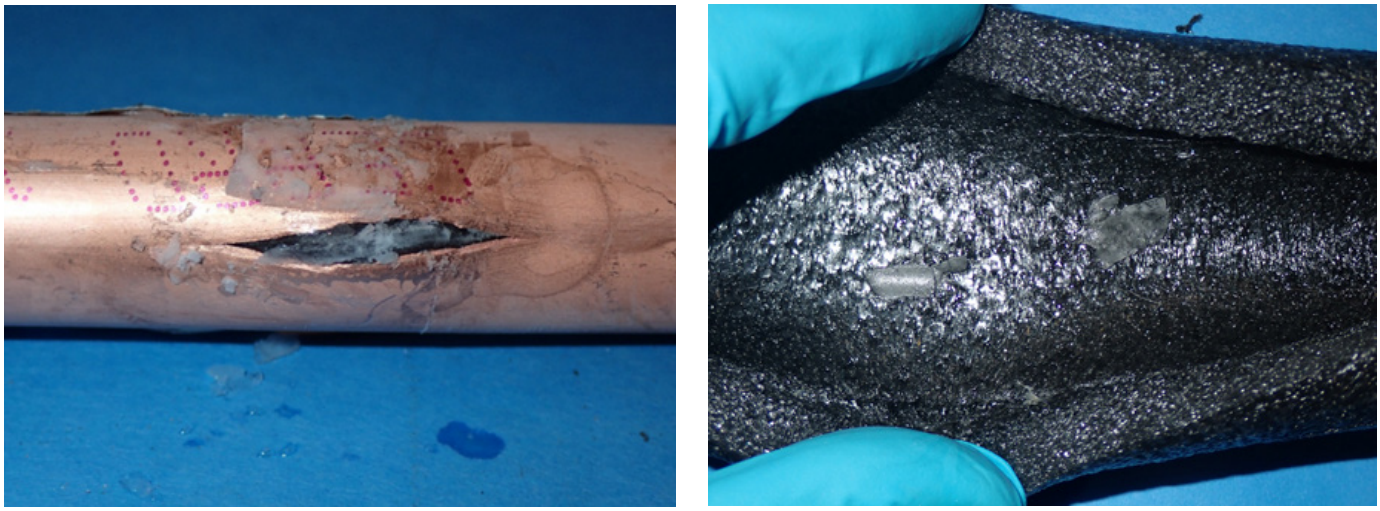

Figure 20
Photographs of ice that formed in the annual space between the tube and insulation.

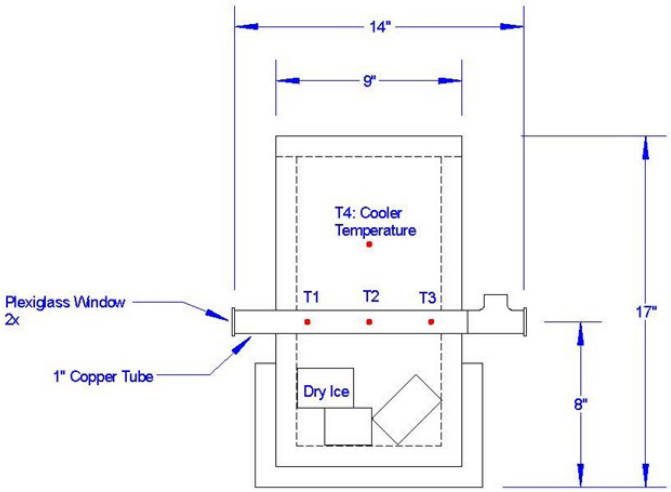

Figure 21
Diagram of ice plug formation test apparatus.

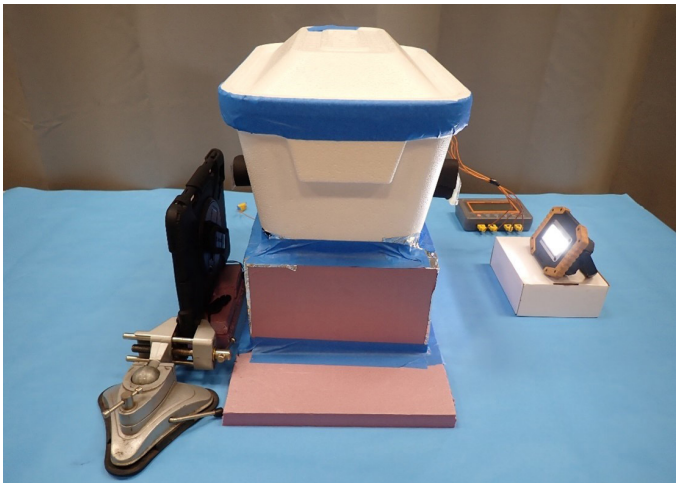

Figure 22
Photograph of ice plug formation test apparatus.

failures (**Figure 20**). A thin layer of ice was observed to have formed on the outer surface of the tube and the inner surface of the insulation at the rupture, indicating liquid water had flowed out of the rupture and into that annular space where it froze.

Ice Formation Process in Tube Experiment

A test was performed to observe the formation of an ice plug in a section of copper tube (**Figures 21, 22** and **23**). A horizontal straight length of 1-inch copper tube with plexiglass windows on the ends was positioned horizontally through a cold chamber so that both ends extended through the walls and were located outside the chamber. Thermocouples were installed on the portion of the tube located inside the chamber (T1, T2, and T3). The freezer air temperature was also measured (T4). The tube was filled with distilled water, and the dry ice was placed inside the chamber with an air space of several inches between the tube and ice, assuring no contact between the two. A video camera was positioned at the front window to view the interior of the pipe, and lighting was positioned at the rear window to illuminate the interior of the tube. **Figure 24** illustrates the temperature data for a test run.

The cold chamber air temperature ranged between approximately 15°F and 22°F. As expected, the temperature of the copper tube decreased from room temperature with the center of the tube being the coldest, since it was in the middle of the chamber. The temperature of the center of the tube decreased below 32°F at an elapsed time of 56 minutes. The liquid water in the tube became supercooled at that point and remained in a supercooled state until an elapsed time of 3 hours and 6 minutes. Accordingly,

the supercooled period lasted for 2 hours and 10 minutes.

At the 3 hour and 6 minutes point, dendritic ice began to form on the interior of the tube wall. Ice was observed initially forming on the upper-left quadrant wall and growing circumferentially along the wall in both directions (clockwise and counterclockwise). At the same time, the ice layer began to grow longitudinally along the tube toward the camera. This initial part of the process occurred over a 17-second period after the first ice was observed. The ice growth then accelerated significantly in both the circumferential and longitudinal directions. The layer grew into a solid plug, completely obstructing the tube. This second part of the process, which occurred over a 5-second period, was recorded on video. The total elapsed time was 23 seconds. Screen shots of the video are presented in **Figure 25**.

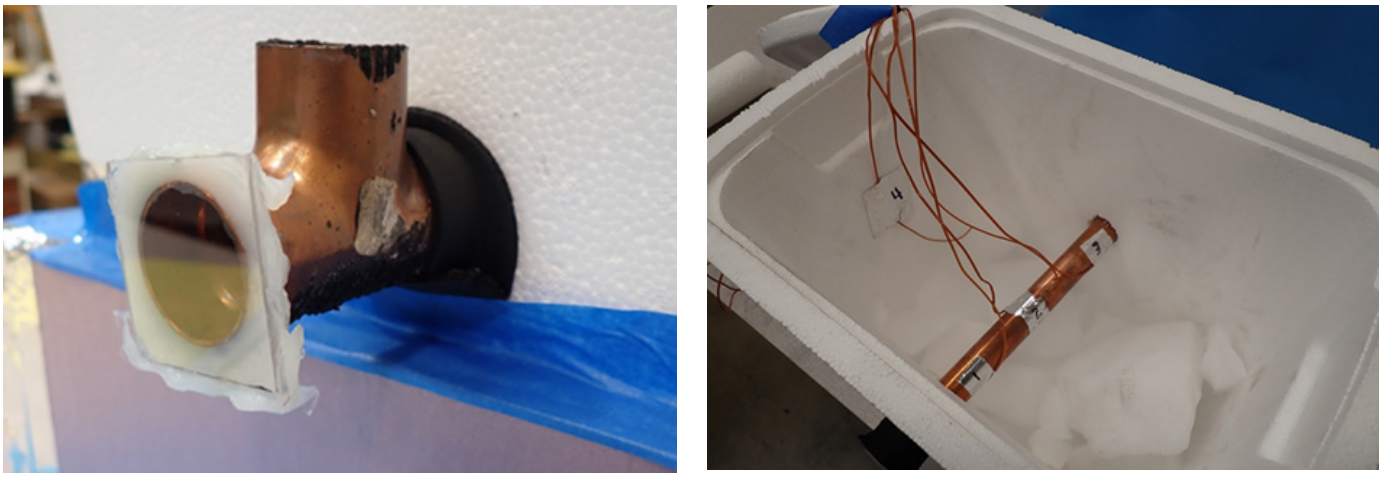

Figure 23
Photographs of ice plug formation test apparatus.

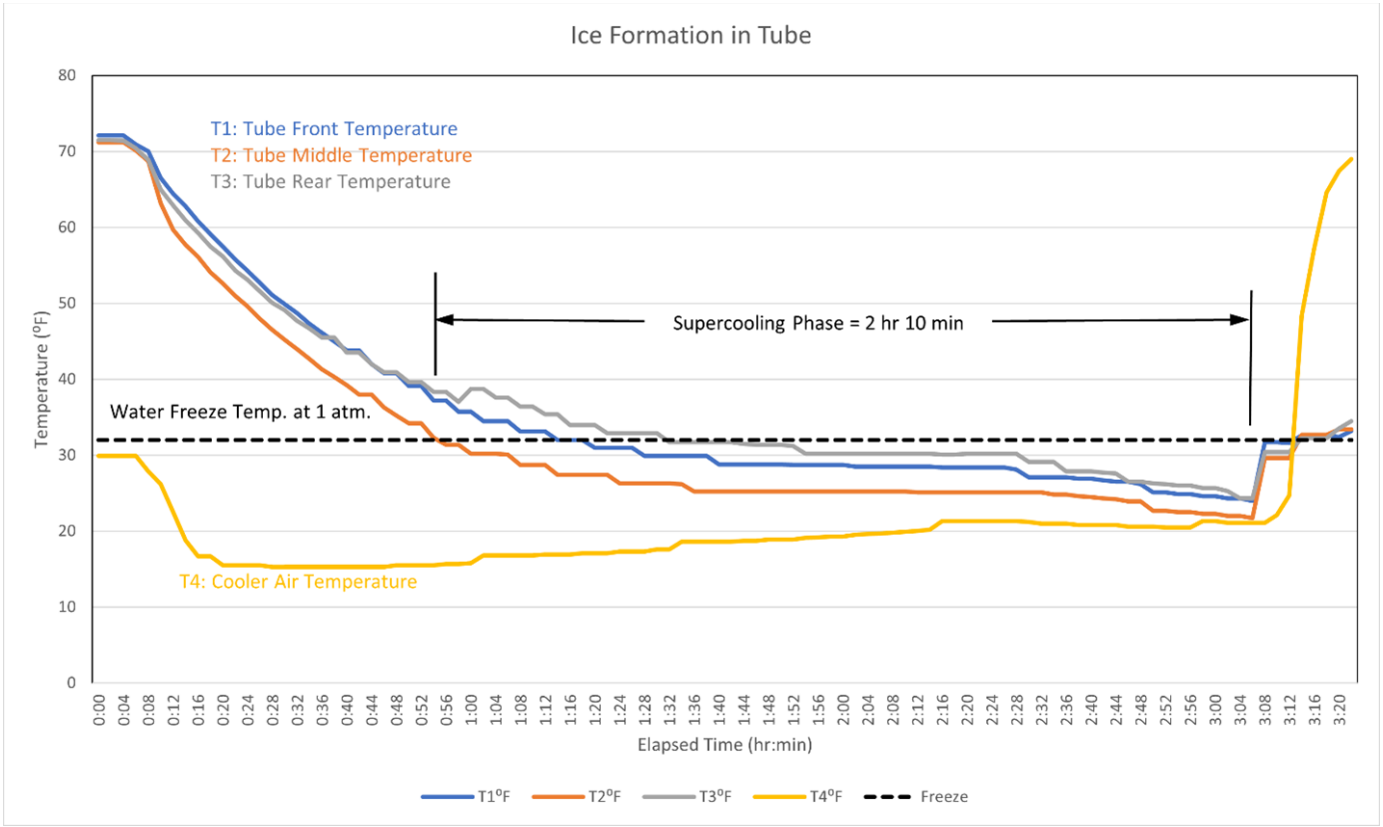

Figure 24
Graph of ice plug formation test data.

Figure 25
Screen shots of video depicting ice plug formation inside copper tube.

Conclusion

Experimental testing was performed to investigate three basic issues related to a building copper tube water piping system freeze failure investigation:

- Downstream pressures generated from ice plugs forming and growing inside a piping system were investigated. The pressures necessary to fail copper tube, copper fittings (elbows and caps), solder joints, push-to-connect components, and compression components were included in that investigation. Pressures as great as 7,133 p.s.i. were developed in the liquid water-filled portion of the test apparatus, including the copper tube assemblies, at temperatures that were well above freezing. The pressures were great enough to burst/rupture common components of copper tube water systems, including Type M tube, solder fittings, push-to-connect fittings, and compression fittings.

- The ½-inch Type M copper tube ruptured at an average pressure of 5,373 p.s.i. (see **Figure 15**), which was 88 percent of the published burst pressure of 6,135 p.s.i. (see **Figure 1**). The ½-inch Type L copper tube was pressurized to 7,133 p.s.i. without failure, which was less than the published burst pressure of 7,765 p.s.i.

- The push-to-connect fittings and compression fittings leaked but did not burst.

- The locations of the failures were investigated to determine if they occurred at the point of the ice formation (ice plug) where the tube was in direct contact with the ice or in liquid-filled closed portions of the system due to increased water pressure from ice plug growth inside the piping. When water-filled copper tube assemblies were subjected to freezing, the failures occurred in areas that were insulated, and froze later in time than the non-insulated areas. The ruptures occurred in liquid-filled areas as evidenced by liquid water flowing out of the rupture into the annual space between the tube and insulation (and freezing there) and a recorded spike in the temperature at the moment of the failure caused by the sudden drop in water pressure from the rupture in the area of the rupture.

- The process of the formation of an ice plug inside copper tube was investigated. The interior of a water-filled copper tube inside a cold chamber was observed and recorded. The temperature of the copper tube decreased from room temperature and became supercooled for a period of 2 hours and 10 minutes. At that point, dendritic ice formed on the interior of the tube wall. Ice was observed initially forming on the inner surface of the tube wall and grew circumferentially along the wall in both directions (clockwise and counterclockwise). At the same time, the ice layer began to grow longitudinally along the tube toward the camera. The ice growth then accelerated significantly in both the circumferential and longitudinal directions. The layer grew into a solid plug, completely obstructing the tube. The elapsed time of ice formation was 23 seconds.

- No solder joints failed during the testing, indicating those joints were not the weak points of the piping system. Failed solder joints found by investigators in the field would be inconsistent with this testing. Additional analysis of those failed joints may be warranted to determine if they had been properly soldered when they were made or became damaged before the freeze event.

References

1. U.S. House of Representatives, “28 USC App, FEDERAL RULES OF EVIDENCE, ARTICLE VII: OPINIONS AND EXPERT TESTIMONY,” Office of the Law Revision Counsel United States Code, 1 December 2011. [Online]. Available: https://uscode.house.gov/view.xhtml?path=/prelim@title28/title28a/node218/article7&edition=prelim. [Accessed 10 September 2021].

2. C. Kohut, “Illinois Chapter Community Associations Institute: Frozen - Flooded and Frustrated,” [Online]. Available: https://www.cai-illinois.org/frozen-pipes-flooded-and-frustrated/. [Accessed 6 July 2021].

3. International Code Council, Inc., “2021 International Residential Code ((IRC),” November 2021. [Online]. Available: https://codes.iccsafe.org/content/IRC2021P2/chapter-29-water-supply-and-distribution#IRC2021P2_Pt07_Ch29_SecP2903.3. [Accessed 28 February 2022].

4. International Code Council, Inc., "2021 International Residential Code (IRC)," November 2021. [Online]. Available: https://codes.iccsafe.org/content/IRC2021P2/chapter-29-water-supply-and-distribution#IRC2021P2_Pt07_Ch29_SecP2906.5. [Accessed 28 February 2022].

5. International Code Council, Inc., "2021 International Property Maintenance Code (IPMC)," September 2020. [Online]. Available: https://codes.iccsafe.org/content/IPMC2021P1/chapter-5-plumbing-facilities-and-fixture-requirements#IPMC2021P1_Ch05_Sec505. [Accessed 28 February 2022].

6. *ASME B16.18-2018 Cast Copper Alloy Solder Joint Pressure Fittings*, ASME, New York, NY 2018.

7. *ASME B16.22-2018 Wrought Copper and Copper Alloy Solder-Joint Pressure Fittings*, ASME, New York, NY 2018.

8. *ASTM B32-20 Standard Specification for Solder Metal*, ASTM International, West Conshohocken, PA 2020.

9. *ASTM B 88-20 Standard Specification for Seamless Copper Water Tube*, ASTM International, West Conshohocken, PA 2020.

10. Copper Development Association, Inc., "Search for Nation's Oldest Copper Plumbing Continues," March 2005. [Online]. Available: https://www.copper.org/consumers/copperhome/HomePlan/projects/search_for_nations_oldest_copper_plumbing_continues.html. [Accessed 27 February 2022].

11. E. Avallone and T. Baumeister III, Marks' *Standard Handbook for Mechanical Engineers*, McGraw-Hill Book Company, New York, NY pp. 4-81.

12. J. R. Gordon, "An Investigation into Freezing and Bursting Water Pipes in Residential Construction," Insurance Institute for Property Loss Reduction, Champaign, IL 1996.

13. J. Cruz, B. Davis, P. Gramann and A. Rios, "A Study of the Freezing Phenomena in PVC and CPVC Pipe Systems," Materials Science, Engineering, p. 1, 2010.

14. Copper Development Association, Inc., *Copper Tube Handbook*, McLean: Copper Development Association, Inc., New York, NY 2020, pp. 66-68.

15. D. Edwards, K. Smith, Jr., D. Duvall, and J. Grzetic, "Analysis and Testing of Freezing Phenomena in Piping Systems," in Proceedings of IMECE2008, Boston, MA 2008.

16. R. Gilpin, "The Effects of Dendritic Ice Formation in Water Pipes," *International Journal of Heat and Mass Transfer*, vol. 20, p. 693, 1976.

17. J.P. John R. Rumble, "Properties of Ice and Supercooled Water," in CRC Handbook of Chemistry and Physics, Boca Raton, London, New York, CRC Press, 2018-2019 99th Edition, pp. 6-12.

18. A. Harvey, "Properties of Ice and Supercooled Water," in *CRC Handbook of Chemistry and Physics*, CRC Press, Boca Raton, FL 2018-2019 99th Edition, pp. 6-12.

19. Rigid SF-2300/SF-2500 Manual Super Freeze Pipe Freezing Units, Ridge Tool Company, Elyria, Ohio, USA, 2013 p. 3.

20. C. Auyeung, "13.20 Phase Diagram for Water," CK-12 Foundation, Palo Alto, CA. [Online]. Available: https://flexbooks.ck12.org/cbook/ck-12-chemistry-flexbook-2.0/section/13.20/primary/lesson/phase-diagram-for-water-chem/. [Accessed 9 September 2021].

FE Use of Arc Mapping/Arc Fault Circuit Analysis in a Residential Kitchen Fire Investigation

By Jason McPherson, PE (NAFE 852M)

Abstract

A fire occurred in a single-story, single-family residence. At the time of the fire, two individuals (a husband and wife) occupied the residence. During the early morning hours, the wife was awakened by the smell of smoke, and discovered a fire in the kitchen. Initially, the area of origin for the fire was the kitchen. Utilizing arc mapping, the area of origin was further defined. This enabled fire investigators to use available fire effects to ultimately determine the point of origin and cause of the fire. The intent of this paper is to detail those efforts, enabling others to benefit from this case study.

Keywords

Electrical survey, arc, arc site, arc mapping, area of origin, point of origin, fire effects, fire patterns, electrical safety, arc fault circuit analysis, forensic engineering

Introduction

A fire occurred in a single-story, single-family residence during the early morning hours (**Figure 1**). Prior to the discovery of the fire, the two occupants (husband and wife) were asleep. The wife was sleeping in the master bedroom, and her husband was sleeping on a sofa in the family room. At approximately 1 a.m., the wife was awakened by knocking at the front door. A friend of the husband came to the residence to drop off one jacket and pick up a different one that was mistakenly taken home by the husband. The wife went back to bed approximately 15 minutes later. She reported that at the time she went back to bed, the television/lights were still on. Therefore, she assumed the husband had fallen back asleep on the sofa.

Figure 1
Exterior photograph of the residential structure.

At approximately 3:30 a.m., the wife was awakened by the smell of smoke. She exited the master bedroom to investigate the source of the odor. Walking down the hallway toward the family room and kitchen area, she noticed it was now dark inside — and eventually realized there was a fire.

She returned to the master bedroom and exited the residence via one of the master bedroom's windows. She traveled around the exterior of the residence to the garage vehicle door, entered the code for the vehicle door, and the garage door opened. She entered the garage, and

Safety

"Electricity can be very dangerous occupational hazard." [sic] *Working within fire scenes may expose investigators to electrical hazards. Documents such as the National Fire Protection Association's NFPA 70E,* Standard for Electrical Safety in the Workplace[1]*, address safety-related work practices that can help reduce the risk of electrically related workplace injuries. — **National Fire Protection Association***

Jason McPherson, PE, PO Box 888682, Grand Rapids, MI 49588-8682; 616-566-5669; jasonmcpherson05@gmail.com

then proceeded to open the service door that led from the garage into the kitchen. After entering a few feet into the kitchen, she was met with heat from the fire, and could not proceed any farther. She recalled seeing fire to her right and overhead. She exited the kitchen into the garage, and then proceeded to the back of the residence. With the aid of a neighbor, she attempted to gain access to the residence by breaking the door wall glass, but those efforts were not successful. The husband expired in the fire.

Arc Mapping Primer

Arc mapping, also referred to as arc fault circuit analysis, is a generally accepted method within the forensic engineering community whereby a trained, experienced, and skilled practitioner uses the electrical system to reconstruct the fire scene to assist in the determination of its origin and progression. Several papers have been published on the topic of arc mapping[2,3,4].

Arc mapping is often thought of only in the terms of origin determination. However, it is not simply a one-dimensional approach. More accurately, it is a multi-dimensional method that can also be used for such tasks as scenario development and scenario testing. Additionally, it seems that when investigators speak of arc mapping, the presence of an arc site (see **Figure 2** as an example) is the emphasis. Skilled practitioners will understand that the lack of electrically caused damage can be just as important as finding electrically caused damage.

Arc mapping is not simply a pattern recognition tool. The practitioner cannot plot arc-site locations on a fire scene diagram and — by those locations — discern the area of origin of a fire or determine heat flow through a compartment. The practitioner must have a grasp of the installation that is provided through the performance of an electrical survey, which provides the foundation for being able to discern the data that can be gathered from the post-fire condition of the electrical system.

Figure 2
Arc site found at the fire scene.

Presumptions

When performing arc mapping, certain foundational presumptions are made, including:

1. The electrical system was energized at the time of the fire.

2. The electrical system available fault current will be such that an arcing event will leave physical damage.

3. Circuit lengths and installation methods are such that fault current will not be attenuated to the point that physical damage will not be made.

The fire will affect conductor insulation in the same manner as other combustible materials. In addition to the above, it is expected that the practitioner who possesses the skill necessary to perform arc mapping will recognize when circumstances exist that require additional considerations.

Fault Current

The amplitude of current a transformer can supply to a fault is directly related to the utility system's available fault current, transformer impedance, transformer secondary voltage, transformer kVA rating, circuit impedance, and fault impedance. Guidance related to the calculation of fault currents is provided in references such as the *Standard Handbook for Electrical Engineers*[5].

Electrical Insulation

The intent of electrical insulation, when placed between conductors at different potentials, is to permit only a "small or negligible current to flow through it."[5] Electrical insulation can be considered a combination of resistors and capacitors. The basic circuit representation of electrical insulation is shown in **Figure 3**. When exposed to heat from fire of sufficient time and magnitude, the insulation can go through a decomposition process that results in the insulation no longer functioning as intended.

Initial Scene Examination by the Lead Fire Investigator

The lead fire investigator retained by the property insurance company conducted an initial scene examination. During this examination, the lead fire investigator documented the fire scene and collected information

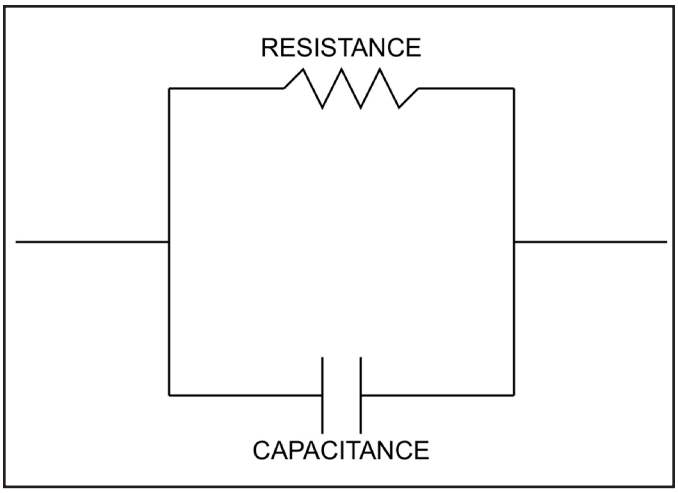

Figure 3
Basic circuit representation of electrical insulation.

related to the discovery and response to the fire. The area of origin determined by the lead fire investigator at this point was, for all intents and purposes, the entirety of the kitchen area. Several potential ignition sources were present in the kitchen, including a gas stove, small remote-controlled toy, appliances, and structural electrical and attached devices.

Forensic Electrical Engineering Scene Examination

A joint-scene examination was scheduled and conducted in conjunction with the attending experts for the identified interested parties that were notified of the fire loss.

Forensic engineers should follow a systematic approach[6]. The author's post-briefing scene documentation efforts began with an initial walk-around. This consisted of photographic documentation and note-taking in conjunction with an exterior electrical survey.

For the purposes of the examination, the residence was considered to face east. The residence was supplied with electricity via an overhead service drop to a weather-head that was located on the northwest corner of the residence. The copper service entrance conductors (enclosed in metallic raceway) were then routed on the exterior of the residence, and traveled east where they eventually terminated within the service meter enclosure. The service conductors then exited the service meter enclosure, entered the residence, and terminated at the main service disconnect located within the main circuit-breaker-style load center mounted to the interior north wall of the garage.

During the electrical survey, it was noted that an arc site was present on the service entrance conductors in the area of the west side of the kitchen window (**Figure 4**). This was the sole site in this area, meaning it was the only site on this section of the circuit. This provided the following information:

- The utility service consisted of enough available fault current to result in an arcing event that would leave physical damage to circuit conductors.
- At the time the wife utilized the garage vehicle door keypad to open the door, the fire had not yet breached the kitchen window and caused the service to fault.
- The west side of the kitchen window was the location where the fire first breached the kitchen window and service entrance.

The electrical examination then turned to the area of the load center, which was attached to the garage's south wall (near the service door that led into the kitchen from the garage). As stated, earlier the wife passed this area and entered the kitchen through this same door. Therefore, it can be concluded that the fire damage to the equipment happened after this occurred.

Electrical survey efforts proceeded to examination of the electrical system within the kitchen. In this area, the electrical system consisted of such items as light fixtures, receptacles, light switches, non-metallic sheathed cables, and connected appliances. Most of the branch-circuit

Figure 4
Arc site found on service conductors.

wiring was concealed behind wall and ceiling finishes that provided initial protection from heat from the fire. However, it was noted that in addition to the connected appliances located on the kitchen counters, one ceiling surface-mounted light fixture, one surface-mounted fluorescent light fixture located above the kitchen sink, and powered range hood were all permanently wired. The branch-circuit wiring within these devices would not be physically protected by wall and ceiling finishes and would present circuit areas of opportunity for a developing fire to affect the branch-circuit wiring.

The electrical survey in the form of circuit tracing efforts revealed that the branch-circuit cable supplying the junction box that the ceiling light fixture was attached to consisted of a three-conductor with ground cable. From the ceiling light junction box (**Figure 5**), one section of two-conductor with ground non-metallic sheathed cable was routed to the surface-mounted fluorescent light fixture positioned over the kitchen sink. Further examination revealed that the branch circuit was constantly energized — and that the same section of branch circuit also supplied the range hood that was mounted above the stove.

Another section of two-conductor with ground non-metallic sheathed cable was routed from the ceiling light junction box to the west wall — where it was eventually terminated to the duplex receptacle that supplied the gas stove. Based on this information, it was logically inferred that the developing fire attacking one of these would result in an arc site that could be used to further define the area of origin and help to determine the path of fire travel.

Further Defining the Area of Origin Using the Electrical System

Examination efforts then turned to attempting to further define the area of origin of the fire. Due to the damage to the combustible surfaces (such as hanging cabinets), fire pattern analysis was initially of little benefit. Therefore, arc mapping was heavily relied upon to collapse the origin to a more defined area.

The question of whether the origin could be at or near the coffee maker was posed. If this was the case, then the principles of fire dynamics would dictate that the first location of the fluorescent light fixture/range hood circuit affected by fire would be either at the fluorescent light fixture located above the sink or the ceiling-mounted light fixture. Examination of the wiring related to the light fixtures revealed no arc sites within the fixture wiring or the portion of the branch-circuit conductors that would be an opportune target for heat from the fire.

Figure 5
Ceiling light junction box in relation to over-sink light fixture.

The location of the arc site on the service entrance conductors and lack of arc site(s) related to the over-sink fluorescent light fixture, ceiling-mounted light fixture, and associated wiring for both led to the determination that this, in fact, would be a strong indicator that the fire originated toward the west side of the kitchen. Attention then turned to the range hood (**Figure 6**). Since the range hood consisted of a metal enclosure, heat from the fire would easily be conducted through the metallic walls to the wiring. Examination of the wiring within the range hood revealed an arc site (**Figure 7**). Based on the understanding of the electrical system from performing an electrical survey, the arc site in the range hood, the arc site on the service entrance conductors, and lack of an arc site within

Figure 6
Range hood.

Figure 7
Arc site found on range hood wiring.

the fluorescent fixture wiring indicated that the fire had originated at the west side of the kitchen.

Point of Origin and Cause of the Fire

After the area of origin was narrowed down to the west side of the kitchen using the electrical system, fire investigators were able to utilize fire effects. Examination of the range hood revealed fire effects in the form of oxidation patterns on the surface that would have faced downward toward the cooktop. The range hood was more oxidized on the right side than the left side.

This discovery led to the examination of the cooktop and four gas burners. Examination of the cooktop revealed differential damage to the four gas burners. While all four burners exhibited melting from heat, the right front burner was more melted from heat than the other three.

Remains of melted aluminum mesh were found on top of the right front burner grate (**Figure 8**). It was first thought that the remains consisted of the remains of aluminum filters from the range hood. By reconstructing the range hood position — and then using documentation techniques to determine if the filter material would drop onto the front burners or not — investigators determined this would not be the case (**Figure 9**).

The wife was interviewed again regarding the use of aluminum mesh screens for cooking. She indicated that the husband liked to cook jalapeno peppers stuffed with cream cheese and wrapped with bacon on the grill, using a small aluminum mesh screen. She did not recall seeing the husband ever use the stove for that purpose. The kitchen area was searched, and additional aluminum mesh screens of the type that the husband would use were found (**Figure 10**). When compared with the remains found on the right

Figure 8
Reconstructing the range hood.

Figure 9
Mesh found on right-front burner.

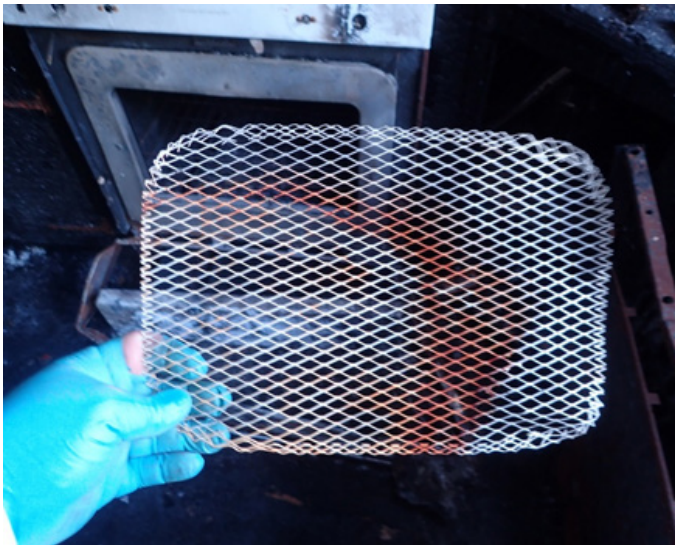

Figure 10
Exemplar mesh screen.

front burner grate, they matched.

Examination of the cooktop gas control valves revealed that all control valve stems (except one) were in the OFF position. The stem associated with the right-most gas valve control, which controlled the right front burner, was not in the OFF position. During the initial interview, the wife stated that when she had gone back to bed the husband was not cooking anything. As a result, examination efforts were then focused on determining if the valve was truly not OFF (due to it falling and physically being out of position).

The cooktop was raised so the gas valve positions could be compared. It was determined that the right-front gas valve was slightly dislodged from its installed position (**Figure 11**). Further comparing it with the remaining three gas valves revealed that when the gas valve was rotated back to its installed position, the gas valve stem would still have been in a position other than OFF. It was estimated that the burner was at a medium-high setting (**Figure 12**).

Based on the available data, it was determined that at some point the husband started cooking and fell asleep with the stove on with foodstuffs on the right front burner grate.

Summary

Based on the examination of the electrical system, it was determined that the fire was contained within the structure at the time the wife entered the garage. The fire first affected the electrical system within the structure prior to breaching the kitchen window and affecting the service entrance conductors. The location of electrical damage to the service entrance conductors indicated the fire first breached the window at the west side. The location of the arc site on the service conductors (combined with the results of the arc mapping in the kitchen) showed the fire originated at the west end of the kitchen. This enabled origin and cause investigators to use the available fire effects related to the range hood and stove to determine the point of origin and cause for the fire.

Figure 11
As-found position of the right-front burner control valve.

Figure 12
Estimated setting of the right-front burner control stem.

References

1. Standard for Electrical Safety in the Workplace, NFPA 70E, National Fire Protection Association, Quincy, MA, 2018 Edition.

2. L. I. Rothschild, "Some Fundamental Electrical Concepts in Locating the Cause and Origin of a Fire," JotNAFE, vol. 3, no. 2, Jan. 1986.

3. Delplace, M. and Vos, E. "Electric Short Circuits Help the Investigator Determine Where the Fire Started," Fire Technology 19, 185–191 (1983).

4. NicDaeid, N. and Carey, N., "2010 Arc Mapping," *Fire and Arson Investigator,* vol. 61, pp. 34-37, Oct. 2010.

5. H.W. Beauty and S. Santoso, *Standard Handbook for Electrical Engineers, 17th Edition.* New York, NY USA: McGraw Hill, 2018.

6. L. Liptai and J. Cecil, "Forensic Engineering and the Scientific Method," Journal of the National Academy of Forensic Engineers, vol. XXVI, no. 1, 2009.

Forensic Engineering Investigation of a High-Voltage Transmission Line Anchor Shackle Failure

By Daniel P. Couture, PEng, DFE (NAFE 951S)

Abstract

A forged alloy steel anchor shackle, one of a batch of more than 2,600 produced for the project, failed catastrophically in service on a newly erected 66-kilometer high-voltage transmission line in northern Canada. A failure analysis led to a hypothesis that forging laps had created the critical crack size to initiate propagation under cold weather conditions. An extensive Charpy fracture toughness test program based on CAN/CSA C83.115-96 parameters was performed on 150 shackles, but the data did not support the initial hypothesis of temperature dependence. The forensic engineering team designed experimental tensile tests at ambient temperatures as low as -40°C to evaluate the propagation response of lap cracks in a statistically valid sampling of shackles. The trimmed forging flash area disguised laps from the manufacturing process, and subsequent galvanizing steps prevented detection by magnetic particle inspection. A focused recommendation for removal and replacement of the shackles was issued for those bearing major loads in the tower array.

Keywords

High-voltage transmission line, shackle hardware, Charpy tensile test, low-temperature fracture toughness, experimental design, statistical sample, forensic engineering

Failure Context and Procurement History

The forensic engineers were engaged on behalf of the owner to confirm the probable cause of the fracture of the single anchor shackle's arms in service on a new transmission line. Standards and specifications that are part of the procurement documents were studied to determine how a decision on fitness for service could be derived. The goal was to provide a technically based criteria for deciding whether all, most, or some fraction of the shackle batch should be replaced while neither endangering the public nor compromising the integrity of the transmission line.

The Number 9 anchor shackles (**Figure 1**) are employed in an array to support insulators on the steel towers (**Figure 2**). The load path goes through the two arms

Figure 1
Typical Number 9 anchor shackle with clevis pin.

Figure 2
High-voltage transmission tower.

Daniel P. Couture, PEng, 9033 Leslie St, Unit 18, Richmond Hill, ON L4B 4K3 Canada, daniel.couture@arconforensics.com

of the shackle, splitting evenly at the eyes by the contact from the clevis pin. By inspection, the cross-sectional area at the midpoint is therefore at the maximum tensile stress when the insulator assembly is loaded in service. Number 9 shackles have a nominal rating of 440 kiloNewtons (kN). The load divided by the cross-sectional area defines the tensile stress in the arms. The position of the broken shackle on the tower is depicted in **Figure 3**.

Statistical Quality Control in Manufacturing Processes and Procurement Documents

Contemporary manufacturing processes employ control systems that are set up to ensure that the quality of raw materials will conform with the engineering design requirements. Master procurement document(s) address these criteria and lay out the means and methods by which the assurance can be obtained to a satisfactory level based on statistical theory. Acceptable Quality Level (AQL) was used because it is uneconomical to test every item in a lot, and these scientifically based sampling criteria are intended to provide the end-user with confidence of the quality of the components[1].

The CAN/CSA C83-96 (2011) "Communication and Power Line Hardware" standard[2] employs the AQL concept to guide the management of risks associated with a product possessing an attribute that is defective. AQL underlies the decision-making process regarding acceptance or rejection of a lot of raw material and (later in the process) the finished products. These are not done in the same way because of process constraints and economic limitations. Inspection by Variables is cited as an "inspection that actual measurement on a continuous scale is made on the unit or article for the quality characteristic under consideration (e.g., tensile testing of steel)."

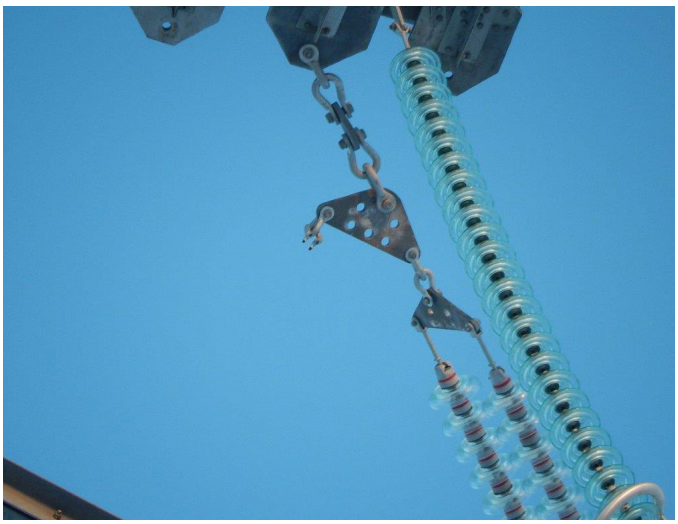

Figure 3
Fractured shackle on the tower.

This contrasts with Inspection by Attributes, which, as set out on page 18, Section A1.4 of the standard, "determines whether the unit or article does or does not conform to the specified requirements for the quality characteristics under consideration (e.g., "GO" or "NO-GO" gauging)".

Defects are discussed in Table 3 of CAN/CSA C83-96, which defines the general classes of defects as follows:

Critical — *Where a failure to meet the specified requirement, through functional failure, would surely result in danger to life. (Class A AQL percent defective* ***0.015%)***

Very Serious — *Where a failure to meet the specified requirement, through functional failure, would surely result in hazardous conditions to personnel or high restoration costs or high consequential costs or any combination of these. (Class B AQL percent defective* ***1.0%)***

According to the Anchor Shackle appendix of CAN/CSA C83.115-96, Class A defects (defined as a critical functional failure) are NOT allowed. It designates surface defects (iii) and energy absorption/toughness (iv) as very serious, or Class B, defects in shackles. The shackle failure that occurred in service may have automatically disqualified the whole batch.

Sampling Plans

The CAN/CSA C83-96 Appendix A sampling programs are recommended to be used for qualification of the component's attributes, while Appendix B inspection by variables programs would be employed for costly destructive testing, such as tensile tests. For example, for a Single Sampling Plan for a run of 1,301 to 3,200 pieces, the sample size would be 150 pieces, whereas under Appendix B, for under 5,000 pieces in the lot, the sample size would be 5. The narrative explicitly states that the best approach for detecting Class A defects is statistical quality control during the raw material selection and production processes.

Participants in the Investigation Process

The utility commissioned Company C, an engineering firm, to complete the design, procurement, and construction of the transmission line. Company A was a European manufacturer of anchor shackles. Company B was a testing laboratory in Europe. Company D and E were both independent testing laboratories in Canada commissioned by the forensic engineer. Company E was a highly

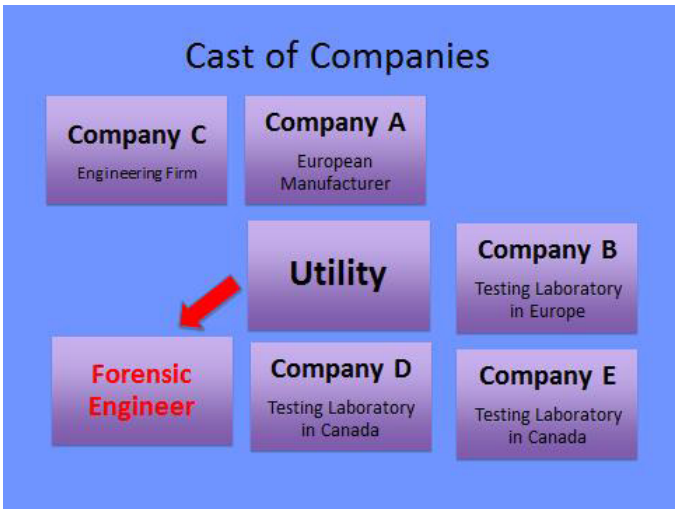

Figure 4
Participants in the investigation.

qualified aerospace metallurgical laboratory (**Figure 4**).

The Anchor Shackle Manufacturing Process at Company A

Six-meter-long bars of 32-mm-diameter 41Cr4 type (equivalent to AISI 5140) heat-treatable and hardenable low alloy steel were cut to size and then hot-forged to shape the anchor shackles. Forging uses mechanical compressive force to plastically deform and change the metallurgical structure of an object, giving it improved strength characteristics. The forging tools may leave flashing when the hammer and anvil are not perfectly aligned; this flashing is typically trimmed as an intermediate step. A "lap" may form if the flashing metal is folded over at the edge of the main body of the forging. Heat treatment (including quenching and tempering) produced the tempered martensitic microstructure, but this process was not revealed in the reviewed documents. A galvanizing step follows in which the product is dipped into a molten zinc aluminum liquid-phase solution. Assembly of the clevis pin and self-locking cotter pins are completed to create the ready-to-use shackle in the final manufacturing step. Approximately 2,600 shackles were made in batch code 2525 by Company A.

According to production records, a sample of the steel bar raw material for the batch was qualified and accepted for cold weather behavior by Charpy test specimens that exceeded the required minimum absorption energy with 24 to 34 Joules at -20°C. The anchor shackles were sampled and subjected to a quality control department tensile test. Each specimen met the rating criteria of CAN/CSA 83.115-96[3] during the room temperature tests, allowing the batch to be accepted and released to the project.

Observations

Company B Failure Analysis Report

The single Number 9 anchor shackle that fractured on the transmission line is shown in **Figures 5** and **6**. Four fracture surfaces of the field failure shackle were examined with metallographic techniques on behalf of the utility and Company A by the laboratory of Company B in Europe. These fractures are displayed in **Figures 7, 8, 9,** and **10**. Each fracture was individually characterized by high-power microscopy. Fracture origins were found along the inboard edge of the eye at forging laps on two of the four fracture surfaces, while the other fractures appeared to be consequential to the two primary fractures. Thirty-one shackles from Batch 2525 were examined and tested.

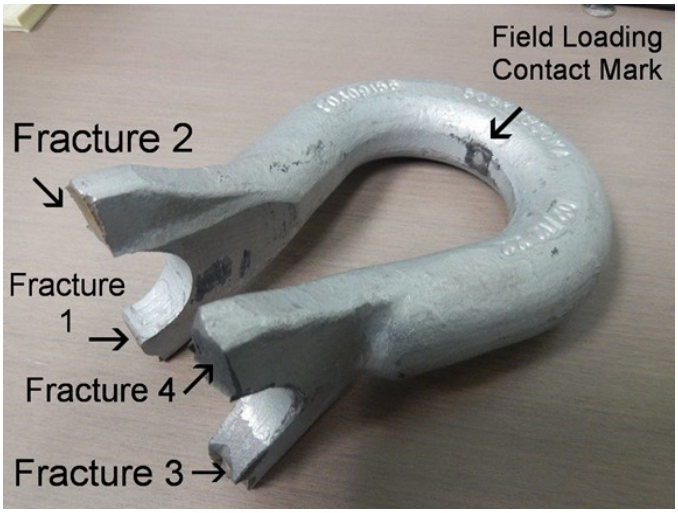

Figure 5
Fractured anchor shackle.

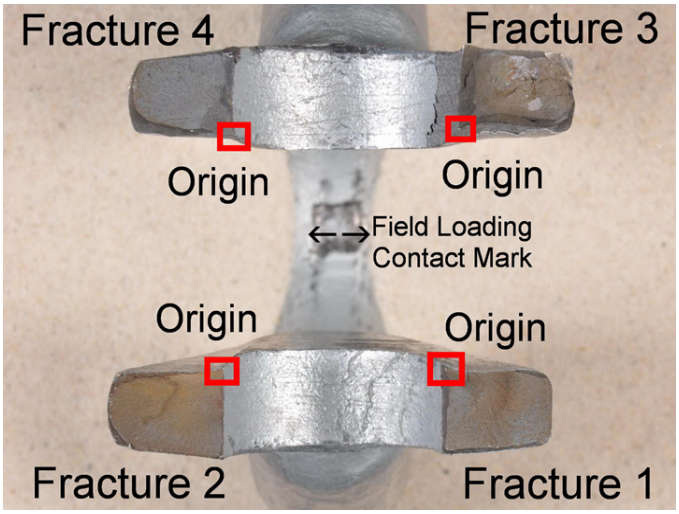

Figure 6
End view of fractures on anchor shackle.

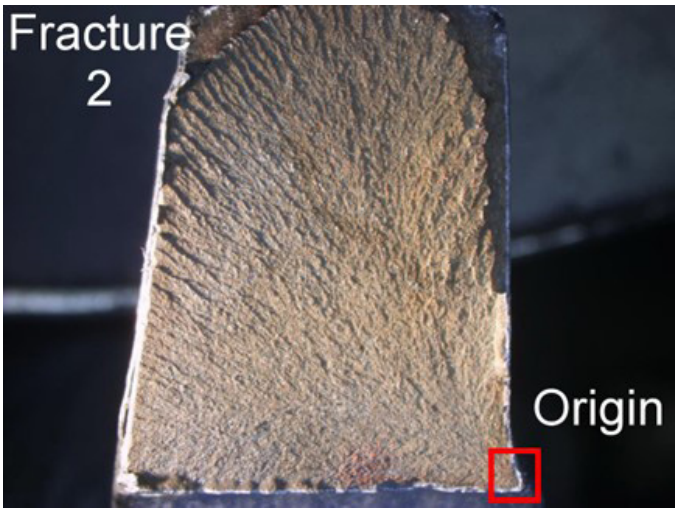

Figure 7
Shackle fracture 2 at the inner eye, origin at lower right.

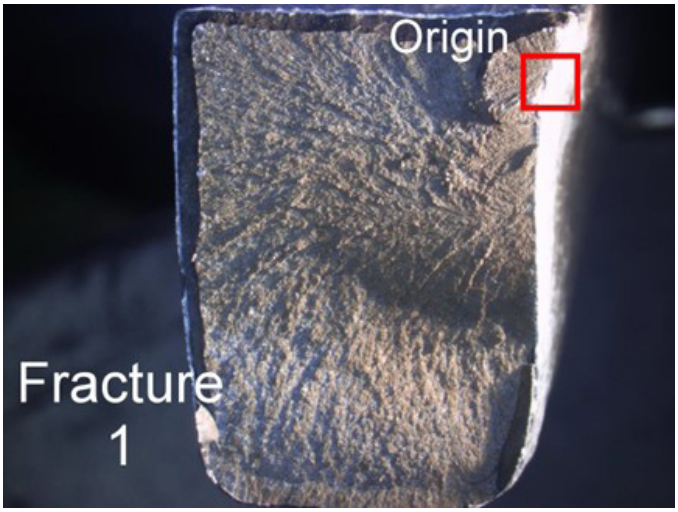

Figure 8
Shackle fracture 1 at the inner eye, origin at upper right.

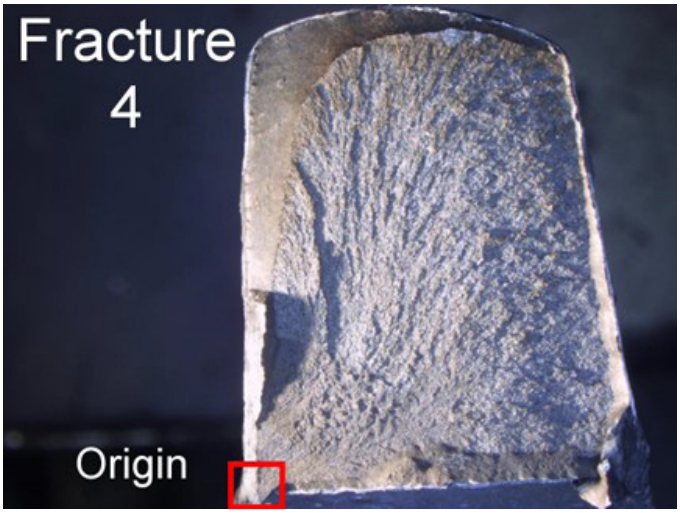

Figure 9
Shackle fracture 4, origin at the inner eye on the lower left.

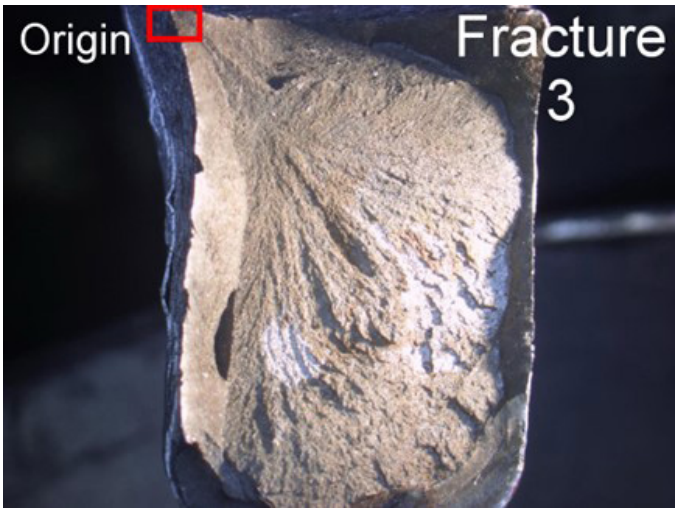

Figure 10
Shackle fracture 3, origin at the inner eye on the upper left.

The essence of the Company B working hypothesis was that these forging laps, coincidental with a trimming line (**Figures 11** and **12**), had created the critical crack size necessary for the crack to propagate through the arm under cold weather service conditions at Fracture 1 area shown in **Figure 8**. The forensic engineers concurred with the first part of the hypothesis, but disagreed that the service conditions were necessarily contributory, based on prior fracture mechanics and failure analysis experience. The low alloy 41Cr4 (5140) steel has a ductile/brittle transition temperature near -100°C (-148°F), and tempered martensite does not undergo this transition. The cold weather effect hypothesis was tested with a factorially designed series of experiments developed by the forensic engineers to quantify the effect of service temperature.

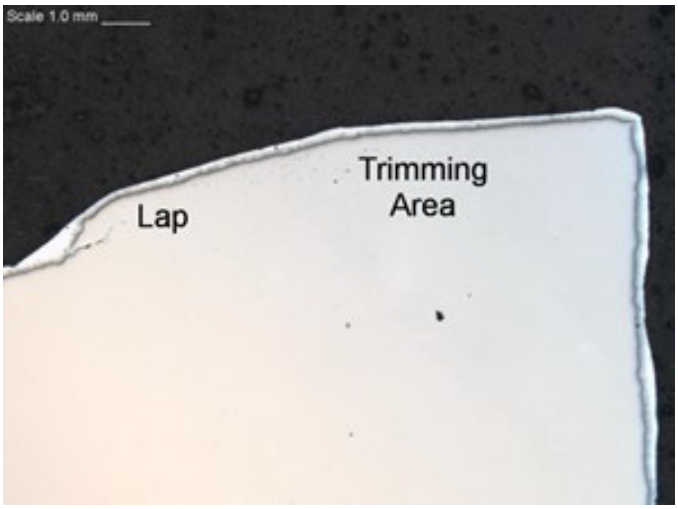

Figure 11
The trimming area with underlying lap.

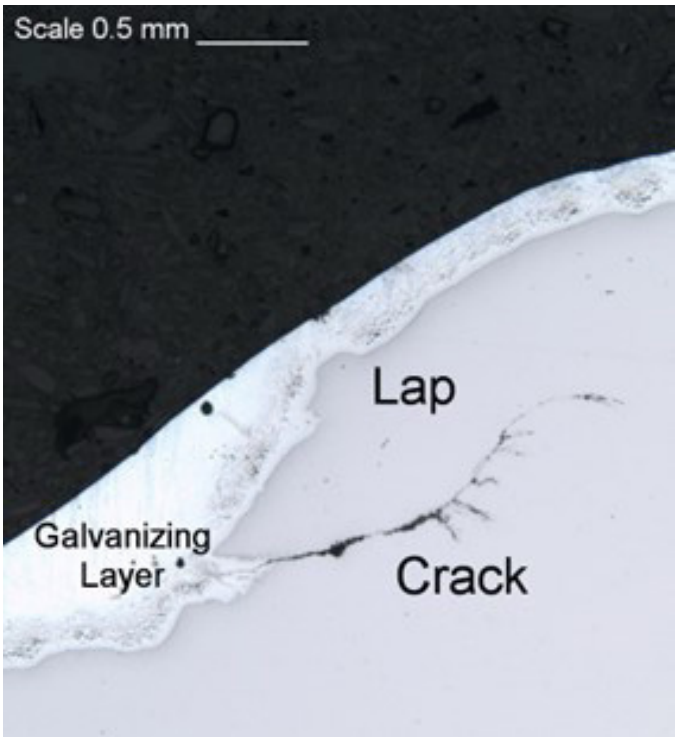

Figure 12
Magnified view of the crack in the trimming area.

Charpy Tests on Raw Material and Anchor Shackles

Charpy tests are employed to measure the notch toughness or impact strength of a metal, that is, its ability to absorb energy prior to failure. In this test, a notched specimen is broken by impact from a falling pendulum, and values are determined by the height the pendulum striker rises in the absence of a specimen versus the height the striker rises after the fracture of a specimen. The governing specifications for Charpy tests are ASTM A370-19e1 "Standard Test Methods and Definitions for Mechanical Testing of Steel Products"[4] and CAN/CSA G40.20 "General Requirements for Rolled or Welded Structural Quality Steel."[5]

Under CAN/CSA C83-96 Section 6.2.4 Energy Absorption/Toughness, the Charpy test criteria evaluate the raw material's conformance in Level 1 Energy Absorption, not the subsequent components, with the testing performed at -20°C and a minimum 20 Joules requirement to pass as Level 1 material.

Furthermore, ASTM E23-12c: "Standard Test Methods for Notched Bar Impact Testing of Metallic Materials"[6] clearly expresses in its Appendix XI that Charpy tests do not reflect actual service stress conditions. Charpy results are not an effective means of retroactively assessing a component once it has been placed in field service. Processed metal components become anisotropic — they have properties that depend on orientation as discussed in Hertzberg[7] and Hosford and Caddell[8].

Although it was clearly laid out as a "variable" of the raw material to be inspected prior to production rather than as an "attribute" inspected in a finished component, Company C attempted to verify the Charpy test behavior of 150 shackles taken from the utility company inventory using the tightened inspection format of Table A1 of Appendix A of CAN/CSA C83-96. A variation was discovered in the response at -20°C, in which some sample bars did not meet the specified minimum value of 20 Joules.

The variation appeared to be related to the location of the samples, taken from one of three places in the body of the shackle shown in **Figure 13**, with those in #2 central position testing significantly lower and not meeting the acceptance criteria. These are not the area where the shackle failed adjacent to the clevis pin hole, shown in

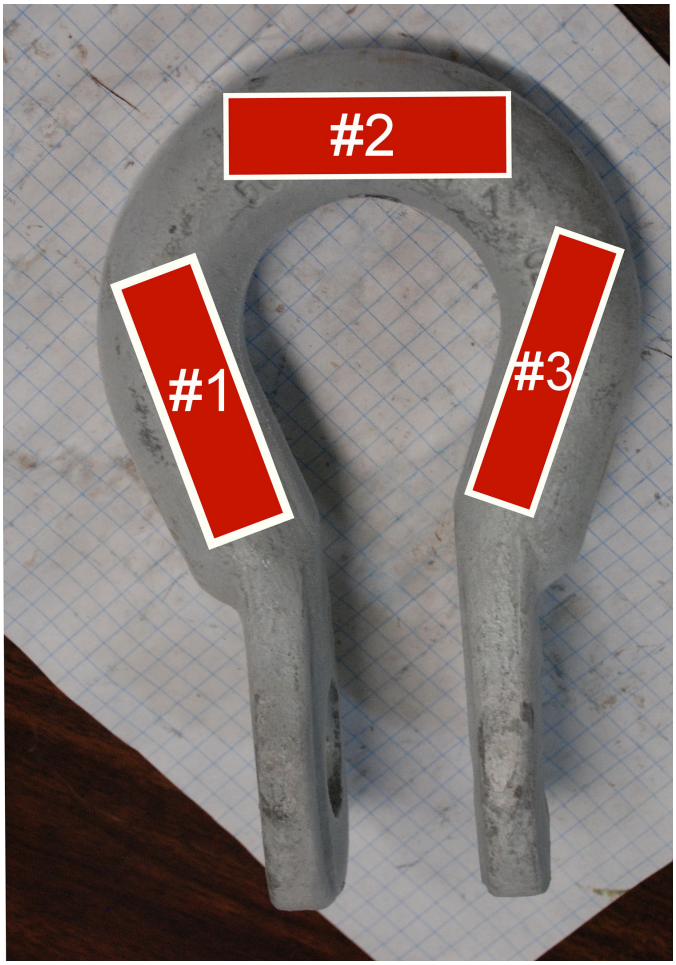

Figure 13
Locations of typical Charpy tests for Company C.

Figure 5. A summary of data from the Charpy tests is presented in **Figure 14**.

Place	Lower (J)	Upper (J)	Accept?
Position 1	21	27	Yes
Position 2	15	17	No
Position 3	21	27	Yes

Figure 14
Overview of Charpy testing results range by Company C.

Company C's series of tests further involved cutting cross-sections of the four portions of the arm adjacent to the pin and evaluating these for the presence of cracks/laps arising from the forging process. This was performed by Company B on contract. Six hundred specimens were mounted, polished, and examined under low power using an optical microscope.

There were seven cross-sections (4.67%) that showed internal cavities longer than 2.5 mm at a location 5 mm or less from the surface on the inner pin side. There were cracks longer than 1.5 mm at a position no more than 2 mm away from the critical area, and only 35 shackles possessed lap defects that could have been detected by magnetic particle inspection (MPI) methods, according to the authors of the Company B summary report.

At this point of the investigation, it appeared that the components' raw material had not met the minimum specified Charpy values for one group of specimen orientation. It became clear that there were cracks associated with lap defects, of which there should be none in an acceptable batch under the CAN/CSA C83-96 Table 3 requirements. This information confounded the owners because a clear decision on acceptance or rejection could not be made based solely on the summary prepared by Company B. A different approach was required to solve the puzzle, and the task was assigned to the forensic engineers.

Cold Temperature Shackle Tensile Testing

A statistically valid fit-for-purpose testing program[9,10] was designed by the author to evaluate a sample of the 2525 batch of shackles procured by the project manager from the European manufacturer but that had not entered service. The program design included the following elements:

1. Selection and design of a customized test method with factors and response functions chosen to emulate field service tension conditions;
2. Selection of a set of temperatures representing the winter extremes encountered by the product at the site in Northern Canada's high latitudes;
3. Procurement of specialized fixtures and a cold-environment stage for the tensile testing machines;
4. Procurement of a random sample batch 2525 shackles held in the utility's stock;
5. Capture of data and live analysis of shackle attributes during the tests; and
6. Post-test metallurgical analysis of shackle fracture surfaces (if these were created).

An additional phase consisting of metallographic specimen evaluation of the cross-sections of the shackles at the midpoint of the eye was instigated to compare and contrast these with results obtained independently by Company B.

The factorial design was chosen with two factors set at two levels, with response functions shown in **Figure 15**, to determine if these factors could explain the field behavior.

Experimental Factor	Low Level	High Level
Load	Reusability load	Breaking/max load
Temperature	-20 Celsius	-40 Celsius

Response Function	Measurement Units
Permanent deflection, nominal rated and maximum load	Percent
Yield strength in tension	MegaPascals
Breaking load in tension or maximun load borne	kiloNewtons
Elongation percent at failure	Percent
Reduction of area at failure	Percent
Mode of fracture (if failure occurs)	N/A descriptive
Time to facture (if failure occurs)	Minutes and seconds

Blocked Variable	Measurement Units
Crosshead speed of machine	mm per minute
Time held under load	Minutes
Shackle production batch	N/A descriptive

Figure 15
Factorial experiment design elements.

Figure 16
Samples as-received from Batch 2525 stock.

Twenty shackles were obtained from the utility's warehouse, and randomly assigned (**Figure 16**) reference identification numbers. The testing run sequence order was set from first to last, according to the size of a random number generated on a calculator, for each run of the factorial design. These shackles were placed into simulated cold temperature field service conditions, with similar parameters to the Company A room temperature tensile test assessments.

Tensile tests were performed by Company D in the special environmentally controlled chamber on an Instron universal test machine for the nominal rated load, and then on a SATEC universal test machine for the maximum load levels. Universal testing machines include electromechanical and hydraulic systems to perform static testing, including tensile, compression, bend, peel, tear, and other mechanical tests. The utility calculated that the maximum load on the shackles would be 127 kN, not including wind oscillation and other cyclic loads. The configurations are shown in **Figures 17** and **18**.

Figure 17
Environmental control stage on the Instron tensile test machine for rated load tests.

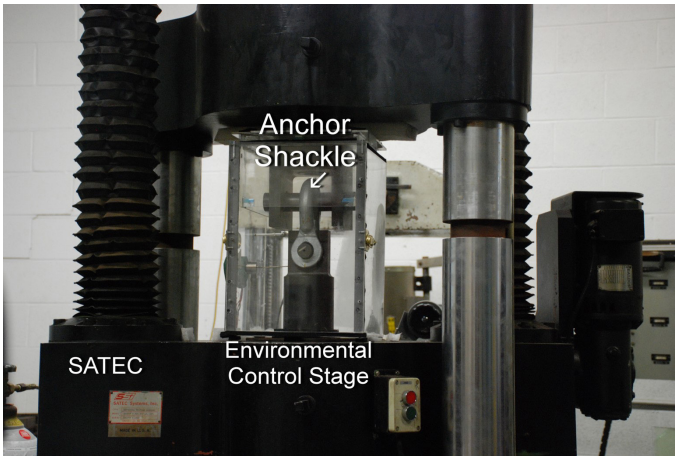

Figure 18
Tensile testing fixture with atmosphere control cabinet on the SATEC machine for maximum load tests.

With respect to a potential Daubert challenge, the hypothesis was tested using well-known techniques on widely owned tension testing equipment used throughout the industry with experimental design methods that are also well-known and employed. Tensile test results have error rates that derive from material property variability. The equipment is calibrated on a regular basis by the laboratories, according to international standards. Tensile testing has widespread acceptance within industry as a method of comparing and assessing material properties. Organized testing was first introduced by the railway companies. In 1901, the first standards were promulgated by the American Society for Testing and Materials (ASTM).

The first stage of mechanical testing consisted of temperature conditioning followed by a low-level load test. Specimens were cooled to the specified test temperature and held long enough to reach thermal equilibrium. Then, they were inserted into the Instron machine, and a pre-load of 0.7 kN was applied. The cross-head was then extended at a rate of 40 mm/minute up to a load of 374 kN (the reusability load) where it was held for 5 minutes before the load was released. The reusability load level is defined on page 319 of the CSA Standard — 374 kN compared to the 440 kN rating of a Number 9 Anchor Shackle.

For the second stage of mechanical testing, the shackle was then conditioned again at the test temperature and moved to the SATEC test machine. The specimen was loaded at a rate of 8 mm/minute to a load of 440 kN, where it was held for 5 minutes. The specimen was loaded at the same strain rate to a load of 530 kN to 575 kN, at which point the fixture pins began deflecting, and the experiments were terminated.

Results of the load testing showed that there were no temperature effects on tensile performance in fitness-for-purpose testing (**Figure 19**). At -40°C, which is a typical minimum winter temperature for Northern Canada, none of the test shackles fractured. As seen in the next section, 1-mm lap cracks were subsequently found to be present on the inboard edges — a little more than 5 mm from the critical area. Despite the presence of these defect-like indications, through-cracks neither developed from the lap positions nor originated from the critical corner when subjected to applied tensile forces up to 575 kN, which is more than 13% above the maximum rated shackle strength of 506 kN.

Factor Levels	Coded Shackles	Factor Details	Response
Low, low	1G, 1A, 2C, 1E, 2B	374 kN reusability load, -20 C	No fractures initiated
High, low	1G, 1A, 2C, 1E, 2B	Max. 575 kN load, -20 C	No fractures initiated
Low, high	1F, 1C, 1I, 1D, 2E	374 kN reusability load, -40 C	No fractures initiated
High, high	1F, 1C, 1I, 1D, 2E	Max. 575 kN load, -40 C	No fractures initiated

Figure 19
Results at factor level settings for fracture initiation.

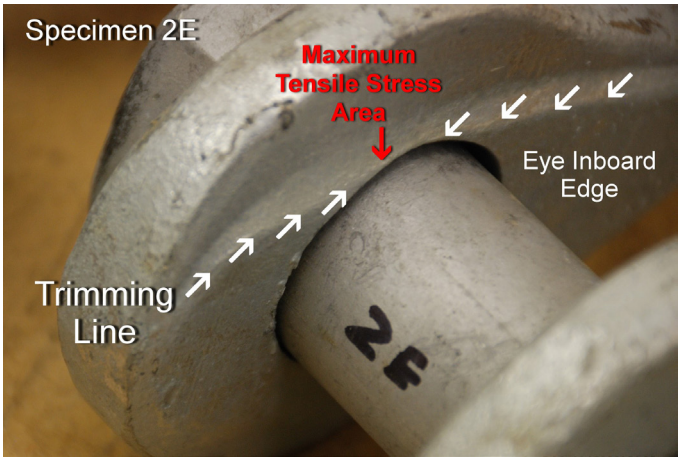

Figure 20
The poor intersection of the trimming line on Specimen 2E.

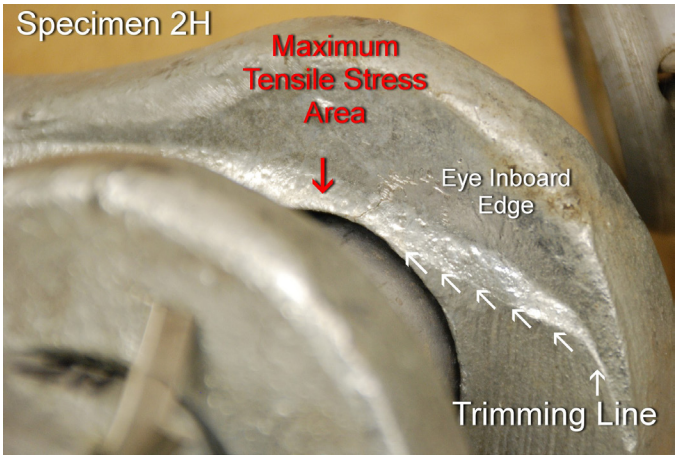

Figure 21
Example of poor trimming line intersection on Specimen 2H.

Illustrations of Poor Trimming Line Geometry

As previously described, the shackles must be trimmed after forging to remove excess flash left over from the forging process. The working hypothesis was that fracture initiation from stress concentrators that develop when the trim line coincides with the edge of the eye — the area of highest stress when the shackle is under load. In field service conditions, these local conditions may create the circumstances for crack propagation and failure.

To illustrate the trimming issue, **Figures 20** and **21** show the trimming line meeting the edge of the eye on specimens 2E and 2H.

Post-Test Sectioning and Metallography

At Company E, the group of 10 shackles were sectioned in a manner similar to the European laboratory, at the midpoint of the eye (**Figure 22**), to inspect the critical area for the presence of lap defects arising from the post-forging trimming process.

Of 40 cross-sectional specimens from 10 shackles, eight were enumerated with laps in the plane of center of the eye, with two laps near the critical area 5 mm from

Figure 22
Specimens cut and polished for metallographic assessment of the critical area.

the eye edge on the inboard side of the shackle arm. These ranged from 0.2 mm long by 0.25 mm wide to 1.8 mm long and 0.6 mm wide, which were comparable to those found by Company B. These are Class B defects (very serious), according to CAN/CSA C83.115-96.

Seven of the laps were located along the inboard edge of an arm, more than 8 mm away from the critical corner. The cross-section of 2E-A was unremarkable under low-power microscope. An 0.8-mm-long by 0.2-mm-wide crack in 2E-B was observed around the midpoint, as shown in the figures. The examination of mounted, polished, and etched specimens using a metallograph (metallurgical microscope) showed that these laps had not opened during the tensile testing processes, such that no through-cracks were observed in any of the 10-shackle sample. Representative images are shown in **Figures 23** through **29**.

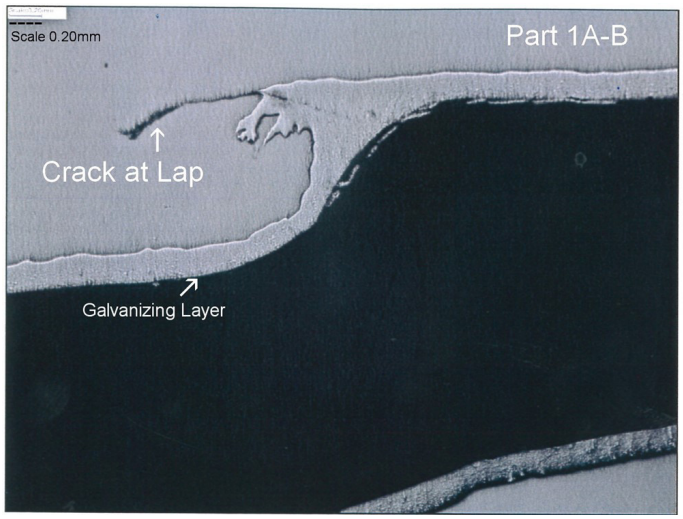

Figure 23
Polished cross-section showing crack at lap in Part 1A-B.

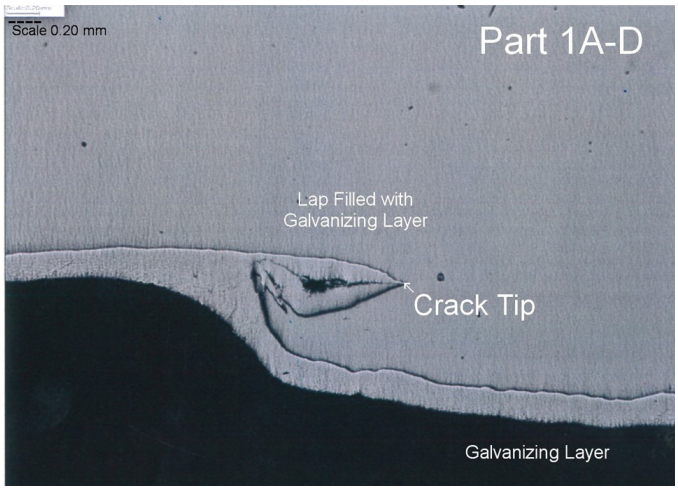

Figure 24
Polished cross-section showing crack tip in Part 1A-D.

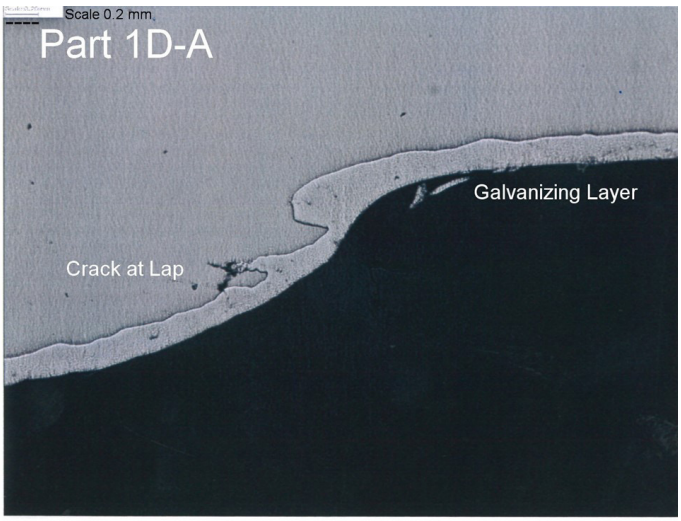

Figure 25
Polished cross-section showing crack at lap in Part 1D-A.

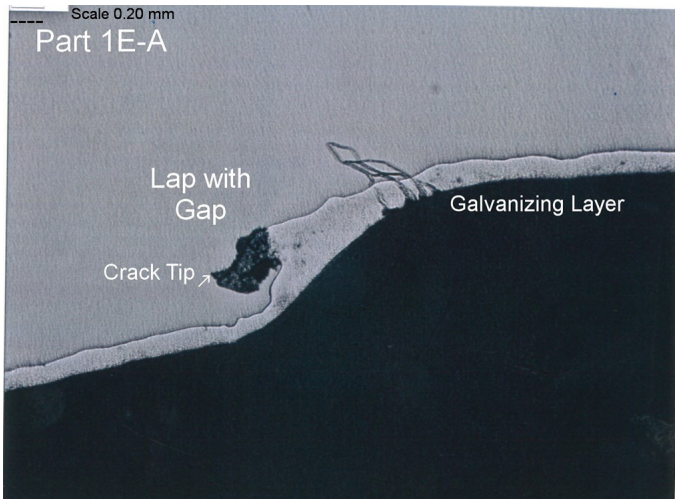

Figure 26
Polished cross-section showing crack tip by gap at lap in Part 1E-A.

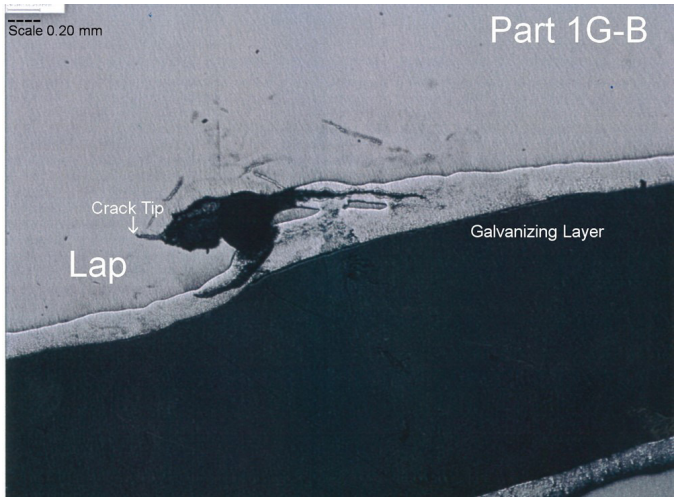

Figure 27
Polished cross-section showing crack tip at lap in Part 1G-B.

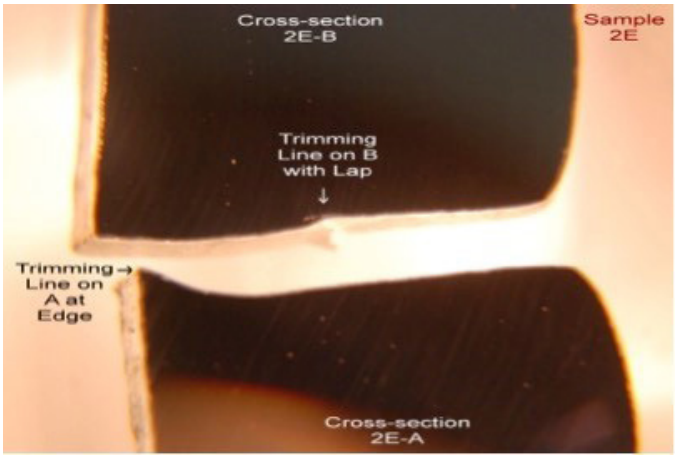

Figure 28
Mounted and polished cross-section of 2E-B with laps.

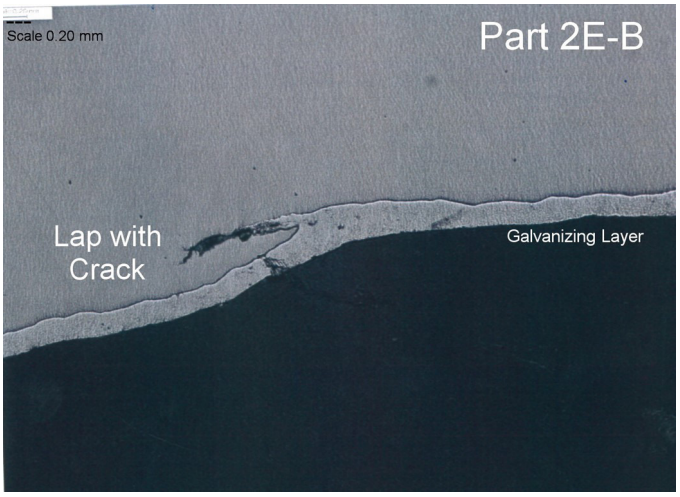

Figure 29
Polished cross-section showing the lap with crack on Part 2E-B.

Discussion

Validity of Observations Established by Representative Statistical Sampling

Through careful factorial design and random sampling, observations made on the random sample group were reasonably extrapolated to be representative of the whole population of shackles and showed results comparable to those in other assessments. Most importantly, the tests were able to replicate extreme loading conditions and temperatures that the shackles would experience in field service.

Insights Confirmed and Gained from the Shackle Assessment

The shackle batch evaluation programs have revealed evidence of conformance issues with Class B defects at frequency levels measured to be higher than the 1% limit in CAN/CSA C83-96 (2011), confirming the following insights:

a. The effects of trimming during the manufacturing process, located at the critical area of the shackle eye, disguised forging lap defects there;

b. Galvanizing in a subsequent step prevented detection of surface cracks by non-destructive techniques, such as magnetic particle inspection (MPI) or dye penetrant inspection (PTI); and

c. Company B identified the trimming line adjacent to the crack origin in the field failure shackle, possibly on both sides, as a factor in the development of the crack that led to the field failure of the anchor shackle.

The assessment supported a new insight that a statistically significant percentage of the shackles in Batch 2525 have forging lap defects, but few cracks are found at the critical eye intersection.

Forging Defects in Metal Products

Forging defects are well known to be a source of concern in components, such as hooks used for lifting materials. Laps introduce stress concentrations and redistribute loads under service conditions in a way that may not have been anticipated during the original design process.

Generally, a manufacturing process should have an inherent ability to avoid the creation of forging laps. If not, active factory quality control processes should be set to detect them and thus allow the manufacturer to remove them or mitigate their effect in a subsequent operation. In this particular instance, the Company A forging process created the laps in a tempered martensite microstructure sensitive to cracks, but did not remove them during subsequent trimming. Laps were then obscured with a galvanizing process. The forging lap crack acts as a stress concentrator in tempered martensite, magnifying the localized stress to a magnitude well beyond the nominal yield stress.

This combination rendered the quality of the shackles unacceptable per the AQL terms of CSA C83.115-96. They should not have entered service as part of an important transmission line assembly if the CSA C83.115-96 criteria had been the sole standard applied to judge their suitability. The anchor shackles would not comply with the letter of the standard.

Critical Defect Characteristics

Laps and associated cracks were observed in a statistically significant proportion of the sample of shackles

evaluated by the forensic engineers (and within the samples evaluated by the European laboratory); however, these were in positions away from the critical region. The designed experiments could not induce fractures when overstressing the shackles under extreme low temperature conditions even in the presence of these defects very close to the critical locations.

The forensic engineering investigation showed that the position of the lap relative to the critical area was the most significant factor when assessing its potential effect on field performance. Unless a forging lap crack intersects exactly with the critical eye region under the highest tensile stress, the pre-condition for induction of a shackle arm failure under field loading is not met. Cracks at the laps in the shackles did not propagate across the arm at the eye to break the shackle when loaded to 575 kN at -40°C.

Probability of the Presence of Forging Lap Cracks

The population of shackles produced for the project likely contained an unacceptably high level (approximately 125 of 2,600, about 5%, compared to the 1% allowable limit) of actual forging lap defects that would not meet CSA C83.115-96 conformance requirements. The probability of a shackle possessing a forging lap crack at the critical juncture was a fraction of that because of the reduced odds of the coincidental geometry in which a forging lap intersects the critical stress area.

The shackles' tensile behavior was shown to be insensitive to very low temperatures. However, the presence of forging laps at a critical area that led to a functional failure event in the field (a Class A Critical unacceptable defect according to the CSA C83.115-96 criteria) disqualified the entire shackle product Batch 2525 as unsuitable for service in critical transmission line infrastructure. The situation was exacerbated by the demonstrated fact that the defects could not be detected retroactively with nondestructive testing techniques.

Ineffective Analysis through Charpy Testing

Charpy testing alone could not distinguish the defect and was an inappropriate screening tool. That method is best used as a quality tool to qualify raw materials, rather than to retroactively approve components — an aspect overlooked by Company C. The forging process changes the fracture toughness of the steel by changing its microstructure permanently, and creates variability within the component by straining the metal such that the Charpy results are skewed when compared to the original material.

Factorial Design Experimental Program Determined the Root Cause

In contrast, the factorially designed program tests subjectively qualified the shackles for use in transmission service, independent of the CSA C83.115-96 criteria, with the explicit restriction of a shackle being redundant within the tower array configuration. The forensic engineer's experimental design evaluated the fault and then tested it with a relevant simulation that could be extrapolated to the set of shackles in the batch. This allowed the root cause to be put into perspective.

Summary

Company A's Number 9 anchor shackle manufacturing process created a technical issue, the magnitude of which could not be resolved by visual inspections on components of the transmission line once a fracture incident had occurred. The utility and Company C ineffectively attempted to requalify the components by retroactively applying one of the raw material acceptance criteria; however, passing a Level 1 Charpy toughness test generally does not replicate field service conditions. The findings of their examination only served to confuse whether the components should have been accepted in the first instance, when cross-sections of the shackles found cracks that were not permitted by the governing standard.

To determine the scope of the problem and to reassure the owner of the fit-for-purpose safety of the Number 9 anchor shackles on the transmission line, it was necessary to carefully design a tensile test to replicate the most extreme service conditions and then apply statistical techniques.

Epilogue

The technical analysis of the root cause by the forensic engineers was employed by the utility's operations group to focus its shackle removal and replacement plan by the project management firm to refine the procurement specification for shackles. To greatly reduce the opportunities for additional field fracture development while avoiding the high cost of full replacement, the shackle arrays were theoretically checked for redundancy. Those in primary load-carrying positions were selected for removal and replacement. The opinions and results were cited in the discussions with the manufacturer about compensation for the replacement program costs prior to litigation proceedings.

Acknowledgements

The author would like to recognize the excellent metallography work performed by Mr. Josh Greenblat.

References

1. For more information on applied quality theory in manufacturing practice, visit American Society for Quality at ASQ.org, and see https://asq.org/quality-resources/quality-glossary/.

2. *Communication and Power Line Hardware*, CAN/CSA C83-96 (2011), Canadian Standards Association, Etobicoke, ON, Canada, 2011.

3. *Communication and Power Line Hardware: Appendix J*, CAN/CSA 83.115-96 Shackles, Canadian Standards Association, Etobicoke, ON, Canada, 2011.

4. *Standard Test Methods and Definitions for Mechanical Testing of Steel Products*, ASTM A370-19e1, ASTM, West Conshohocken, PA, USA, 2019.

5. *General Requirements for Rolled or Welded Structural Quality Steel*, CAN/CSA G40.20, Canadian Standards Association, Etobicoke, ON, Canada, 1998.

6. *Standard Test Methods for Notched Bar Impact Testing of Metallic Materials*, ASTM E23-12c, ASTM, West Conshohocken, PA, USA, 2012.

7. Richard W. Hertzberg, *Deformation and Fracture Mechanics of Engineering Materials*. Hoboken, NJ, USA: Wiley, 1976, pp 327-335.

8. William F. Hosford and Robert M. Caddell, *Metal Forming: Mechanics and Metallurgy Second Edition*. USA: Prentice Hall, 1993, pp 244-303.

9. George E. P. Box, J. Stuart Hunter and William G. Hunter, *Statistics for Experimenters: Design, Innovation and Discovery*. Hoboken, NJ, USA: Wiley, 2005.

10. Bert Gunter and Daniel Coleman., *A DOE Handbook: A Simple Approach to Basic Statistical Design of Experiments*. USA: CreateSpace, 2014.

Resolving Schedule Delay Claims with Forensic Analysis

By Michael D. Stall, PE, DFE (NAFE 955M)

Abstract

This paper demonstrates how the principals of forensic engineering can be applied to evaluation of schedules, daily diaries, status reports, meeting notes, and other project documentation to determine why delays occur on a project and which parties are responsible for delays. To understand the actual project history, the forensic engineer should conduct a thorough and fair evaluation of all available project documentation to understand the contractual requirements, project milestones, effects of changes, magnitude of delays to the Critical Path, and the basis of the delay claim dispute. The forensic engineer should have sufficient knowledge and experience with project planning, scheduling, and cost estimating to understand the technical basis of the project schedule. He or she must also evaluate and understand the schedule resource loading methodology, schedule logic structure, validity of the activity durations, actual sequence of events, and the material issues that affected the Critical Path. Use of the original planning software is usually necessary as well. The forensic engineer should conduct an impartial technical evaluation that addresses the important and material issues so responsibility for the delays can be determined and proven with a reasonable degree of certainty to resolve the dispute fairly.

Keywords

Critical Path Method, network schedule, Critical Path, critical activities, positive float, negative float, predecessors, successors, activity relationships, resource loading, activities, submittals, concurrent delays, procurement, logic, constraints, durations, earned value, status, progress, forensic engineering

Introduction

Planning and scheduling are two powerful project management tools if they are developed in a disciplined manner and maintained throughout the life of a project. However, if planning by the contractor is superficial — and schedules are not detailed and structured in a logical network format — the plans and schedules will have little or no value to the contractor for managing the work or to the owner and architect for understanding earned value and progress. Planning helps determine how to perform work, and scheduling applies a timetable to those plans. Plans must be realistic (and schedules have to be achievable), or they will be used to document failure to meet the schedules.

To demonstrate the forensic schedule evaluation process, this paper evaluates a $25-million project that was completed several months after the contract completion date. In this case, the contractor claimed the owner caused all of the delays; therefore, he was entitled to $2.6 million in direct and indirect costs as a result.

CPM Network Schedule Activities

A properly constructed Critical Path Method (CPM) network schedule, regardless of the software utilized, has several key components that include:

- Critical Path — the path through working activities that has the least amount of float.
- Activity relationships — which activities must be completed prior to starting new activities.
- Date constraints — when the scheduler makes mandatory start dates rather than making them a function of the prior activities status.
- Resource loading — applying the manpower levels to each activity that are required to complete the activity in the time scheduled based on experienced or estimated productivity.

Michael D. Stall, PE, 77 Sugar Creek Center Blvd. Ste 210, Sugar Land, TX 77478, 713-627-1122 (extension 1), mike@mribuilds.com

- Real time resource adjustments based on experience — when experience shows that the productivity level of the work being performed is either better or worse than planned, and the resources are either increased or decreased to compensate for the experience.

These are required to properly develop and maintain a CPM schedule as an effective management tool. The first components of a CPM schedule are the activities, which are graphical representations of the work items required to complete a project or part of the project in a certain amount of time.

Figure 1 shows what could be considered to be several typical construction activities at some point in time during a project's scheduled life. A predecessor is an activity that occurs before the successor activity, and the relationships between the activities define the CPM Network.

The schedule activities shown in this graphic are several typical construction activities that are identified in terms of activity description, activity duration, criticality, and relationships with other activities. The activities are represented as they were scheduled without progress measurement.

CPM Network Schedule Activity Relationships

Figure 2 shows the same activities from **Figure 1** with the addition of the types of relationships between the activities identified with green boxes. The most often-used and therefore most important schedule activity relationships consist of the following relationship types:

- Finish-To-Start (FS) — This is where one activity must finish prior to starting the succeeding activity.

- Start-To-Start (SS) — This is where one activity cannot start until the preceding activity starts.

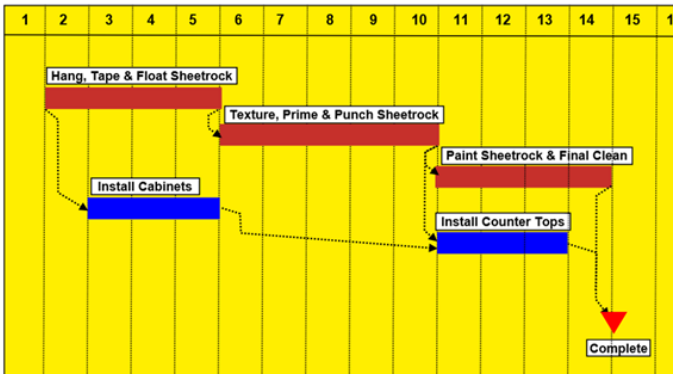

Figure 1
Schedule activities.

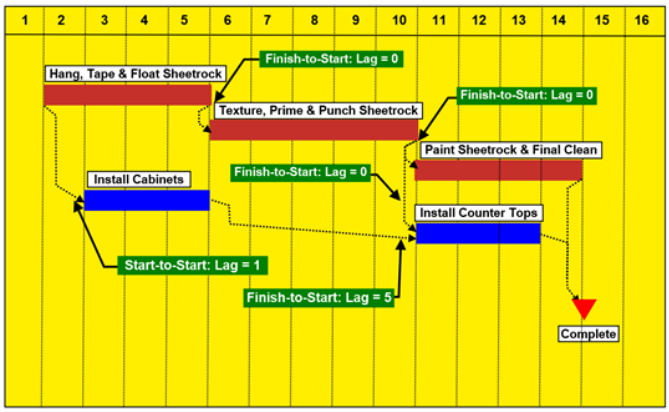

Figure 2
Activity relationships.

Each of these relationship types can be modified by a lag factor, which is the time difference between the predecessor and successor activities. For example, the first blue-colored activity in **Figure 2** cannot be started until one day after the preceding activity starts. The activity relationships also create the Critical Path (shown in **Figure 2** as the red-colored activities). They are on the Critical Path because there is no float between the critical activities while there is float between the blue-colored activities.

Date Constraints Override Logic

When an activity is constrained by a date, the logical relationships that would normally drive the activity start date as a function of preceding activity durations is overridden by the date constraint.

Figure 3 shows a situation where the "install counter tops" activity has been constrained by a date — that is, the scheduler has determined the activity should be started

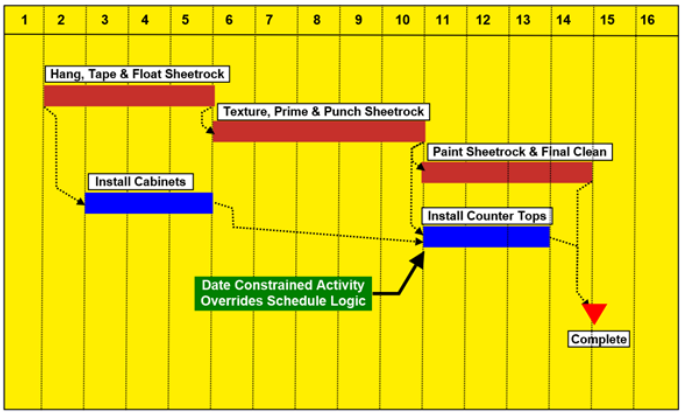

Figure 3
Date constrained activity.

on a certain date rather than be driven by logical activity relationships.

In this example, if the "texture, prime & punch sheetrock" activity were to take a few days longer, the "install countertops" activity will not move with the driving activity relationships because it is constrained by the date requirement. When the date-constrained activities do not move, the schedule provides misleading status information that includes incorrect float times and start dates that will not occur when shown on the schedule.

Schedule Activity Resource Loading

Resource loading is manpower. **Figure 4** shows examples of activity resource loading. For this case, the resources refer to the level of manpower that is to be used for each work activity for each day of the activity duration. The resource loading is expressed in terms of manpower per day for each activity. The basis for realistic activity durations is the resource loading. Without realistic resource loading and knowing earned value, the activity durations and progress are guesses.

Figure 5 shows an example of how resource loading defines and determines the activity duration and the quantity of items being installed. The resource loading is based on productivity factors, such as how many man-hours are required to install a square foot of steel stud and sheetrock walls. This graphic demonstrates how realistic installation unit rates allow the scheduler to determine realistic and achievable activity durations. Effective planning and scheduling require monitoring and maintenance of the schedule to include actual project performance in the schedule updates that provide an accurate picture of the progress.

Figure 6 shows how monitoring and maintaining realistic durations must include the actual experience to determine the differences between the planned and actual performance. The actual performance experienced will result in changes to activity durations — shorter if performance is better than planned and longer if performance is worse than planned. In this case, the actual installation rate was 90 square feet per man-hour, which is less than the planned rate of 106 square feet per man-hour, so the schedule duration must be extended to account for the worse-than-planned installation rate.

Forensic Schedule Evaluation Goals

The goals of forensic schedule evaluation include evaluation of the CPM network scheduling process elements that are required to develop a realistic and achievable schedule with a well-defined Critical Path that can be evaluated in terms of what delays occurred and which parties (if any) not in the control of the contractor caused delays to the Critical Path.

To determine what was required and actually occurred during the life of the project, the following issues should be evaluated and understood:

- Contract terms and conditions.
- The basis of the contractor's delay claim.

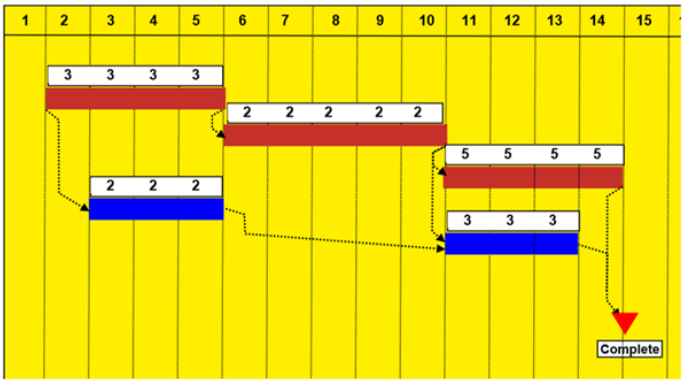

Figure 4
Activity resource loading examples.

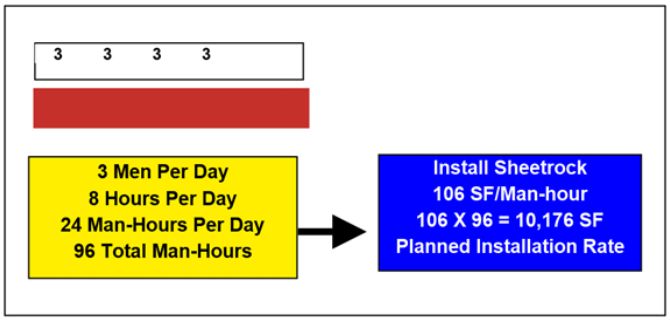

Figure 5
Resource loading establishes realistic activity durations.

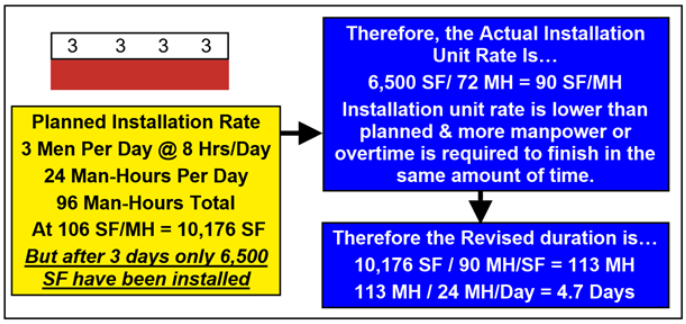

Figure 6
Monitoring and maintaining activity durations with actual experience.

- Determine if there was an approved project schedule.
- Determine if there was a procurement schedule.
- Understand the submittal scheduling process.
- Determine if the schedule met the contract requirements.
- Understand the activity relationships and schedule logic.
- Understand the activity resource loading methods.
- Determine which activities were on the Critical Path.
- Understand if there were concurrent delays.
- Compare the actual manpower to the planned manpower levels.
- Understand logic and resource differences between the different schedules.
- Determine if the activity durations are realistic.

Methodology

The forensic evaluation must be fair and thorough. The actions related to the dispute by all participants must be evaluated to determine and apportion responsibility for delays. The schedules provided by the contractor were evaluated to determine the following:

- If the schedules met the standard of care required for large projects, which is typically defined in the contract.
- If the schedules were functional management tools with proper logic that could be used to plan and schedule the work based on the available resources.
- If the schedules could be used to measure earned value (and therefore the actual status of the activities/project) and make adjustments as necessary.

A functional and valid CPM network schedule must include valid resource loading, valid activity durations, and proper logic. If not, it cannot be used as a management tool or as a basis to prove a delay was caused to the Critical Path by parties not in the control of the contractor.

Standard of Proof Required for Delay Claims

The standard of proof required for delay claims has been established by the Courts in Wilner v United States, 26 Cl. Ct. 260 (1992). The following elements provide a basis for the standard of proof required to prove a delay claim:

- *Realistic schedule*: The starting point for a compensable claim must be a realistic schedule that establishes the contractor's intent and documents actual experience.
- *An achievable schedule*: Courts hold that claims will be disregarded when schedules that have not been agreed to by the parties (or that the contractor never intended to follow or could not achieve) are used as a basis for the delay claim.
- *Submittal schedule*: The submittal process is important to work progress because this is how the contractor obtains approval for procured items from the architect during the life of the project. The contractor must schedule each submittal because submittal approvals are a prerequisite to the start of procurement and construction. If the submittal review process is not scheduled — or is scheduled unrealistically — subsequent construction activities that are a logical function of the submittals cannot be started until the submittals are reviewed and approved by the architect and/or owner. Inaccurate submittal scheduling results in inaccurate construction scheduling, and inaccurate schedules cannot be used as a basis for establishing a delay was caused to the Critical Path.
- *Realistic resource loading is required*: Schedules that contain unrealistic resource loading cannot form a delay claim basis because without resource loading, the activity and schedule durations cannot be realistically established. Courts have determined that CPM schedules must include valid resource loading as a required scheduling element.
- *Proper schedule maintenance is required*: When schedule updates are used to report the project status, the contractor must start with a realistic

plan and prove that it has taken appropriate action to: (1) revise durations to reflect actual experience; (2) revise logic to address out-of-sequence work to provide a network analysis system that reflects the actual status of the project and the current critical path; and (3) track actual start and finish dates.

- *Schedule changes must be communicated and documented*: The contractor must abstain from any manipulation of logic in updates to conceal contractor activities that could not be completed as scheduled. No material changes in important schedule elements, such as resource loading or logic ties, shall be made without informing the owner of the changes.

These parameters define the standard of proof for a delay claim that are required to prove a delay was caused to the Critical Path. A contractor's delay claim that is based on a schedule with invalid resource loading, improper/missing logic, and unrealistic activity durations should be denied because a faulty schedule cannot be used to prove the schedule was accomplishable — or that a delay to the Critical Path was caused by others.

Evaluation of CPM Network Schedule

Detailed evaluation of a CPM network schedule must be done with the native files and the scheduling program originally used to develop the schedule. **Figure 7** shows part of a graphical print-out that shows bars and lines, but no functional evaluation can be performed with this picture.

Without the native files and the scheduling software, the important informational reports, such as resource loading, activity logic relationships, float, predecessors, successors, and earned value (progress), cannot be accessed and evaluated.

Figure 8 shows one example of the type of information and detail that can be obtained from the native files using the appropriate software. It is a screen shot from the scheduling software program that was used to generate the native files. This particular report page shows the activity name, activity cost code, the resources assigned to this activity, the manpower units per hour, the resource availability window, and the budgeted quantity. This report showed that the resource loading was incomplete, undefined, and worthless for measuring earned value or progress.

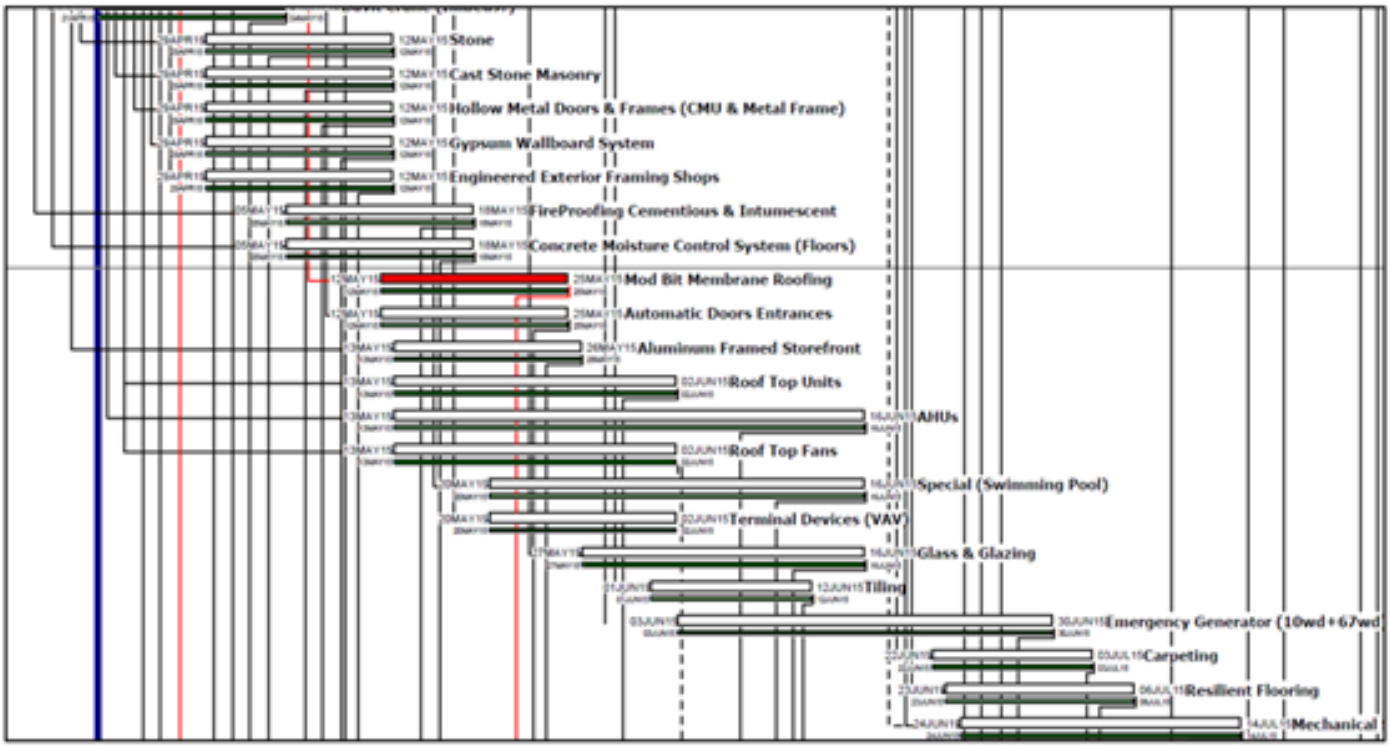

Figure 7
Graphical prints are not useful for accurate forensic evaluation.

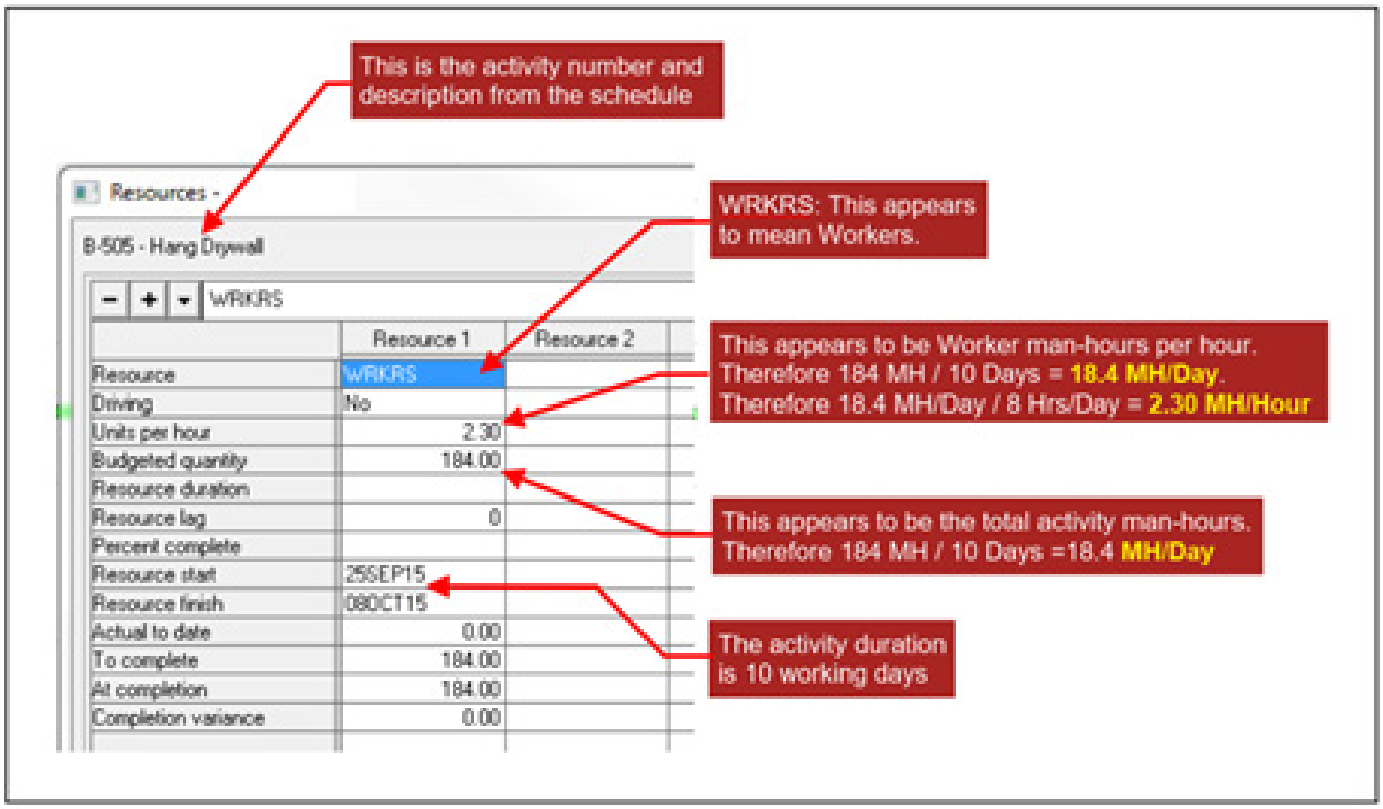

Figure 8
Native files provide information for detailed forensic evaluation.

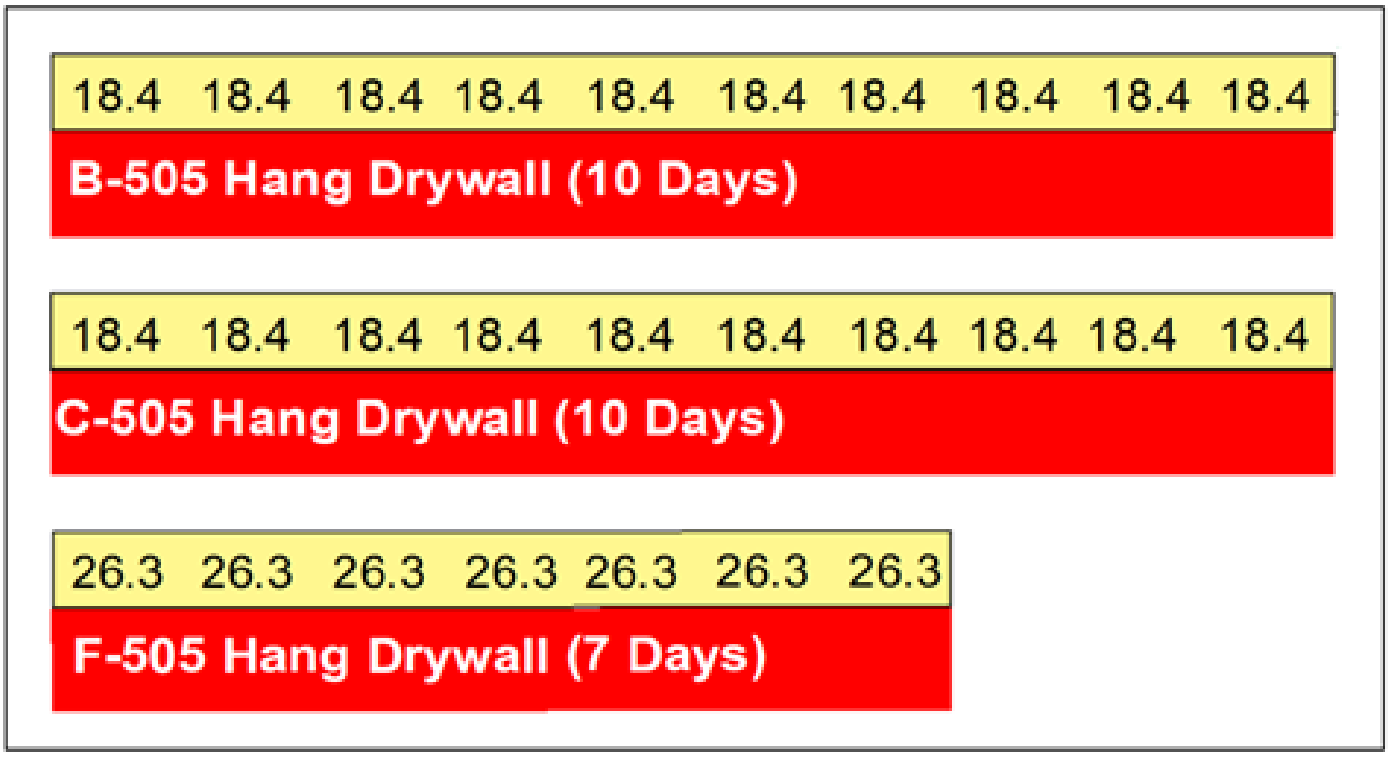

Figure 9
Evaluation of native files exposes faulty resource loading.

Figure 9 shows the manpower resource loading factors that were applied to three drywall installation activities. These are three examples of activities with faulty manpower loading.

The resource factors shown (18.4 and 26.3) do not make sense with respect to actual resources such as manpower, equipment, or other required resources. For example, it is impractical to work partial man-days or man-hours on an activity, which is what the values indicate — that is, resources should be assigned to activities in a manner that would actually be done on a job site rather than a mystery factor that provides no basis for measuring earned value.

Figure 10 shows the same three activities that were illustrated in **Figure 9** with the addition of the drywall quantities by area in the middle yellow boxes and the calculated unit installation rate in the blue boxes.

Figure 11 shows results of the quantities, resources, and unit rate evaluation compared to the *Walker's Building Estimator's Reference Book*, 26th Edition, drywall installation unit rate of 106 square feet per man-hour. It demonstrates how the contractor's resource loading has provided activity durations that are not realistic and cannot be attained. In Area B, for example, the scheduled unit rate of 616 square feet per man-hour is unrealistic and

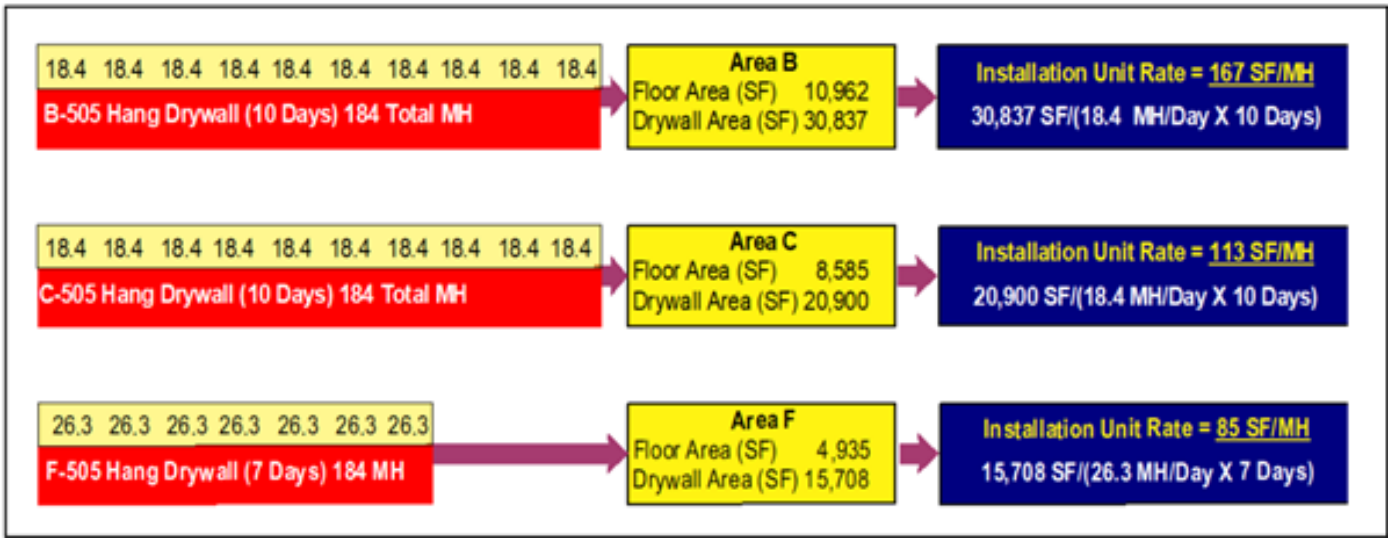

Figure 10
Evaluation of native file exposes widely divergent installation unit rates.

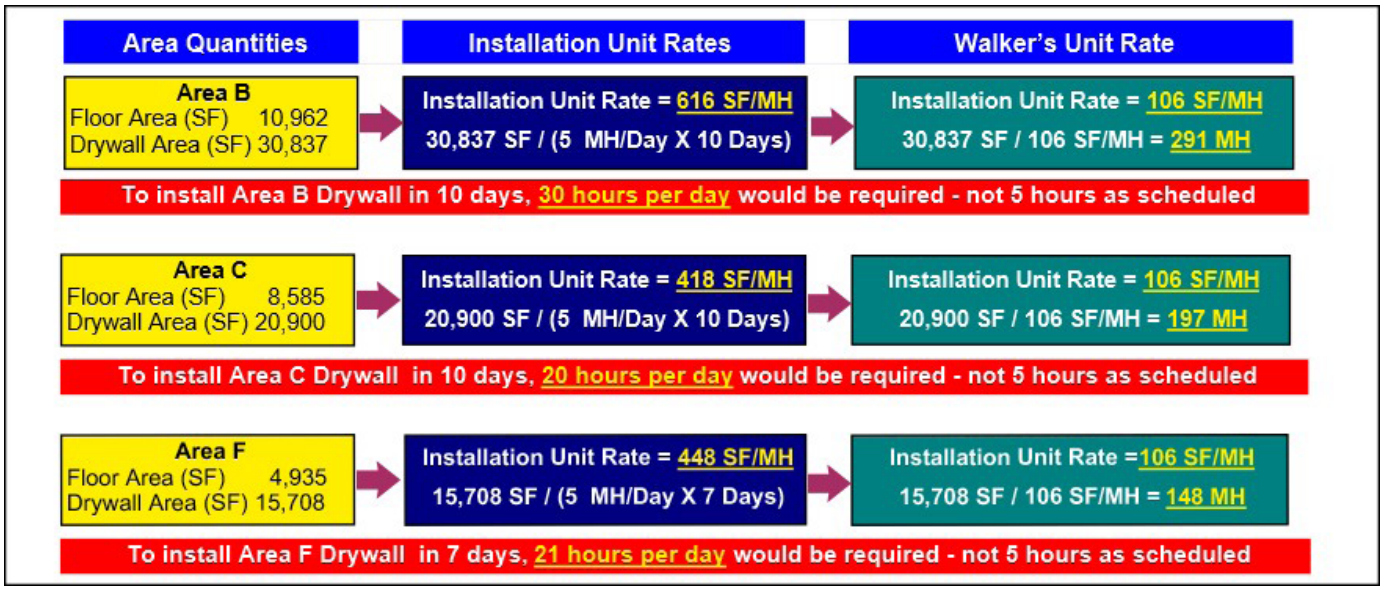

Figure 11
Poor scheduling practices result in unrealistic durations.

unattainable. With a more reasonable unit rate of 106 SF per man-hour, the resources required would be 30 hours per day rather than the 5 hours per day that was scheduled. The other two examples are similar in that they show the work cannot be accomplished as scheduled.

Forensic evaluation of the information that is only available in the native files showed the details of the resource loading methodology. The conclusion of this evaluation was that the resource loading method is not achievable.

Figure 12 shows a comparison of the resource loading for the same activities in two different schedule revisions issued approximately one month apart that is materially different. The different resource loading (15 and 5) — and the resulting installation unit rates (59 to 302) for the same activities in two different schedule revisions — provides unrealistic activity durations.

Figure 13 shows another report generated with the native files. The details of the report are highlighted, and the note boxes explain how the submittal scheduling practices are misleading (do not provide an accurate picture of the project's progress).

Figure 14 shows the planned manpower curve, which was derived from the original project schedule resource loading plan compared to the actual manpower during the project that was derived from forensic evaluation of the contractor's daily diaries.

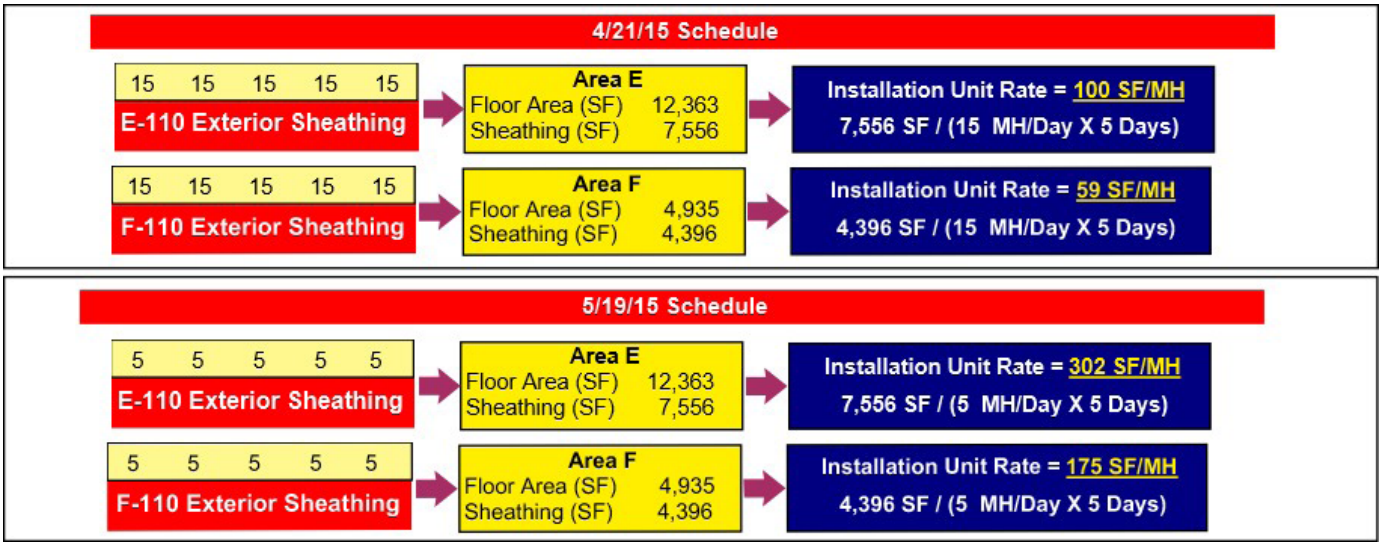

Figure 12
Different schedule revisions used different resources for the same activities.

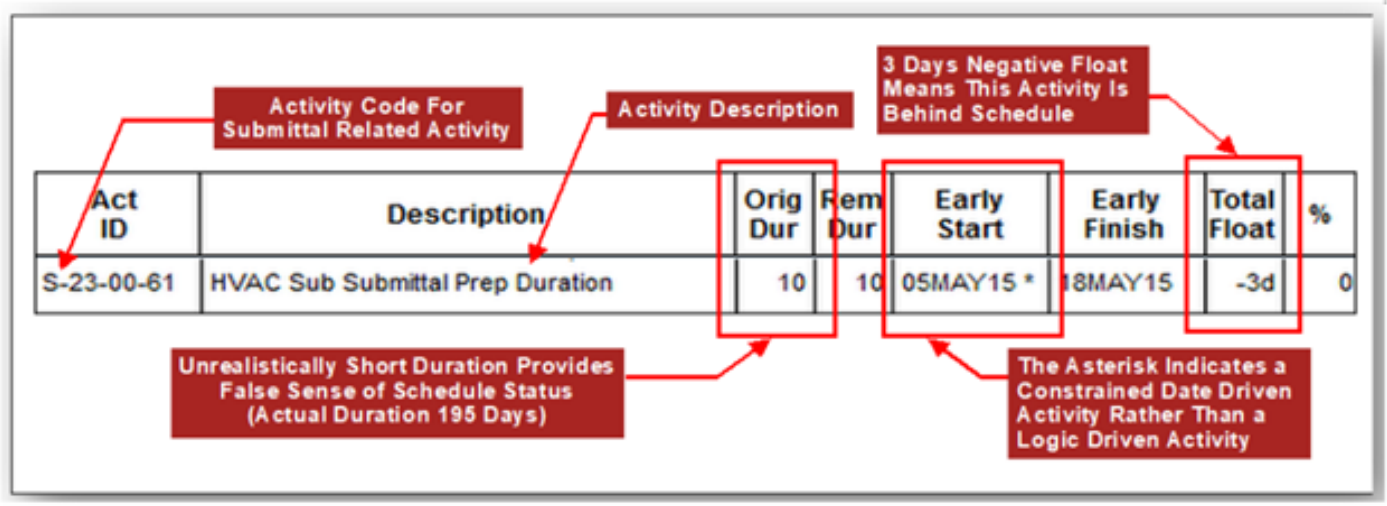

Figure 13
Native file evaluation exposes insufficient and incomplete submittal scheduling.

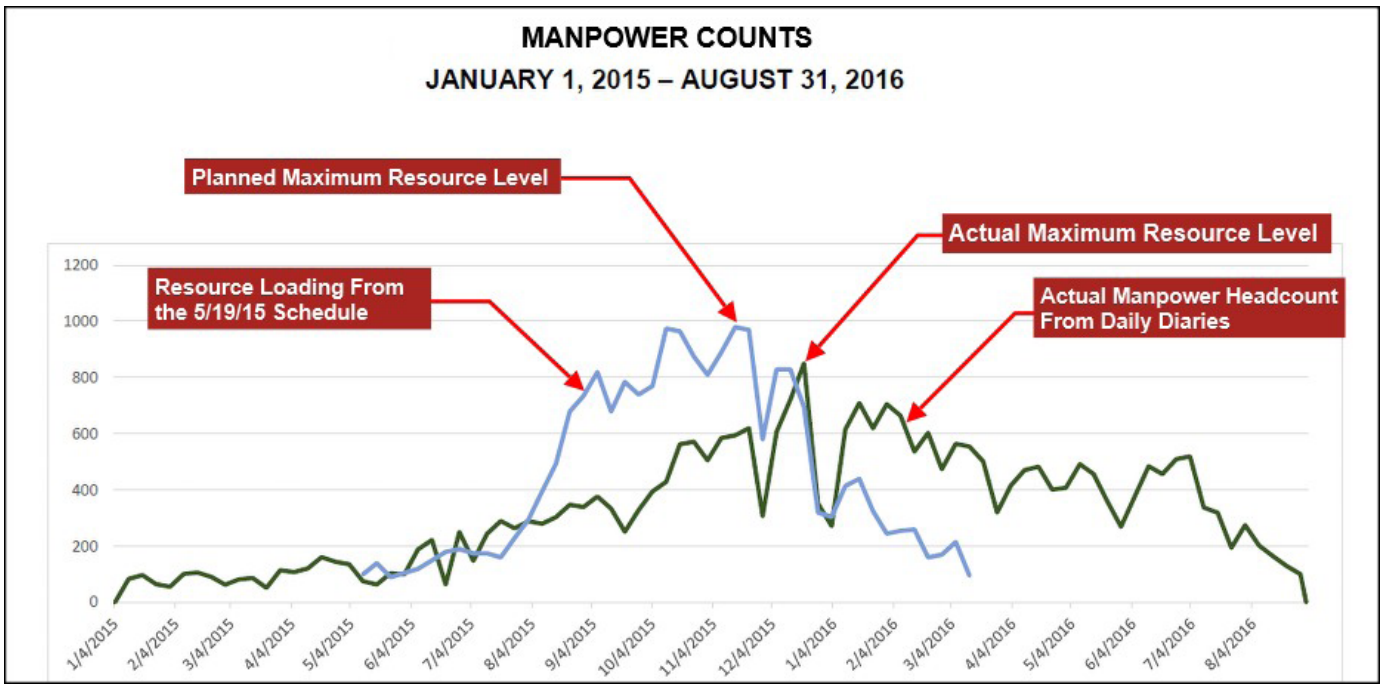

Figure 14
Actual manpower curve shows original schedule was not attainable.

Forensic evaluation of this information helped determine that the planned manpower levels were not very close to the actual manpower for most of the actual project life cycle. This actual experience information also shows that the schedule was extended several months past the originally scheduled completion date.

Indications of Inadequate Scheduling

The forensic evaluation should evaluate the schedule for inadequacies as well as contract-required elements. The following attributes of inadequate scheduling that were discovered during forensic evaluation of the contractor's schedules demonstrate that the schedules were not adequate for management of a large institutional project:

- Failure to schedule the majority of submittals that are prerequisites for construction.
- Failure to show critical procurement and succeeding installation activities.
- Logic that does not make sense in terms of construction sequencing.
- Failure to resource load the schedules in a manner consistent with CPM scheduling.
- Inaccurate schedule updates or inaccurate as-built information.
- Overly broad, inaccurate, or inconsistent activity descriptions.
- Suppression of information needed to evaluate the schedule.
- Assuming unlimited or unmeasured resources.
- Override logic with constraints results in excessive float or less negative float than actual.

Not only are the schedules not suitable for management of a large institutional project, but they are not sufficient for use as evidence that some other party caused a delay to the Critical Path.

Conclusions

Based on the forensic evaluation, the contractor's schedules provided for this matter cannot be reliably used to prove that a delay to the Critical Path was caused by another party that the contractor did not control for the following reasons:

- *Schedule was not approved*: The architect requested that the contractor provide a contract-compliant schedule numerous times, but R&M never

produced a schedule that was approved by the architect or owner.

- *Resource loading was inconsistent, limited, and missing*: The contract clearly defines when the project schedule is to be submitted to the owner in Section 3.10.1, which states: "At the time of his issuance of the guaranteed maximum price, the contractor shall submit for the owner's and architect's review a contractor's Critical Path Method (CPM) construction schedule (construction schedule) for the work." The schedules developed by the contractor were not properly resource-loaded, and did not meet these basic contractual requirements to be a resource-loaded CPM schedule.

- *Contract requires alternate plans in case of delay*: The contract also states that: "The contractor propose an affirmative plan to correct the delay." Forensic evaluation of the project documentation and correspondence revealed no work-around plans or other schedules were developed to address alternate work plans, increased manpower, or other similar efforts to meet the schedule.

Summary

The practice of Critical Path scheduling and the required elements of realistic Critical Path network schedules have been well-established during the past 50 years. The standard of care for proving delay claims and the contractual and legal requirements of CPM Network schedules have been established by the courts — and must be used as the performance standard in any schedule delay claim evaluation.

The forensic engineer should understand these practices, procedures, requirements, and standards to fairly and appropriately apply the practice of forensic engineering to evaluation of delay claims for a fair and reasonable resolution of the claim.

FE Investigation and Analysis of Poor Electrical Connections and Related Fire Investigation Case Studies

By Timothy C. Korinek, PE, DFE (NAFE 1023M)

Abstract

Overheating poor electrical connections (OPCs) are a ubiquitous ignition source of structure fires. Yet, knowledge of the intimate process between conductors at the connection point is relatively undocumented on the microscopic scale. For an OPC, it is ordinary for a filament or pool of liquid oxide to be the main current-carrying conductor at the point of overheating. This paper examines the overheating phenomena from a materials science perspective using photography through the stereo microscope, cross-sectioning, electron microscopy, and specialized techniques under the metallurgical microscope. Two case studies are presented in the second half of this paper. The first presents an artifact from field testing performed by a commercial cooking appliance manufacturer and introduces a real-world example of an OPC that did not ignite surrounding materials. The second is from a fire investigation of a food processing plant where prior research on OPCs informed expert opinions at trial and influenced the results.

Keywords

Poor connections, glowing connections, electrical overheating, electrical ignition sources, liquid oxides, liquid oxide conductor, high-resistance connections, high-temperature oxidation, forensic engineering

Background

Overheating poor connections (OPCs) are also referred to as glowing connections or high-resistance connections. These terms are often used interchangeably in the context of fire investigation. All overheating connections are, by their nature, high-resistance connections, but this paper focuses on OPCs that have some portion of the connection area glowing red-hot or higher. It aims at giving the investigator a better understanding of how a liquid oxide conductor behaves in an OPC and some unique features that can serve as evidence to prove an OPC occurred in the field. Readers are encouraged to seek out the references cited in this paper for additional information. The chapter on contacts and connections in *Electrical Fires and Explosions*[1] includes the results produced by many different investigators and is highly recommended.

The presence of liquid oxide as the stable electrical conductor at an established OPC is the predominant feature observed in the research performed by this author with currents in the range of 1 to 15 amps[2,3], and is well documented in the literature for currents ranging between 0.5 to 50 amps for various material combinations[1,4]. In the tests performed by this author — even when an OPC appears to be statically glowing — a liquid filament bridge was always observed to exist. This was determined by careful visual observation of the connection under the stereo microscope in real-time during overheating — and by metallographic cross-sectioning afterward, which reveals the existence of a formerly liquid region on top or within a larger oxide mass.

The oxide mass is sometimes referred to as the "nugget" in this paper. It consists of mostly solid oxide, but all areas of it were part of the liquid filament at some previous point in time. In many cases, the glowing liquid filament can be observed to wander around like a worm, causing further oxidation of the metal conductors and growth of the oxide mass. The liquid oxide filament is sometimes referred to as the "worm" in this paper. The worm-like action of the liquid filament is one characteristic that helps OPCs be stable for long periods of time. As the worm wanders around, it's continuously melting and remelting regions of the oxide mass that produces a self-healing

Timothy C. Korinek, PE, N144 W6466 Pioneer Rd., Cedarburg, WI 53012, 414-791-2434, tim.korinek@efiglobal.com

effect regarding the mechanical stresses caused by thermal gradients and volume expansion from oxide growth. If there were no wandering melt zone, these stresses would tend to crack the brittle oxide and open the electrical circuit.

The types of OPCs studied in this paper involve connections between Cu-Steel, Cu-Cu, and Brass-Brass. The data in **Figure 1** outlines the materials and circuit parameters examined in this study. All of the samples researched by this author produced evidence of a liquid oxide conductor at the connection interface.

The ranges of currents (as provided in **Figure 1**) represent different electrical loads. For example, about half of the Cu-Cu AC tests employed a number of incandescent light bulbs such that the current was 1.5 amps through the connection. Additional light bulbs were added in parallel for other tests to increase the current through the connection to 2.2 amps. For every situation studied, the overheating connection did not appear to be the controlling factor of the current.

It can be convenient to think of an OPC as a high-resistance hot-spot composed of a solid material (such as a miniature Nichrome heating element), but there are some distinct differences between the two. There is also a point where this analogy fails to properly characterize what actually happens in an OPC. OPCs involve one or more oxide species as an electrical load, and these oxides have a negative temperature coefficient of resistivity (NTC)[1], whereas metals like Nichrome have a positive temperature coefficient of resistivity (PTC)[5]. For the oxide semiconductors involved in an OPC, the electrical resistance decreases with increasing temperature, which is the opposite behavior observed for metals.

At a given temperature, metallic heating elements have resistivities many orders of magnitude lower than oxides such as Cu_2O (cuprous oxide). A useful chart of material resistivities is given in *Principles of Electronic Materials and Devices* [p. 130 Fig. 2.7][5]. By modeling an OPC as a resistance heating element, the overheating contact area can be as small as a thin film. The comparative difference in resistivities between a metallic heating element and an oxide can certainly be offset by the difference in lengths. Since the circuit resistance also depends on the conductor geometry, it is plausible that a very thin oxide with high resistivity can have the same resistance as a longer metal conductor with much less resistivity.

OPC material Combination	Nominal Circuit Voltage	AWG & Wire Type, or Conductor	Number of Samples Produced	Range of Current Through the Connection (Amps)	Duration of Test[c] (minutes)
Cu-Cu	120 V AC	14, Solid	28	1.5[a] — 2.2	35 — 480
		12, Stranded	6	1.6 — 2	40 — 450
	12 V DC	14, Solid	17	2.2 — 7.2	16 — 180
		12, Stranded	2	3.7—3.75	60 — 255
Brass-Brass	120 V AC	Plug blades	28	1.5[b]—2.3	15—420
	12 V DC	Plug blades	3	2.2—3	115—150
Cu-(Ni plated Steel)	120 V AC	Copper wire-Steel Terminal Screw	50	12	20—7200

[a] One sample was tested at 0.5 V for 120 minutes as a low current example.

[b] Two of the tests were performed at higher currents, 9.2 Amps and 13.8 Amps.

[c] The test duration was sometimes stopped before the connection melted open. Some tests were also stopped at the end of the business day.

Figure 1
Table of different OPC configurations tested.

The behavior of a metallic heating element is to have the highest current upon startup when the element is cold (i.e., inrush current). After startup, the resistance increases as the element heats up (often to red or orange hot), and the circuit reaches a steady state balance between the resistive heating (aka joule heating or I^2R heating) and the corresponding PTC material response.

In contrast, when an oxide with NTC behavior acts as a high-resistance element in a circuit, the resulting joule heating causes a decrease in resistance. This introduces one divergence with the analogy of the oxide as a conventional high-resistance heating element. The second divergence comes with the fact that, when an OPC glows red hot, high-temperature oxidation of the metal occurs next to (and at) the connection interface. For the copper oxides at temperatures above 300°C, the rate of high-temperature oxidation growth is parabolic with respect to time[6].

If the oxide conductor is modeled as existing only as a solid, the basic materials behavior described above has important implications on how an OPC develops in a real-world application. It is apparent that any significant overheating that takes place at the interface may also be in competition with an oxide thickness increase, which would increase the connection resistance and decrease the overheating wattage. If the effects of the NTC behavior upon heating predominate over any thickness increase, then it is possible a connection will proceed in "run-away" heating, which can cause the oxide layer to melt[1]. This behavior may explain why OPCs can sometimes be re-initiated again after being separated[7]. Experiments have shown the molten oxide has an additional order of magnitude drop in electrical resistance associated with the phase change from solid to liquid[1].

For the OPC samples prepared in the lab by this author, the method of initiating the OPC was by establishing the molten oxide worm by causing series micro-arcing, after which the worm starts out as a very small-sized ball or bridge. Much attention has been given to vibrations as a means to initiate micro-arcing. However, even at small currents, the high local temperatures created from one or a few micro arcs can be sufficient to establish the molten oxide worm. In fact, it has been the experience of this author that it is easier to initiate an OPC by separating the current-carrying conductors ultra slowly, compared to repeated vibratory micro-arcing. For example, this author employed a small DC motor with an eccentric weight (such as a cell phone ringer), which was used to cause vibrations and continued micro-arcing. When the vibratory motor was used to attempt OPC initiation, it was sometimes very difficult and took many hours to start an OPC, especially with direct current OPCs.

This author also employed a rack and pinion fixture with one moveable contact. With a little practice, it was easy to get all types of the studied OPCs to initiate by lightly "kissing off" the conductors with the rack and pinion fixture. It took some practice with the rack and pinion fixture to make the motion small enough, but this method was observed to initiate OPCs far easier than a condition subjected to regular vibrations. This same mode of initiating an OPC is reported in *Electrical Fires and Explosions*[1] and is described as "extremely low separation of the contacts," where the researchers used controlled thermal contraction as a means to slowly separate a connection.

Aspects of How OPCs Can Occur

It's well known that light contact is the main prerequisite to OPCs[1]. There are many routes by which this can happen in a real-life circumstance. Below is a list of some scenarios that may be causative of an OPC. This list is not exhaustive, and many of the factors can also be interrelated or exist in combination.

1. Aside from thermal run-away of an overheating solid oxide layer, the remainder of the causative conditions are due to series micro-arcing as the OPC initiator.

2. Oxidation at or next to the connection interface from any source, such as high-temperature oxidation or aqueous corrosion. An accelerated scale or medium that causes a mechanical separation and a decrease in metallic contact area (and eventual separation of the contacts) can cause parting micro-arcing. The Pilling-Bedworth (PB) ratio compares the volume of an oxide with its corresponding metal. Most metal oxides have a PB ratio greater than 1, which means the volume of the oxide is greater than the metal. Cu_2O has a PB ratio of 1.67[8]. When the copper oxide layer is formed on a copper substrate, a mechanical volume expansion occurs that can separate conductors previously in contact. The nature of a liquid conductor also provides an extra degree of freedom considering the electrical circuit. Reference 1 shows how the worm size is affected by the current density on a Cu-Cu OPC.

3. Stress relaxation of spring elements that make

connections, such as receptacles. Spring elements made from copper and copper alloys are known to relax over time under stress[9]. External stresses from either normal or abnormal use can exacerbate these effects.

4. Environmental conditions, such as thermal expansion and contraction from temperature changes, can influence a loose connection.

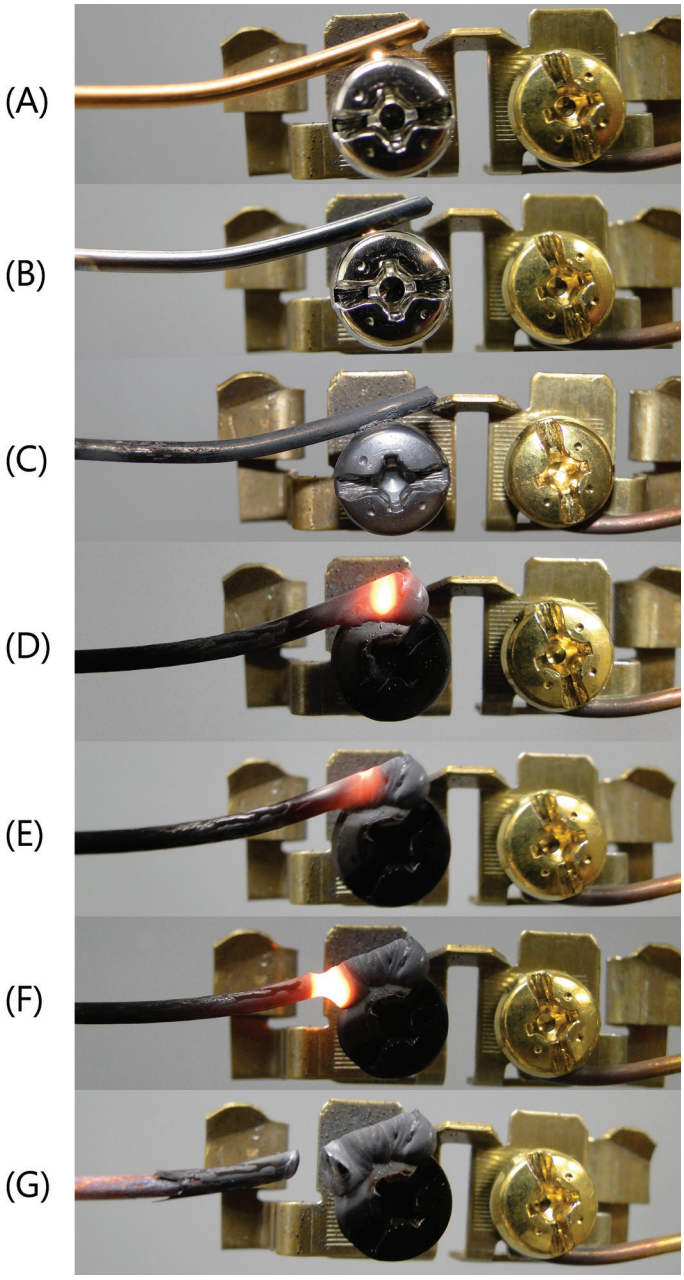

Figure 2
Common sequence of overheating for a loose connection between copper and steel, such as an improperly tightened wire on a receptacle screw terminal.

5. Installation error, misuse, normal wear, abuse while in service, or design defects that result in unnecessary connection looseness should all be considered when evaluating a possible OPC.

Figure 2 shows a time lapse sequence of an OPC produced in the lab between a 14-gauge solid copper wire and a nickel-plated steel screw with 12 amps of current running through the connection. These photos were taken as part of the research presented in "Pre- and Post-Flashover Characteristics of an Electrically Overheated Poor Connection Between Copper and Steel"[2]. This connection is ordinarily made by wrapping the wire around the shaft of the screw resembling a pig-tail, but the configuration of a wire simply in contact with the top of the screw was chosen to bring the overheating features into full view.

In many common scenarios, such as plug-blade receptacle connections or crimp terminals, the actual connection interface is hidden out of sight, making it difficult to demonstrate what occurs inside of an overheating connection. Research in "Electrical Receptacles - Overheating, Arcing, and Melting,"[10] used the same connection materials and similar circuit conditions as **Figure 1**. They used a pigtail configuration and produced OPCs that have identical features (except the oxide nugget assumes the shape of the pigtail). This is consistent with the observations of this author that the remnants of an OPC often are a function of the original connection geometry, but the essential characteristics of why the overheating happened (and what evidence is left behind) are the same.

Figure 2(A) shows micro-arcing at the contact point caused by manually making and breaking the contact. The OPC can be initiated with as little as one light touch. Soon after, a ball of molten oxide is established in series with the circuit, and significant heating of the surrounding conductors begins.

Figure 2(B) shows the OPC within minutes of establishment of the molten oxide. The copper wire has now darkened because a layer of adjacent oxide has formed. This layer is caused by high-temperature oxidation and is a secondary effect of the heating taking place at the contact point. The secondary high-temperature oxidation is a solid-state process.

Figure 2(C) displays the appearance of the OPC on the order of several hours after initiation. A nugget of oxide about the size of a grain of rice exists at the interface between the wire and screw. At this stage, the wire

sometimes glows red-hot due to the heating taking place at the connection point. The molten oxide also glows, but is not always visible when viewing the connection from the exterior because the liquid filament is inside the nugget. As the oxide mass at the connection point grows, the liquid path is often a fraction of the entire mass. It will wander around, re-melting formerly molten areas. The thickness of the secondary high-temperature oxide layer has also thickened over time, and the screw is beginning to show secondary high-temperature oxidation on the surfaces away from the connection point. The OPC can stay in this stage for a considerable amount of time before transitioning to (D), if at all. As emphasized throughout this paper, the geometry and circuit conditions can influence the form an OPC will take.

Figure 2(D) shows the stage in which the oxide nugget has grown to the point where the molten pool is large, and more than half of the wire nearest to the connection point has been converted to oxide. The bright yellow area is the molten region. A needle or probe can easily be inserted into the molten pool without it dripping due to the surface tension.

Figure 2(E) shows the molten pool wandering at a later stage. More of the wire and screw have been converted into oxide due to the molten pool. For the copper-to-steel connections studied at 12 amps, more of the copper wire was converted to oxide compared to the iron from the screw. In addition, it took between 10 and 100 hours of runtime to reach the stage shown in (F).

Figure 2(F) shows the molten pool, which is only supported by surface tension in this stage, but still conducting all of the circuit current.

Figure 2(G) shows the connection after it melted open.

The scanning electron microscope (SEM) image in **Figure 3** shows a mounted and polished longitudinal cross-section through a sample in a state comparable to **Figure 2(C)**, where the oxide nugget is about the size of a grain of rice. This image was taken with a backscattered electron detector (BSE), which produces a grayscale contrast based primarily on the local atomic weight of the sample regions. Higher atomic weight results in lighter shades, and lower atomic weight will have darker shades. The copper wire is the brightest; the dark background is the epoxy mounting material. The red arrow points to the formerly liquid oxide nugget between the wire and screw, and the blue arrow points to the secondary high-temperature oxide growth layer. This sample was stopped after 107 hours of overheating.

Figure 4 shows the secondary high-temperature oxidation of a copper wire in greater detail. This image is an unmounted cross-section of the oxide layers after some of it fractured away. The oxide is a dual layer composed of Cu_2O grown at the Cu metal interface, and CuO grows on top of the Cu_2O. The ratio of Cu_2O to CuO thickness is dependent on temperature[6]. The CuO grows into the atmosphere as whiskers, which would resemble something like a winding staircase on the atomic level. The whiskers then coalesce into a polycrystalline CuO layer with the Cu_2O underneath. For the time and temperatures of the Cu-Cu

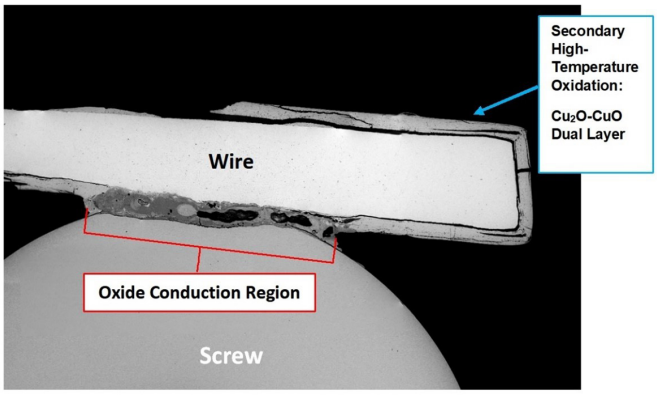

Figure 3
Mounted and polished cross-section[2] showing the overheating interface between a loose wire making contact with a steel screw. Evidence of the worm is not always found in a cross-section because it is only a single two-dimensional slice — the worm can be in a different location.

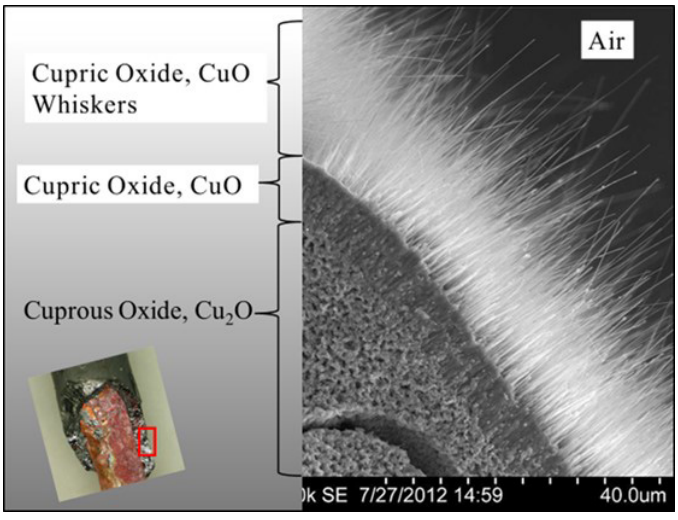

Figure 4
SEM image showing the dual copper oxide scale plus the whisker morphology of the outer layer after high temperature growth[2].

OPCs studied, the Cu_2O layer predominates in thickness. For those readers who are only familiar with aqueous electrochemical oxidation of metals (usually referred to as corrosion), the mechanism of dry high-temperature oxidation is different — but not entirely. With aqueous corrosion, the chemical reactions take place via ionic conduction of dissociated species through an electrolyte. High-temperature oxidation still involves species with an effective charge, but the transport takes place via electronic conduction through the layer, such as with positively charged holes and vacancies in the crystal.

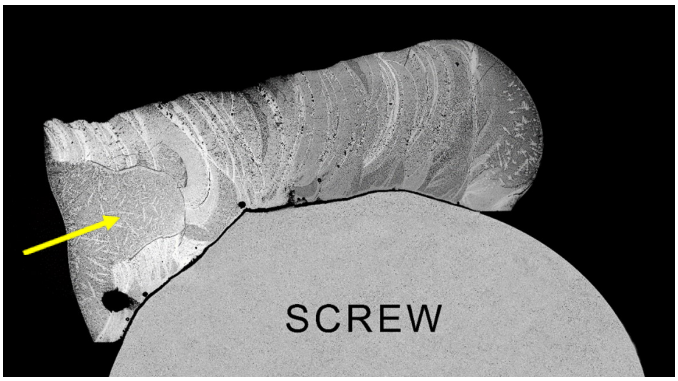

Figure 5
An as-polished metallurgical cross section[2] of an OPC remnant from a connection between a 14-gauge copper wire and a steel screw as shown in **Figure 2**. All parts of the wire in the vicinity of the screw have been part of the molten oxide worm at some point, and the region that was molten immediately prior to the connection melting open is the bell-shaped feature on the left-hand side (as indicated by the yellow arrow).

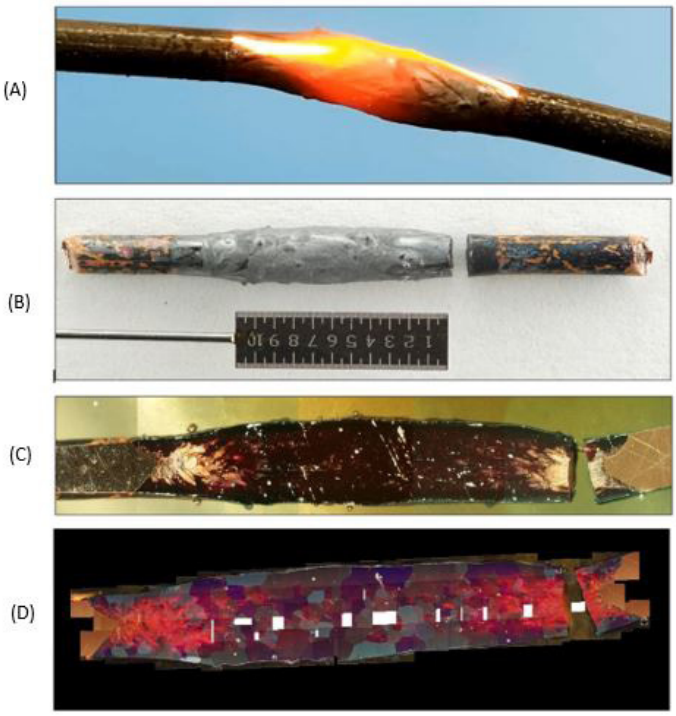

Figure 6
A Cu-Cu OPC showing (A) the worm and oxide nugget growth after a period of overheating, (B) remnants after shutting the circuit off, (C) as-polished cross section of the connection with incident lighting under the stereo microscope, and (D) composite image of photos taken with the metallurgical microscope using crossed polarizing filters[3].

Figure 5 is a SEM-BSE image, and shows the sample from **Figure 2(G)** after being mounted in epoxy and polished to achieve a cross-section. There is no evidence of any melted copper wire or melted steel. The species that were molten consist entirely of copper-oxides and copper-iron-oxides[2]. Despite these observations, it is possible for melting of the metallic conductors to take place (this will be discussed later in the paper).

Figure 6 shows a copper-to-copper OPC produced in the lab with 1.6 amps of current flowing[3]. After the overheating connection is established, the liquid filament acts like a worm that wanders through the already-oxidized mass. The liquid oxide is stable on a time frame of minutes to hours, and there is a self-healing effect of the worm wandering around — melting and remelting — which helps sustain the process and keeps the connection intact.

Figure 6(A) shows a photograph of the molten worm and oxide mass during the experiment, which exists as a bridge more than 1 cm long after 4 hours of overheating since the OPC was initiated.

Figure 6(B) shows the sample after the circuit was shut off. When the circuit was shut off, the sample cooled and fractured, which can be seen on the right-hand side of the photo. The scale shown in the photo is 1 cm total in length, and the numbered divisions are millimeters.

Figure 6(C) shows the same sample mounted and polished longitudinally, viewed under the stereo microscope.

Figure 6(D) is a composite image of more than 100 long-exposure photos taken through the metallurgical microscope using completely crossed polarizing filters and stitched together afterward. The exposure time for each photograph was approximately 30 seconds. With completely crossed polarizers, the field of view when framing these shots is completely dark. The filters are not perfect materials (or perfectly crossed), so some light gets through, resulting in the images shown. The white areas in the image compilation were missed areas because it was difficult to know where the shot was before taking it.

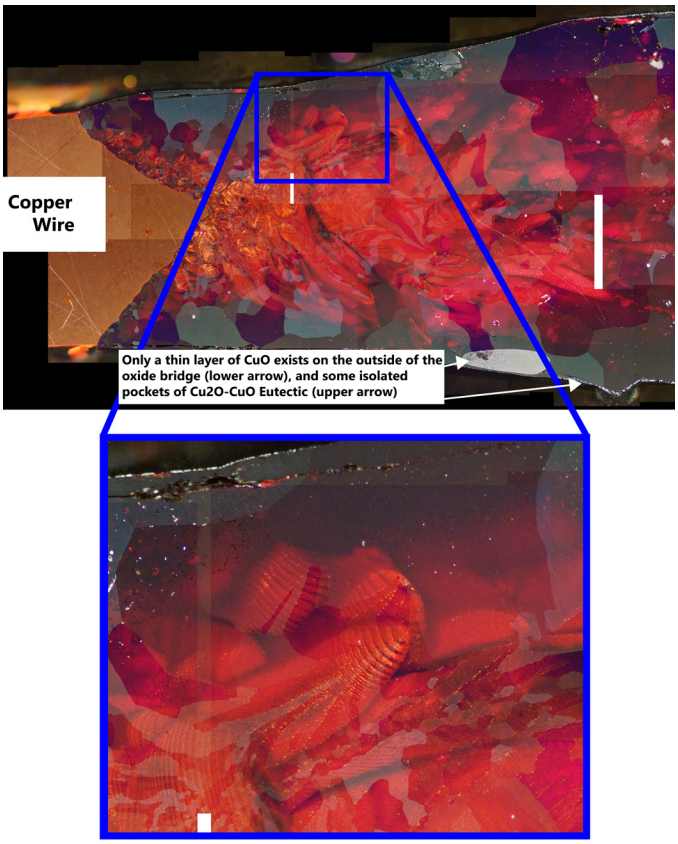

Figure 7
Images from **Figure 6(D)** at higher digital zoom. There is a thin outer layer of CuO and some pockets of Cu_2O-CuO eutectic, as indicated by the white arrows. The segmented morphology of the worm microstructure is apparent[3].

Cuprous oxide (Cu_2O) is a semitransparent material, so the photos also display features inside the cross-section below the plane of polish. Cu_2O also shows up as red colored under the microscope when using polarized filters[11].

Figure 7 shows the left-hand region from **Figure 6(D)** at a higher magnification. The microstructure of the worm can be seen; it actually represents many past locations of the worm. One aspect to reiterate is that Cu_2O is semitransparent, and using crossed polarizing filters allows features below the plane of polish to be observed — so some areas inside the material can be seen. It is also important to note that only a thin layer of CuO is found on the outside of the nugget, except for a few small pockets containing Cu_2O-CuO eutectic. This is also consistent with the dual layer discussed earlier. The cross-section is useful because if only energy dispersive spectroscopy (EDS) were to be performed non-destructively on the surface of the nugget, one could come to the incorrect conclusion that the whole nugget is composed of CuO.

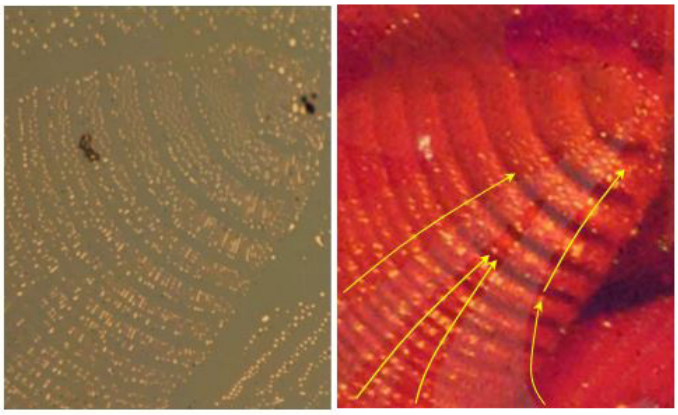

Figure 8
Image of the worm microstructure with normal brightfield reflected illumination under the metallurgical microscope (left); the copper globules are peach colored, and the Cu_2O matrix is gray and opaque. Same region of the worm under crossed polarizing filters with long camera exposure time (right); the copper globules are gold colored, and the Cu_2O matrix is red and translucent, which shows additional copper globules below the surface and surface macro grain morphology (as shown by the yellow arrows)[3].

Figure 8 shows a comparison of the worm microstructure with different illumination techniques under the metallurgical microscope. One interesting aspect of this microstructure is that it displays banding and segmentation similar to an earthworm. The cause for this morphology deserves more research. While the glowing oxide worm from the outside looks visually similar for many OPCs between different materials (including both AC and DC currents), the microstructure of the worms in the plurality of scenarios has yet to be studied in greater detail and deserves more research.

A temperature-composition equilibrium phase diagram of the copper-oxygen system is shown in **Figure 9**, which is from "Critical Assessment and Thermodynamic Modeling of the Cu–O and Cu–O–S Systems,"[12] and some additional overlays have been provided by this author to show the Cu-Cu OPC situation. Additional thermodynamic data for the Cu-O system can be found in *Phase Diagrams of Ternary Copper-Oxygen-Metal Systems*[13].

Beside the temperature and composition of the elements involved, oxygen pressure isobars are included. A value of 0.21 atmospheres (atm) represents air (i.e., 21% oxygen). The 0.21 atm line in the phase diagram is shown by the highlighted labels in red, and the rest of the isobars are shown in terms of $\log_{10}(P(O_2)$, in atm. The melting point at (E) in **Figure 9** for the two-phase region consisting of Cu_2O+CuO is about 1,125°C in an ambient 21% oxygen environment.

The vertical blue line indicates the stoichiometric Cu_2O compound at 33% atomic oxygen concentration. The congruent melting, which occurs at (C) at 1,231°C, is commonly cited as the melting temperature for copper oxide. Yet, care must be taken when interpreting the phase diagram. The kinetics (i.e., rate) of a particular reaction are also not represented at all in the phase diagram — as well as the fact that the partial pressure of oxygen will not be 0.21 atm. inside the oxide.

The molten L1 + L2 region in **Figure 9**, as highlighted in yellow, shows the compositional region relating to the worm. The worm involves a copper-rich L1 and liquid oxide L2. Below the critical point at (G) is a miscibility gap region below which liquid copper and liquid oxide exist analogous to oil and water at room temperature, and the solid structure upon cooling creates the microstructure of the worm. This is part of the monotectic transformation resulting in solid Cu + Cu_2O. The monotectic reaction is bounded by the two regions labeled (B) in **Figure 9**.

As mentioned earlier, the kinetics of the reaction are also important and not represented in the thermodynamic phase diagram. The red highlighted path in **Figure 9** shows how the 0.21 atm. isobar can be followed down the diagram to predict which substance is stable at a given temperature at a constant $P(O_2)$. In fact, the thermodynamic phase diagram dictates that CuO is the stable phase at ambient conditions (room temperature and oxygen partial pressure of 0.21 atmospheres). The diagram predicts metallic copper is not stable and should transform to CuO. The reality is that the kinetics of this reaction can be so slow that it's often not practical to consider. For example, metallic copper lasts on earth for thousands of years under

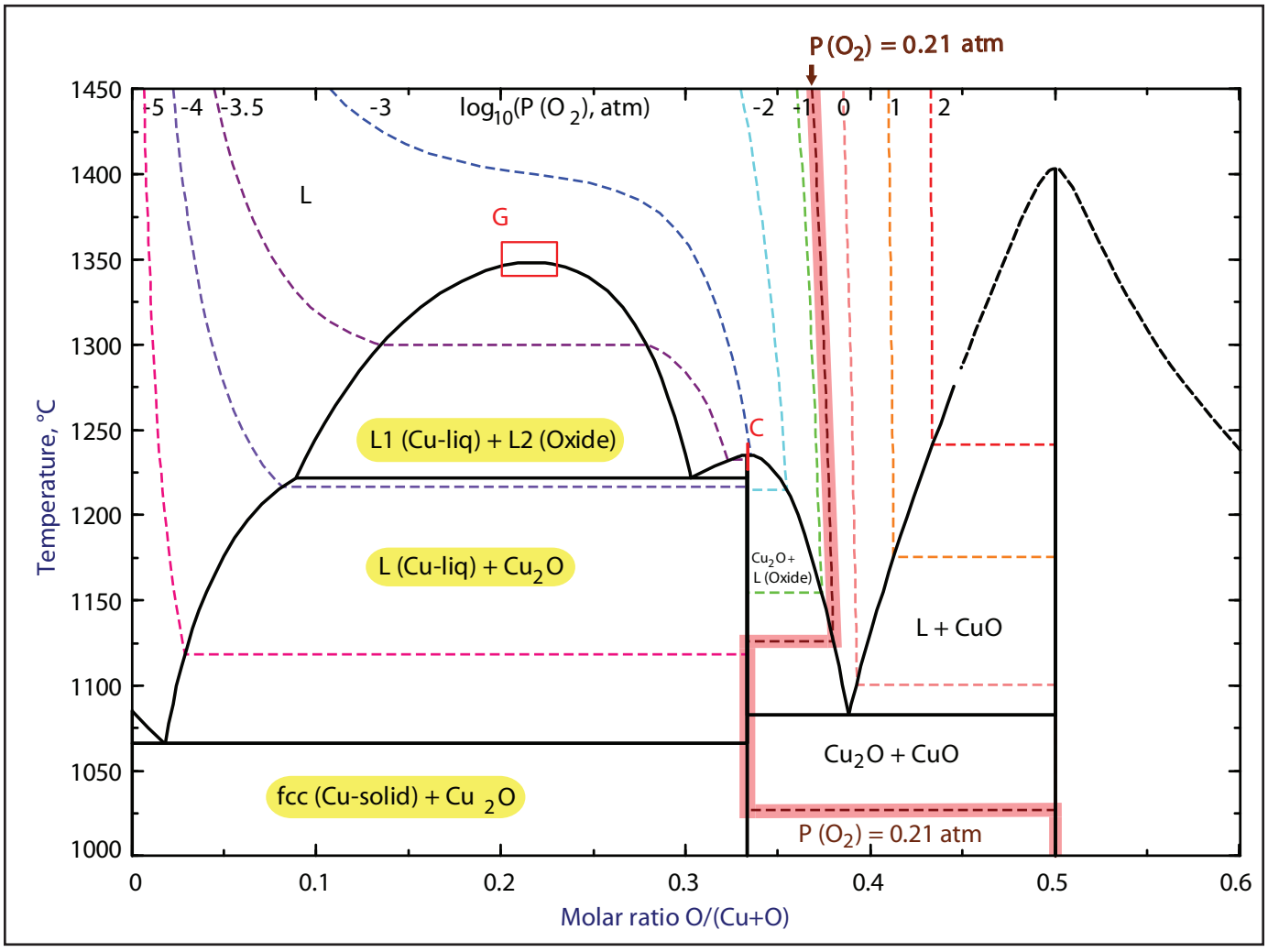

Figure 9

Phase diagram of the copper oxygen system with oxygen pressure isobars. The diagram was produced by the researchers in "Critical Assessment and Thermodynamic Modeling of the Cu–O and Cu–O–S Systems,"[12] and used the software program FactSage to generate the chart from available thermodynamic equations. The red and yellow highlights are overlays added by this author.

standard conditions (aqueous corrosion aside).

Nevertheless, the partial pressure of oxygen $P(O_2)$ is useful for predicting many reactions, and a three-dimensional oxide layer will be subject to a gradient of $P(O_2)$, depending on the depth. The partial pressure of oxygen decreases with depth into the solid layer, as shown in **Figure 10**[15]. This fact is consistent with the microstructure of the Cu-Cu OPC nugget, worm, and the dual scale phenomena for high-temperature oxidation of copper in air.

Figure 11 (A) shows an OPC with 12-volt DC with an overheating connection running 6 amps of current after several hours of overheating time. Note that with a DC current, the nugget only grows in the direction of the positive anode. This behavior is rather unusual in terms of basic heat transfer and may relate to the semiconductor nature of the oxide. More research is warranted in this regard. The unidirectional growth of the oxide nugget has been noted by other researchers[1].

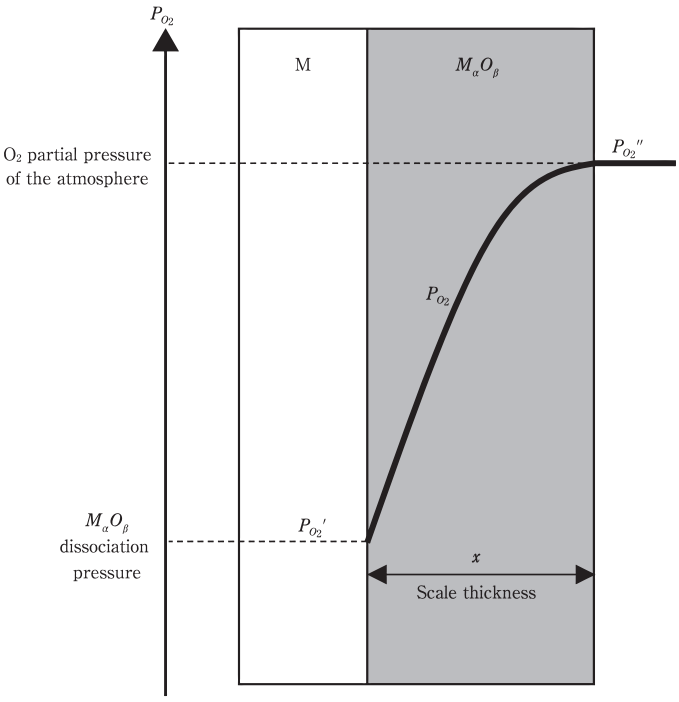

Figure 10
Diagram of how the partial pressure of a gas decreases inside a solid.

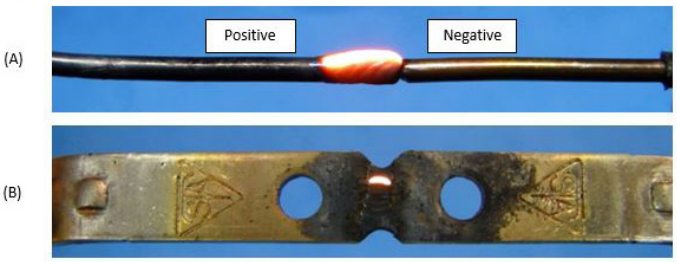

Figure 11
(A) shows a DC OPC where the liquid conducting worm only consumes the positive electrode. (B) shows a brass-to-brass OPC where the worm is shown to behave similarly to the other experiments. Metallurgical cross-sections of similar samples are documented in "Poor Electrical Connections: Physical Features, Materials Characterization, and Newly Identified Characteristic Traits, Before and After a Fire."

Figure 11 (B) shows the glowing worm between two brass plug blades with 2.2 amps of current flowing across the connection. The nominal circuit voltage is 120V AC, and the voltage drop across the connection was measured to be 7V.

In the examples studied in "Pre- and Post-Flashover Characteristics of an Electrically Overheated Poor Connection Between Copper and Steel"[2] and "Poor Electrical Connections: Physical Features, Materials Characterization, and Newly Identified Characteristic Traits, Before and After a Fire,"[3] it was also possible to identify the characteristics of the worm after samples were exposed to a fire environment. This was done primarily with metallography, though some features were still observable by surface examination.

Case Study 1

This case involves a thermal cut out (TCO) switch from a commercial cooking range. The subject TCO, as shown in **Figure 12**, was presented to this author's laboratory by the range appliance manufacturer for a failure analysis. The subject TCO was part of a range that was being field tested under the control of the manufacturer. The range had been in service for approximately 10 months prior to the failure of the TCO crimp terminal connection. The current through the subject TCO is 20 amps during normal operation when both range heating elements are

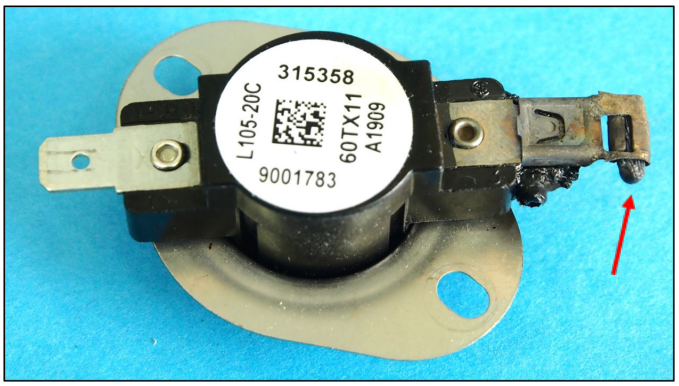

Figure 12
Subject TCO with overheated terminal crimp on the right-hand side. The TCO manufacturer markings have been blurred out.

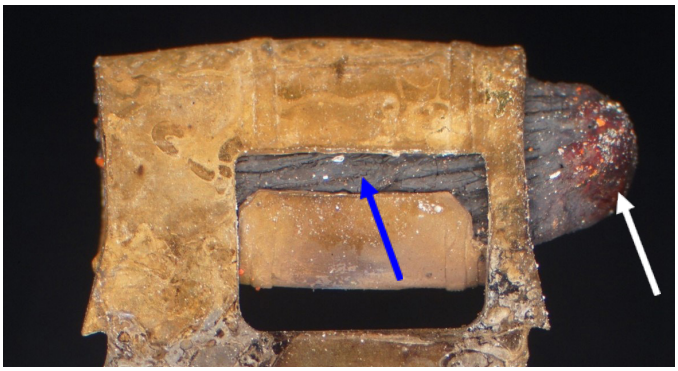

Figure 13
Digital image taken through the stereo microscope with crossed polarizing filters.

on. There is some melting and thermal decomposition of the plastic insulation materials close to the terminal, but no other surrounding materials ignited before the subject OPC melted open at the region indicated by the red arrow.

Figure 13 shows a stereo microscope image of the subject crimp connection between the brass terminal and a stranded copper wire. This image was taken with crossed polarizing filters and the region where the stranded wire melted open is red colored, as indicated by the white arrow. The red color under crossed polarizing filters is consistent with Cu_2O (cuprous oxide), which is semi-transparent and red colored under polarizing filters[11]. Also apparent is a gap in the crimp barrel, as indicated by the blue arrow.

Figure 14 shows the subject crimp from the other side. It is clear there is a melted mass where the stranded wire once exited the crimp barrel, as indicated by the red arrow. The blue arrow points to localized melting of the female brass terminal body. In all the experiments performed by this author, where OPCs were produced in the lab under various conditions, essentially no evidence of melting was observed on the metallic conductors in the connection area. Yet, melting of the metallic conductor can occur for several reasons. The OPC may thermally degrade the surrounding materials such that parallel arc tracking across a carbonized path occurs between adjacent conductors.

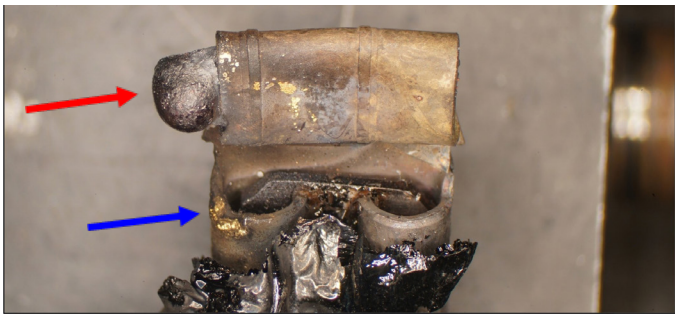

Figure 14
The red arrow points to the melted brass that formed after the subject circuit melted open. The blue arrow points to melting of the brass terminal body, which may have been caused by series arcing from contact with the stranded wire as it separated.

An OPC may cause parallel arcing if the insulation breakdown from the localized heating causes conductors to touch and short circuit. If an OPC ignites a fire, the fire may become hot enough to melt conductors. These aforementioned potential causes for melting do not appear to have caused the brass melting on the subject terminal. When the OPC melted open and severed, the stranded wire segment (not available for analysis) likely contacted the brass terminal body causing a 20-amp series arc and local melting. In general, circuits with higher amperage loads would be likelier to cause melting under series arcing conditions.

Figure 15 shows the subject crimp at the end opposite the melted-open region. The subject crimp was improperly made because it failed to properly compress the copper strands, which can easily be seen by the large gaps between the strands. The copper strands themselves have undergone a significant amount of secondary high-temperature oxidation from the OPC. The red arrow points to a formerly liquid oxide mass, which, at some point, was undoubtably part of the molten worm. The rippled appearance, shiny gray exterior, and engulfed strands are a dead giveaway. Surface analysis of this worm region also shows micro-sized oxide spatter droplets. The blue

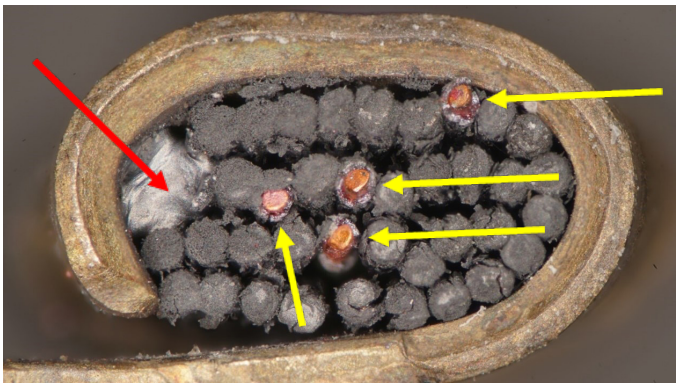

Figure 15
This shows a positive identification of an OPC worm between a brass crimp body and a stranded copper wire. This component had been installed in a real-world application, and the failure resulted in an open circuit. The red arrow points to a globular region, which was a worm at some point in time. The yellow arrows point to fractured high-temperature oxidation scale on the individual copper strands, which is a secondary effect of the heating caused by the worm. All of the wire strands not consumed by the worm globule display this secondary scale.

arrows point to the layer of high-temperature oxidation scale surrounding the copper strands.

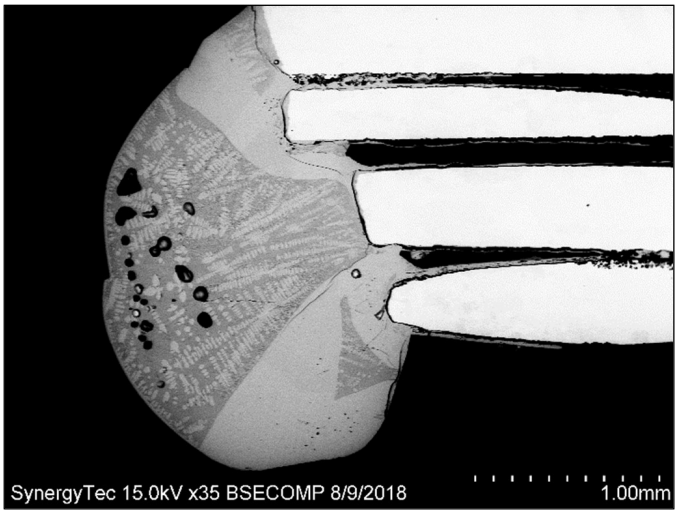

Figure 16
Above is an as-polished cross section[3] of a sample produced in the lab between copper electrodes with an AC current (2 amps for 20 minutes, then 13 amps for 20 minutes until the connection melted open).

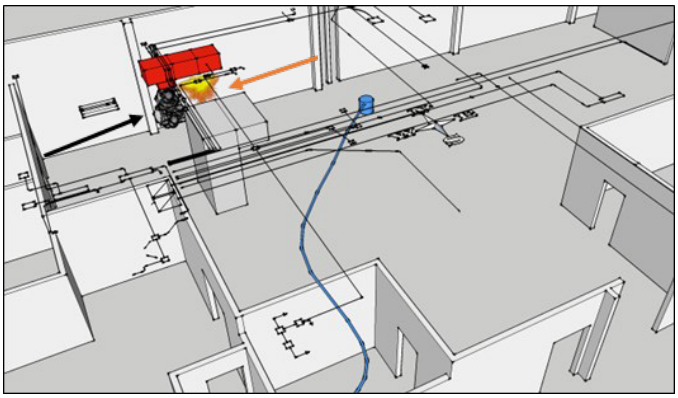

Figure 17
A model of the room where the fire took place. The blue wiring is the security camera and wiring; the red item is the furnace where the fire was first discovered. The furnace is above a drop ceiling.

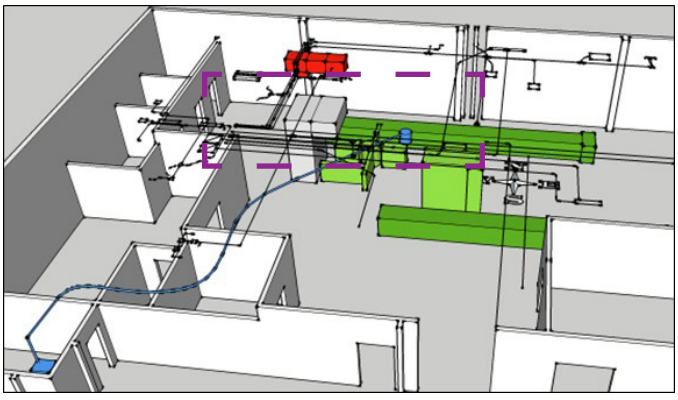

Figure 18
Macro view of the area identified by the plaintiffs as the origin, indicated by the dashed purple box.

Figure 16 shows a polished cross-section of a solidified oxide mass from an experiment performed on a copper-to-copper OPC produced in the lab[3]. This sample ran with a current of 2 amps for 20 minutes (after which the circuit current was switched to 13 amps for 20 minutes), and the OPC proceeded to melt open. The last oxide liquid to solidify can be seen coming from one strand. It is expected the melted open cross-section (as shown in **Figure 11**) would display similar features if examined in similar detail.

Case Study 2

A fire at a commercial bakery was the subject of an investigation led by a colleague of the author, who was hired by one of the defendants in a lawsuit and trial that followed. This defendant was an electrician who was working on an installation of a security camera system in the room of origin on the day of the fire.

The subject structure was used as a warehouse until 1998, after which the building was converted into a facility for pizza crust production. In the weeks prior to the fire, a video security system was being installed, which consisted of 16 cameras, two DVRs, and two power supply panels — each containing a power supply transformer. On the day prior to the fire, bakery maintenance personnel smelled overheating plastic in the room containing the camera power supply panels. The maintenance staff then shut off the circuit breakers serving these panels.

The following day, the defendant electrician discovered one of the camera power supply transformers had shorted and failed. He replaced the transformer, continued setting up camera circuits, and disconnected the camera circuits at the panels before leaving for the day. At least 4½ hours passed between the electrician leaving and the first smoke or fire observed by production workers.

Figure 17 shows the location of where the first smoke and fire was observed by workers on the production line, as indicated by the black and orange arrows, respectively. The smoke was observed coming out of a return vent, and the first fire was seen about 7 feet from the return vent.

Figure 18 shows a more zoomed out view of the subject structure compared to **Figure 17**. The production line in the room of fire origin is shown in green. The furnace where the first smoke and fire were observed is shown in red. This furnace was installed above a drop ceiling. The components shown in blue are a camera in the upper right, the power supply panel with the transformer is in the lower left, and the camera wiring is in between. The

region shown enclosed by the dotted purple box is the plaintiff's area of origin, which includes the camera/wiring and excludes the furnace. Other items in this region included a ceiling exhaust fan, fluorescent lighting, and associated wiring. The experts who were hired on behalf of the electrician defendant included the furnace in their area of origin and requested it be retained as evidence. This was based on the fire patterns in this area and the fact this was the location where smoke and fire were first witnessed.

At the first joint laboratory examination of the artifacts collected at the fire scene, the plaintiff's experts tested the transformer that had failed one day prior to the fire as well as the replacement to this transformer installed by the electrician defendant on the day of loss. The failed transformer, which was not in service on the day of loss, was found to have an open circuit in the primary windings. The transformer installed on the loss date exhibited no failure and was found to operate normally. At this exam, the expert on behalf of the electrician defendant requested the furnace and related components be examined further. The plaintiff's experts objected and concluded the joint exam.

Despite continued requests to examine the subject furnace, the plaintiff's experts maintained their objections. It was not until after the plaintiff's experts provided deposition testimony that additional examination of the furnace was found agreeable.

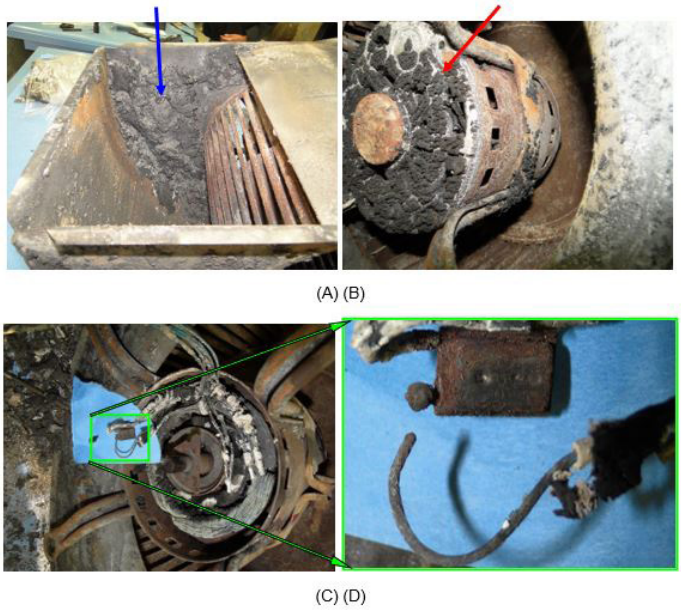

Figure 19
(A) shows caked-on flour deposits inside the blower volute, as indicated by the blue arrow. The witness who first spotted flames identified a location close to this component. (B) shows the motor end bell, which is caked with flour deposits. This is where the cooling fan within the motor housing draws in air to cool the motor. (C) is the thermal protector with the overheated connection, and (D) is a close-up of the melted open connection.

Figure 19 shows four images from the subsequent examination of the furnace. (A) shows the furnace fan discharge with a thick layer of burnt flour deposits, as indicated by the blue arrow. (B) shows more burnt flour deposits on the end-bell of the motor for the furnace air handling fan, as indicated by the red arrow. (C) shows an image after the fan motor end-bell was removed, and (D) shows an enlarged view of the thermal protector switch, which exhibited a formerly molten bead consistent with an OPC and a solidified oxide that melted open. The stranded wire, which was previously crimped into the steel thermal protector body, also displayed localized melting consistent with an OPC.

Figure 20 shows a close-up stereo microscope image of the formerly molten mass on the end of the subject motor thermal protector switch, as indicated by the blue arrow. This thermal protector employs a steel casing that carries the circuit current between the crimp connections and the interior contacts as well as the crimp connections. The other crimp connector is shown by the yellow arrow. Both of the subject crimp connectors are a copper to steel connection.

Conclusions

For the conductor materials and circuit conditions studied, the liquid oxide conductor (aka worm) has been shown to be ubiquitous and identifiable. The phase diagram for the copper-oxygen system shows very clearly a region with

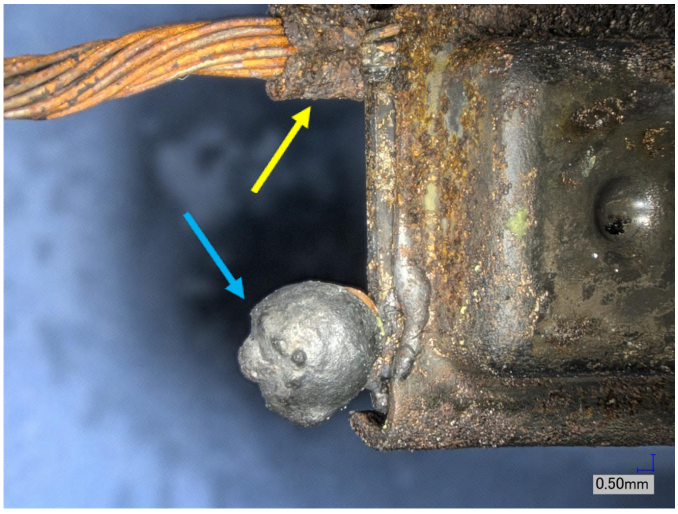

Figure 20
The blue arrow points to an oxide mass resulting from an OPC on the subject switch.

two immiscible liquids, which explains the microstructure of the conducting filament worm for Cu-Cu alternating current OPCs. Since the worm involves copper-rich particles, it would make sense that this is the favored electrical path. Given particles of copper dispersed in a matrix of Cu_2O, it would be expected that the electrical conductivity would follow the rule of mixtures as a first order approximation. This is another area for continued research. The conductivity measurements performed on Cu-Cu OPCs by others in the past deserve reconsideration in light of the fact that the material they were measuring was not monolithic CuO or Cu_2O, as in "Glowing Contact Physics."[4]

Other areas deserving more research have been identified in this paper, such as potential causes for metallic melting observed on materials involved in an OPC. Aspects of higher current OPCs that are expected to last for shorter time periods are under researched.

The first case study in this paper is a real-world example of an OPC from the field. This analysis shows some of the characteristic traits of an OPC, such as the worm traveling to the rear of the connection and creating an oxide mass that consumed several individual copper wire strands.

One major takeaway from Case Study 2 is never discount or ignore the witness accounts of where the smoke and fire were first observed.

References

1. V. Babrauskus, *Electrical Fires and Explosions*, New York: Fire Science Publishers, 2021.

2. C. Korinek, T. Korinek and H. Lopez, "Pre- and Post-Flashover Characteristics of an Electrically Overheated Poor Connection Between Copper and Steel," in *Fire and Materials*, San Francisco, 2013.

3. C. Korinek and T. Korinek, "Poor Electrical Connections: Physical Features, Materials Characterization, and Newly Identified Characteristic Traits, Before and After a Fire," in *Fire Science and Technology* (ISFI), Chicago, 2018.

4. J. Shea, "Glowing Contact Physics," in *IEEE Holm Conference on Electrical Contacts*, Montreal, 2006.

5. *Principles of Electronic Materials and Devices*, New York: McGraw-Hill, 2006.

6. G. Garnaud, "The Formation of a Double Oxide Layer on Pure Copper," *Oxidation of Metals*, vol. 11, no. 3, 1977.

7. J. Shea and X. Zhou, "Material Effect on Glowing Contact Properties," in *IEEE Holm Conference*, 2007.

8. S. Bradford, Chapter on Fundamental of Corrosion in Gasses, Handbook Volume 13 - Corrosion, Materials Park, Ohio: ASM International, 1987.

9. *Properties and Selection: Nonferrous Alloys*, Materials Park, Ohio: ASM International, 1990.

10. M. Benfer and D. Gottuk, "Electrical Receptacles - Overheating, Arcing, and Melting," in *FIRE SAFETY SCIENCE*, 2014.

11. *Introduction to Practical Ore Microscopy*, 1989.

12. D. Shishin and S. Decterov, "Critical Assessment and Thermodynamic Modeling of the Cu–O and Cu–O–S Systems," *CALPHAD: Computer Coupling of Phase Diagrams and Thermochemistry*, vol. 38, pp. 59-70, 2012.

13. Y. A. Chang and K.-C. Hsieh, *Phase Diagrams of Ternary Copper-Oxygen-Metal Systems*, Materials Park, Ohio: ASM International, 1989.

14. E. Ehlers, *The Interpretation of Geological Phase Diagrams*, San Francisco: W. H. Freeman and Co., 1972.

15. M. Noguchi and H. Yakuwa, *Lecture on the Fundamental Aspects of High Temperature Corrosion and Corrosion Protection Part 1: Basic Theory*, 2016.

16. W. J. Meese and R. Beausolie, "Exploratory Study of Glowing Electrical Connections," NIST, Washington, D.C., 1977.